Annual Report of Investigations Carried Out Under the Director's Research and Development Fund

September 30, 2001 to September 29, 2002

January 31, 2003

Jet Propulsion Laboratory
California Institute of Technology

FOREWORD

The Jet Propulsion Laboratory (JPL) Director's Research and Development Fund (DRDF) was established in 1969 as one provision of a Memorandum of Understanding between the National Aeronautics and Space Administration (NASA) and the California Institute of Technology (Caltech). The principal objectives of the DRDF are to promote innovative seed efforts for which conventional program resources are not available, and to encourage collaborative work with faculty and students at Caltech and other universities.

In 2002, the level of support for DRDF was $3.5 million. For a typical mix of in-house labor and procurements, this level of funding provides about 13 workyears per year of research effort. In contrast to the NASA civil service centers' flexibility of action afforded by the availability of research and program management (R&PM) resources, JPL must cover all cost of in-house labor, services, and related burdens by the R&D funds themselves.

The current level of funding has had a significant impact at JPL by enabling expanded efforts in selected technologies regarded as especially important for the future of the Laboratory. The technologies selected for emphasis by the Director for 2002 were those aligned with the JPL strategic implementation plan. The emphasis is on innovative science and breakthrough technologies. Since space missions are fundamentally limited by the technology, any breakthrough offers a possibility of bypassing today's limitations and will lead to revolutionary improvements in space science and missions.

This annual report deals primarily with the technical content of the work supported by the DRDF. It is a collection of task reports prepared by individual investigators that describe the objectives, progress and accomplishments, significance of the results, and financial status of the various tasks. Care is taken by authors to credit other persons, especially university faculty and students, who contributed to the effort. Publications and conference presentations related to the work are listed at the end of each summary. The material has been lightly edited to ensure consistency in format, correctness of spelling and punctuation, completeness of thought, and so on, but the substance of style of the reports reflects the individuality of their authors.

The individual summaries are categorized as either "interim" or "final," according to the status of the task efforts. Most of the DRDF tasks that were active during FY 2002 are represented in the report, but in few instances contributions were not forthcoming in time to be included in this volume. Submissions of this kind that eventually appear will be retained in the task files for reference.

The table of contents groups the summaries by technology area.

Individual task reports are intended to be informative stand-alone narratives. However, readers who have questions or desire additional details about any task should not hesitate to contact the authors directly.

CONTENTS

Task	*Title and Investigators*	*Page*
ADVANCED MEASUREMENT TECHNIQUES		
983	**SENSOR WEB FOR REMOTE AND UNATTENDED ENVIRONMENT MONITORING** Kevin A. Delin, In-Situ Technology and Experimental Systems Section (384) Arthur L. Lane, Earth and Space Sciences Division (32)	3
1021	**A COHERENT MATTER WAVE QUANTUM GRAVITY GRADIOMETER FOR SUBSURFACE REMOTE SENSING** Lute Maleki, Tracking Systems and Applications Section 335 Robert Thompson, Tracking Systems and Applications Section 335 Nan Yu, Tracking Systems and Applications Section 335 James Kohel, Tracking Systems and Applications Section 335	7
ADVANCED OPTICAL SYSTEMS		
974	**NARROW LINEWIDTH LIGHT SOURCES FOR SPACE INTERFEROMETRY** Alexander Ksendzov, Section 346 Johan Burger, Section 346 Serge Dubovitsky, Section 346	13
1016	**A MEMBRANE TRANSFER TECHNOLOGY FOR A CONTINUOUS MEMBRANE MEMS DEFORMABLE MIRROR** Eui-Hyeok Yang, In Situ Technology and Experiments Systems Section (384) Dean Wiberg, In Situ Technology and Experiments Systems Section (384)	17
1038	**ULTRA-LIGHTWEIGHT OPTICAL COLLECTOR USING IN-SPACE BUBBLE BLOWING AND METAL EVAPORATION TECHNOLOGIES** Yu Wang, (Section 387)	21
ASTROBIOLOGY		
964	**MECHANISMS OF RESISTANCE TO HYDROGEN PEROXIDE IN MICROBES ISOLATED FROM A JPL SPACECRAFT ASSEMBLY FACILITY** Kasthuri Venkateswaran, Biotechnology and Planetary Protection (3544) Michael J. Kempf, Biotechnology and Planetary Protection (3544)	27

CONTENTS

Task	*Title and Investigators*	*Page*
978	**A NOVEL INVESTIGATION ON BIOTIC AND ABIOTIC MOLECULES IN AN ICE MATRIX UNDER ENERGETIC CONDITIONS** Isik Kanik (Instrument Development and Spectroscopy Research Element-3264)	33
1006	**ORGANIC ENVIRONMENTS IN THE OUTER SOLAR SYSTEM** Patricia M. Beauchamp, JPL In-Situ Exploration and Sample Return Center of Excellence (303) Jonathan I. Lunine, University of Arizona Jesse L. Beauchamp, Department of Chemistry, California Institute of Technology Dennis A. Dougherty, Department of Chemistry, California Institute of Technology Mark Smith, Department of Chemistry, University of Arizona	39
1010	**NANOFLUIDIC LAB-ON-A-CHIP FOR BIOMOLECULE DETECTION** Sabrina Feldman, In situ Technology and Experiments Systems Section (384) Danielle Svehla, In situ Technology and Experiments Systems Section (384) Frank Grunthaner, In situ Technology and Experiments Systems Section (384) Jason Feldman, In situ Technology and Experiments Systems Section (384) Joseph Wang, New Mexico State University (NMSU)	47
1022	**NOVEL NON-DESTRUCTIVE MICROWAVE EXTRACTION OF ORGANIC MOLECULES FROM ROCK AND SOIL SAMPLES** Luther W. Beegle, Instrument Development and Spectroscopy Research Element (3264) Isik Kanik, Instrument Development and Spectroscopy Research Element (3264) Nasser Budraa, Instrument Development and Spectroscopy Research Element (3264)	51
AUTOMATION AND CONTROL		
919	**PASSIVE ATTITUDE CONTROL OF A SPIN-STABILIZED SPACECRAFT BY SOLAR RADIATION PRESSURE ON CANTED VANES** Thomas R. Spilker, Mission & Systems Architecture Section (311)	57

CONTENTS

Task	*Title and Investigators*	*Page*
961	**A NOVEL APPROACH TO PLANETARY PRECISION LANDING USING PARAFOILS** Marco B. Quadrelli, Autonomy and Control Section (345) Fred Y. Hadaegh, Autonomy and Control Section (345)	61
INFLATABLE STRUCTURES		
966	**A NEW TYPE OF SELF-RIGIDIZABLE SPACE INFLATABLE STRUCTURE** Michael Lou, Mechanical Systems Engineering and Research Division (35) Houfei Fang, Thermal and Propulsion Engineering Section (353)	69
969	**TITAN BALLOON BUOYANCY CONTROL ANALYSIS AND DEMONSTRATION** Jack A. Jones, Science and Technology Development Section (354) Andre Yavrouian, Thermal and Propulsion Engineering Section (353) Ralph Lorenz, University of Arizona, Lunar and Planetary Laboratory	73
INFORMATION SYSTEMS		
1035	**QUANTUM INTERFEROMETRY** Jonathan P. Dowling, Exploration Systems Autonomy Section (367)	79
MATERIALS		
973	**SHAPE MEMORY ALLOY THERMAL SWITCH** Virginia Gordon Ford, Mechanical Engineering Section, (352P) Georg Siebes, Thermal and Propulsion Engineering Section, (3536) Eric Sunada, Thermal and Propulsion Engineering Section, (3536) Sean Haggart, Mechanical Engineering Section, (352)	85
MICRO/NANO DEVICES		
935	**NANOTUBE ENGINEERING** Brian Hunt, In Situ Technology and Experiments Systems (384) Michael Hoenk, In Situ Technology and Experiments Systems (384) Flavio Noca, In Situ Technology and Experiments Systems (384) Prof. Jimmy Xu, Brown University Prof. Axel Scherer, Caltech	91

CONTENTS

Task	*Title and Investigators*	*Page*
939	**INFRARED DETECTORS BASED ON SELF-ORGANIZED CARBON NANOTUBE ARRAYS** David Z. Ting, Section 384 Sumith V. Bandara, Section 384 Sarath D. Gunapala, Section 384 John K. Liu, Section 384 Sir B. Rafol, Section 384	97
960	**NANOTUBE ACTUATORS AND OSCILLATORS** Brian D. Hunt, Space Microsensors Technology (384) Michael Hoenk, Space Microsensors Technology (384) Flavio Noca, Space Microsensors Technology (384) Dan Choi, Space Microsensors Technology (384) Bob Kowalczyk, Space Microsensors Technology (384) Prof. Michael Roukes, Dr. Jim Hone, Caltech	101
1018	**CARBON NANOTUBE FIELD EMITTERS FOR MINIATURE MASS SPECTROMETERS AND NANOKLYSTRONS** Harish M. Manohara, Microwave Experiment Systems and Technology Section (386) Peter H. Siegel, Microwave Experiment Systems and Technology Section (386) Michael Hoenk, Section 384 Murray Darrach, Section 323 Ali Husain, California Institute of Technology James Hone, California Institute of Technology Michael Roukes, California Institute of Technology Axel Scherer, California Institute of Technology	105
1025	**SUBMILLIMETER-WAVE MOMED MIXERS FOR EARTH AND PLANETARY REMOTE SENSING** John J. Gill, John E. Oswald, Peter H. Siegel, Microwave and Lidar Technology Section (386) Michael Janssen, Earth and Space Sciences (320)	109
1026	**TOWARD ARTIFICIAL NANOSCALE SYSTEMS: SELF-ASSEMBLED POLYMERIC TEMPLATES FOR FABRICATION OF CARBON NANOTUBE ARRAYS** Michael J. Bronikowski, Michael E. Hoenk, Robert S. Kowalczyk, Eric W. Wong, In-Situ Technology and Experiments Systems Section (384)	113

CONTENTS

Task	*Title and Investigators*	*Page*
1027	**A MICRO TURBINE POWER SOURCE FOR DEEP SPACE APPLICATIONS** Beverley Eyre, In Situ Technology and Experiments Systems Section (384) Dean Wiberg, Section (384), Kirill Shcheglov, Section (384) Dr. Phillip Muntz (USC), Eric Moore (USC)	119
MICROINSTRUMENTS AND SMALL PAYLOADS		
979	**INTEGRATED REFLECTANCE/RAMAN MICROSPECTROMETER** Pantazis Mouroulis, Space Experiments Systems &Technology Section (387) Daniel W. Wilson, Paul D. Maker, In-situ Technology & Experiments Systems (384)	127
980	**A PARTICLE SIZE AND CHARGE ANALYZER FOR INVESTIGATION OF THE ELECTRICAL PROPERTIES OF DUST DEVILS** Gregory Wilson, Geophysics and Planetary Geosciences (3223) Stephen Fuerstenau, In-Situ Technology and Experiments Systems Section (384)	131
1017	**MINIATURE AGE DATING /MATERIALS CHARACTERIZATION INSTRUMENT FOR MARS EXPLORATION** Soon Sam Kim, Thermal and Propulsion Engineering Systems Section (353) Stephen W.S. McKeever and Michael W. Blair, Department of Physics, Oklahoma State University	141
PROPULSION		
991	**A 3-DIMENSIONAL PARTICLE SIMULATION MODEL FOR ION THRUSTER PLASMA FLOW AND GRID EROSION** Joseph J. Wang, Thermal and Propulsion Engineering Section (353)	149
1012	**NANOSTRUCTURED METAL OXIDES FOR HIGH POWER BATTERIES** Ratnakumar Bugga, Will West, Nosang V Myung, (Section 346) Jay Whitacre and Marshall Smart (Section 346) Rachid Yazami and Brent Fultz, Materials Science Dept., Caltech	153

CONTENTS

Task	*Title and Investigators*	*Page*
SCIENCE		
MU994	**A STUDY OF IN SITU CHRONOLOGY IN THE OUTER SOLAR SYSTEM** Leslie K. Tamppari, Mission Systems Engineering Section (314) Timothy Swindle, University of Arizona	159
1007	**EXPERIMENT TO DETECT MARTIAN PERMAFROST BASE/GROUND WATER AND BIOGENIC METHANE FROM AN ORBITER AND/OR LANDERS ON MARS** Natalia Duxbury, Section 3224	163
1030	**TIDAL CORRECTIONS FOR SAR INTERFEROMETRY ON FLOATING ICE SHELVES** Ian R. Joughin, Radar Science & Engineering Section (334)	167
1034	**DISK-AVERAGED SYNTHETIC SPECTRA OF TERRESTRIAL PLANETS** Victoria S. Meadows, Planetary And Life Detection Section (322)	171
1039	**HIRES FOR SIRTF EXTRAGALACTIC SURVEYS** Thangasamy Velusamy, Astrophysics Element (3262) Charles Beichman, Astronomy and Physics Directorate (700) George Helou, IPAC (Caltech)	175
TELECOMMUNICATION		
1015	**FAST & ACCURATE PREDICTION OF ANTENNA-SPACECRAFT MULTIPATH EFFECTS** Dr. Vaughn P. Cable, Spacecraft Telecommunications Equipment Section (336E) Professor Oscar P. Bruno, Applied Mathematics, California Institute of Technology	181

ADVANCED MEASUREMENT TECHNIQUES

SENSOR WEB FOR REMOTE AND UNATTENDED ENVIRONMENT MONITORING

Final Report

JPL Task 983

Kevin A. Delin, In-Situ Technology and Experimental Systems Section (384)
Arthur L. Lane, Earth and Space Sciences Division (32)

A. OBJECTIVES

We planned on demonstrating a Sensor Web [1,2] that can be deployed in a remote and unattended environment, and showing that the information gathered and processed by the web can be transferred to scientists in their offices in real-time. The web will track the spatio-temporal changes in local environments. The systems were tested in environmental laboratory chambers and are presently deployed in-field.

B. PROGRESS AND RESULTS

1. A graphical user interface (GUI) was perfected, suitable for Internet viewing. The GUI is interactive and allows the user to display different pods, different measurements to study, and to look at both archived and real-time data. The GUI is meant to be globally accessible over slow (56K modem) connections, and platform independent (PC, Mac, Netscape, IE).

2. A package was designed to withstand a variety of environments, ranging from temperatures of 70°C to –40°C. The following design changes were incorporated into the package:

   - Improved gasket: Instead of a polyurethane (shore 30-40A) material in the form of an O-ring, a 1/16" silicon sponge with a pressure sensitive adhesive backing was chosen. The location of the gasket moved to outside the groove, which increased the sealing area, minimized unnecessary gasket compression, thus increasing life expectancy, and decreased assembly difficulties. The pressure-sensitive backing also reduced the risk of potential twisting during assembly and in field deployment. The material selection better handles the temperature requirements.
   - Antenna seals: Ethylene Propylene O-rings fitted into counterbores replaced the vibration isolators as the sealing method for the antennas. The material selection handles impermeability, temperature cycling, compression set, and weathering far better than the polyurethane isolator. The design offers easier and faster installment.

- Board deflection was addressed through a change in the antenna/board connection design. Instead of a press contact, which caused the bending, a fixed design was chosen which used a nut and bolt on the antenna stud. This not only improved the connection, it also added robustness and eliminated any loading on the electronics board.
- Thread-forming fasteners replaced the insert/machine screw attachment device in the six middle locations. The thermal cycling seen in the test experiences started to develop cracks in the pod shell due to thermal expansion differences between the polycarbonate box and the brass inserts. The softer, silicon sponge gasket decreased preload on the screws needed for gasket compression, thus allowing the thread-forming fasteners to be used with no operational sacrifices. Inserts were left in the corners due to the large number of assembly and disassembly operations. Additional material at these locations minimized the possibility of a crack-causing leak. Cost per pod also decreased with this alteration.

3. To test system robustness outside the laboratory, we deployed one Sensor Web system inside a greenhouse which simulates the humid, moist environment of a rainforest. Another system will be deployed in Antarctica in late 2002.

C. SIGNIFICANCE OF RESULTS

The task developed a robust Sensor Web system capable of monitoring such diverse environments as the Southern California desert and Antarctica. The Antarctic Sensor Web will be deployed by Prof. Ralph Harvey's team in November, 2002 as a no-cost test of the system.

The GUI associated with the system has been recently deployed and field-tested at both the Huntington Gardens and Cal Poly Pomona. Real-time streaming data may be viewed at http://sensorwebs.jpl.nasa.gov/. This GUI capability allows the Sensor Web team to monitor the Sensor Webs' performance remotely, tracking both extreme environmental conditions and pod failure. For example, during the late summer, the internal temperature of some of the pods at the Huntington Garden rose to 65°C, yet the system did not fail and the communication links stayed synched despite the extreme degree of differential heating on the total Sensor Web system.

The work performed on this DRDF allowed for the solid development of a long-lived, robust system, and a means for shuttling the data back to the laboratory in real-time. This is a crucial and significant step in placing the system for actual applications, including environmental monitoring in harsh environments (Antarctica, Mars) and environmental remediation efforts.

D. FINANCIAL STATUS

The total funding for this task was $100,000, all of which has been expended.

E. PERSONNEL

The JPL Sensor Web team: Scott Burleigh (database management), Shannon Jackson (electronics), Dave Johnson (mechanical), Michael McAuley (servlet), and Richard Woodrow (applet) all contributed to the production of the system. Prof. Ralph Harvey (CWR) is deploying the system as a no-cost test in Antarctica.

F. PUBLICATIONS

1. Kevin A. Delin, "The Sensor Web: A Macro-Instrument for Coordinated Sensing," *Sensors,* **2**, 2002, pp. 270-285.

G. REFERENCES

[1] K.A. Delin and S.P. Jackson, "Sensor Web for *In Situ* Exploration of Gaseous Biosignatures," *Proceedings of 2000 IEEE Aerospace Conference*, Big Sky, MT March 2000. (see also http://sensorwebs.jpl.nasa.gov/resources/Delin-Jackson2000.pdf)

[2] K.A. Delin and S.P. Jackson, "The Sensor Web: A New Instrument Concept," *Proceedings of SPIE's Symposium on Integrated Optics*, San Jose, CA, January 2001. (see also http://sensorwebs.jpl.nasa.gov/resources/sensorweb-concept.pdf)

A COHERENT MATTER WAVE QUANTUM GRAVITY GRADIOMETER FOR SUBSURFACE REMOTE SENSING

Final Report

JPL Task 1021

Lute Maleki, Robert Thompson, Nan Yu, James Kohel
Tracking Systems and Applications Section 335

A. OBJECTIVES

This task is for the development of a coherent matter wave atom interferometer suitable for use in a gravity gradiometer. The quantum interferometer gravity gradiometer (QUIGG) is an enabling technology which will allow remote three-dimensional mapping and the determination of density variations below the surface of a solid or fluid body.

B. PROGRESS AND RESULTS

1. Development of all-optical source of Bose-condensed atoms

We have designed and built an apparatus that will allow us to Bose condense large samples of Rubidium atoms using entirely optical techniques. Bose-Einstein condensation (BEC) is a quantum-phase transition that occurs at low temperatures and high densities for samples of atoms which obey what is known as Bose statistics (most atoms fit this description). A Bose condensed sample of atoms has a large fraction of atoms in a single, macroscopic, quantum state. The atoms are coherent, meaning their De Broglie wavelengths (according to quantum mechanics all objects have both a wave and a particle nature), are in phase with one another. This property is important for a number of sensor applications, in particular those based on atom interferometry, potentially allowing an increase in the sensitivity of the instrument by a factor proportional to the square root of the total number of condensed atoms, a three orders of magnitude improvement for typical BEC experiments [5].

Our apparatus consists of two vacuum chambers, one of which contains a cold atomic beam source which delivers on order of $1 \blacktriangleright 10^9$ atoms per second to the second chamber, which is held at ultra-high vacuum (UHV) ($5 \blacktriangleright 10^{-11}$ torr). Atoms are collected into a standard magneto-optical trap (MOT), consisting of six laser beams which confine the atoms in all directions and cool them to about 20 millionths of a degree above absolute zero. This low temperature is still several orders of magnitude too hot to achieve BEC, so the atoms are moved into a different type of trap called a quasi-electrostatic trap (QUEST), which is formed by a tightly focused crossed pair of CO_2 laser beams. This trap is purely conservative, so there is no lower limit to the achievable temperature. Once atoms are stored in the QUEST, the intensity of the trap is slowly ramped down, allowing the hottest atoms to escape, while the remaining atoms

equilibrate at lower temperatures. This process, called evaporative cooling, is very efficient in a QUEST trap, allowing BEC conditions to be readily achieved.

The current status of this apparatus is that we have observed a cold atomic beam and are currently optimizing the loading into the UHV MOT. Once this stage is completed, we expect that loading into the final QUEST trap will be straight forward, with the only difficulties coming from the need to precisely align the two CO_2 laser beams. Once a suitable initial density of atoms is found in the QUEST, Bose condensation will follow immediately (all that is required is to ramp down the laser intensity slowly, so that evaporation proceeds steadily). All components of the final apparatus have been assembled. The apparatus is shown in figure 1. An image of the cold atomic beam in action is shown in figure 2.

Once Bose condensation is achieved, the next stage of this task is a demonstration of an atomic interferometer. Our approach is to use Bragg scattering as a beamsplitter[4]. Here the coherent matter-wave diffracts off of an optical standing wave which acts as a grating. A standing wave pulse diffracts a fraction of the condensate into momentum states $\pm 2n\hbar\boldsymbol{k}$, where $\boldsymbol{k}$ is the wave vector of the standing wave. A second pulse applied a time t_1 later creates an overlapping copy. The amplitudes of the matter-waves interfere where they spatially overlap. Such a technique is particularly easy to implement for a proof-of-principle test of a coherent matter-wave accelerometer.

2. Characterization of a dual-beam atomic beam source and observation of cold collisions

In the initial stages of this investigation, we converted an existing cold atomic beam source from operation as a cold Cesium beam to a cold Rubidium source (Rubidium is a standard atom for BEC experiments, while BEC has not yet been achieved in Cs). This allowed us to develop a novel and simple two-species (Cs and Rb) atomic beam source, and utilize this beam source to perform a preliminary study of cold collisions in a separate mixed-species trap under UHV conditions [1].

Simple modeling of these observed differences allowed us to make measurements of the heteronuclear (two atomic species) cold collision rate, which we compared to results from recent experiments in vapor cell traps[3].

C. SIGNIFICANCE OF RESULTS

The optical BEC apparatus developed under this task will have vastly superior performance over what has been achieved previously [2]. It features atomic beam loading which gives a hundred times faster loading rates than the vapor cell used in the original demonstration, a vacuum which is also a hundred times better, giving much longer condensate lifetimes, along with an optical trap which has more than a factor of two higher power, which will result in tighter confinement. At a minimum, these improvements will allow us to produce condensates at a much more rapid rate than in the original experiment (by a factor of ten to a hundred), and allow us to study these condensates for much longer times (by about a factor of ten). The latter capability is particularly important for a future space-based instrument, since microgravity allows one to take advantage of significantly longer interaction times to achieve much higher sensitivity than can be achieved on the ground. Other improvements in our apparatus include increasing the amount of optical access, which will allow us to incorporate the additional laser

beams needed to demonstrate an atom interferometer. We also expect that we will be able to produce much larger condensates in our apparatus than were achieved in the original experiment, though this will require a significant effort in optimizing the trap and evaporative cooling parameters.

A gravity gradiometer employing a coherent BEC source such as we have developed will allow, for the first time, the production of three-dimensional mapping of the gravity field by remote sensing. This will enable below-the-surface studies of the solid Earth, oceans, and other solar system bodies. We expect that such a capability will revolutionize Earth and planetary science investigations, and find important commercial and defense applications. The coherent QUIGG has the potential to offer room-temperature operation of a gravity gradiometer with ultra-high sensitivity (up to 10^{-4} E/Hz$^{1/2}$, where E =1►10^{-9} sec^{-2}), and will be capable of long-term reliability. Such a gravity gradiometer will be especially suitable for on-board spacecraft applications.

The measurements of cold collision rates [1] are complementary to what has been achieved previously [3], in that they measure the effect of cold rubidium atoms on a cesium trap decay rate as opposed to the reverse. Understanding each of these rates is important for a variety of experiments involving two co-located samples of cold atoms, including a proposed NASA flight project, the Quantum Interferometer Test of Equivalence (QUITE). Furthermore, these measurements introduce a new technique into the field of cold collision studies, namely the use of cold beams for studying two-species interactions. This technique allows an unprecedented amount of control over the experiments, yielding results that are much cleaner and simpler to analyze. For example, we are able to turn off the loading rates of the two atoms independently, and neglect effects of background atoms because of our superior vacuum.

D. FINANCIAL STATUS

The total funding for this task was $250,000, of which $205,000 has been expended.

E. PERSONNEL

In addition to the co-investigators named above, Nathan Lundblad, a graduate student at Caltech, played a key role in putting together the BEC apparatus described above, and in gathering and analyzing data for the two-species beam/cold collision studies.

F. PUBLICATIONS AND PRESENTATIONS

[1] Nathan Lundblad, David Aveline, Robert J. Thompson, James Kohel, Jaime Ramirez-Serrano, William M. Klipstein, Daphna G. Enzer, Nan Yu, and Lute Maleki, "A two-species cold atomic beam," submitted to *Physical Review A,* Rapid Communications.

[2] Nathan Lundblad, talk: "Production and Characterization of a Dual-Species Cold Atomic Beam", presented at American Physical Society's Division of Atomic, Molecular and Optical Physics Meeting, (5/29/02) Williamsburg, VA.

[3] Nathan Lundblad, poster presentation: "Production and Characterization of a Dual-Species Cold Atomic Beam", presented at Optical Society of America

Conference on Quantum Electronics and Laser Science, (5/21/02) Long Beach, CA .

G. REFERENCES

[1] Nathan Lundblad, David Aveline, Robert J. Thompson, James Kohel, Jaime Ramirez-Serrano, William M. Klipstein, Daphna G. Enzer, Nan Yu, and Lute Maleki, "A two-species cold atomic beam," submitted to *Physical Review A,* Rapid Communications.

[2] M.D. Barrett, J.A. Sauer, M.S. Chapman, "All-optical Formation of an Atomic Bose-Einstein Condensate," *Phys. Rev. Lett.,* 87**,** 010404 (2001).

[3] G. D. Telles, *et al,* "Trap Loss in a Two-Species Rb-Cs Magneto-Optical Trap," *Physical Review A,* 63 033406 (2001).

[4] E.W. Hagley *et al.,* "Measurement of the Coherence of a Bose-Einstein Condensate,**"** *Phys. Rev. Lett*., 83 3112, (1999).

[5] P. Bouyer, M.A. Kasevich, "Heisenberg-Limited Spectroscopy With Degenerate Bose-Einstein Gases," *Phys. Rev. A,* 56 (2): R1083 (1997).

H. APPENDIX: *Figures*

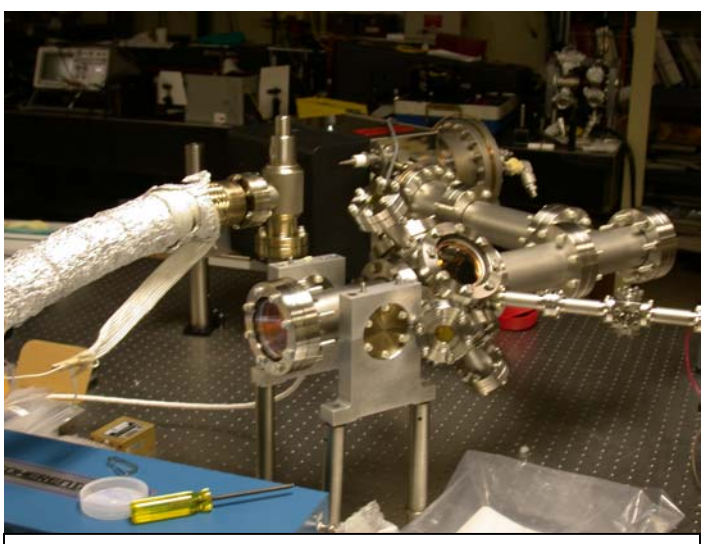

Figure 1.Vacuum chamber for the JPL coherent matter-wave atom interferometer.

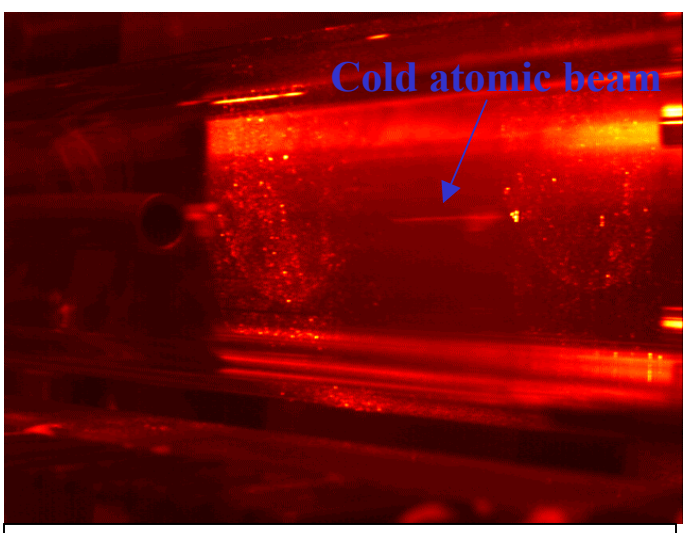

Figure 2. Cold atomic beam in operation.

ADVANCED OPTICAL SYSTEMS

NARROW LINEWIDTH LIGHT SOURCES FOR SPACE INTERFEROMETRY

Final Report

JPL Task 974

Alexander Ksendzov, Section 346
Johan Burger, Section 346
Serge Dubovitsky, Section 346

A. OBJECTIVES

The NASA Origins program theme emphasizes separated space interferometers, tethered interferometers using multiple satellites, and other constellations/formations as enabling technology for very large baseline interferometers in space. The necessary precise positioning of the participating spacecraft will be achieved using optical metrology. The fine-gauge metrology is based on frequency-stable narrow-linewidth light sources. This work will advance the state of the art by producing integrated optics (IO) resonators critical for the narrow linewidth operation of semiconductor and diode pumped Nd:YAG lasers. The potential applications of such components in interferometry projects are numerous.

The most significant result of this work will be enabling absolute metrology in space. The proposed resonator will be the critical component for fabricating pairs of narrow linewidth semiconductor lasers separated by 1-10 nm. One can not perform absolute distance measurement (i.e. determine distance without ambiguity) using a single wavelength -- all distances separated by a full fringe ($\lambda/2 \approx 0.65$ μm) will produce the same reading. This ambiguity could be resolved by using an additional ranging system to determine the distance coarsely, with $\leq\lambda/2$ precision. However, the existing RF and optical ranging systems have ≈1mm precision, and therefore a gap exists between the fine and the coarse measurement gauges. Bridging the gap is required to enable absolute distance measurement. To this end, a pair of narrow linewidth semiconductor lasers separated by 1-10 nm will enable measurements with an ambiguity range of several mm while still enabling submicron precision. (Pairs of Nd:YAG lasers cannot be used for this purpose as they can only be tuned by ≈0.1 nm away from the 1.319 nm line).

Enabling narrow linewidth operation of semiconductor lasers can be of further use for the interferometry projects. While the current light source of choice, Nd:YAG laser, operates at 1.319 μm, the communication industry concentrates its efforts at the 1.55 μm range. Therefore the IO components necessary to build the complete metrology system (e.g. switches, couplers, optical amplifiers and frequency shifters and modulators) operating at 1.3 μm are either non-existent or hard to find. Thus building narrow linewidth semiconductor lasers in the 1.55 μm range will solve difficult systems problems.

Furthermore, metrology systems currently use frequency-stabilized Nd:YAG lasers as light sources for fine-gauge metrology. The lasing frequency is stabilized by closing a frequency control loop using a high quality factor (Q) resonator as a frequency discriminator. The advantage of the proposed IO resonator over Fabri-Perot etalons currently in use will be the

increased flight worthiness and ease in system integration, as well as considerable space and weight savings.

B. PROGRESS AND RESULTS

1. Science Data

We have built two types of ring resonators. The first type (type 1) is built with waveguides that have large modes suitable for the direct fiber coupling. These resonators will replace the bulk Fabry-Perot etalons used in the metrology systems. The type 2 resonators are based on waveguides with oblong modes that fit the semiconductor laser modes. These resonators will be useful in linewidth narrowing of semiconductor lasers. The waveguide cross sections are depicted in Figure 1.

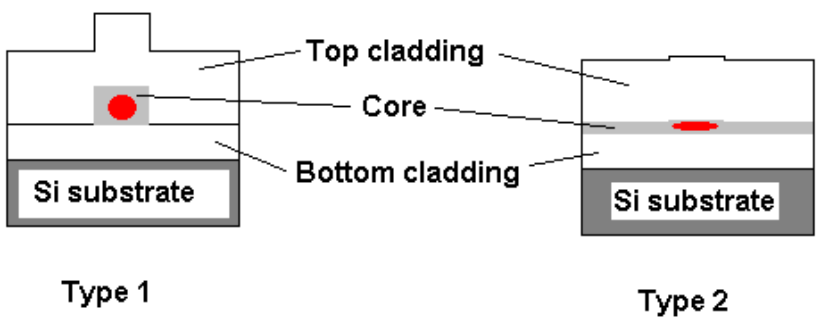

Figure 1. Waveguide layout.

We have calibrated PECVD growth process for a number of materials with different refractive indexes. Table 1 shows the materials with the correspondent stresses and refractive indexes.

Table 1. PECVD material growth calibration

Recipe name	Material	Refractive index at 1.55 μm	Stress dyn/cm^2	Growth rate A/sec.
LORTOX	SiO_2	1.452	-3.2×10^9	382
SION3	SiO_xN_y	1.501	1.5×10^9	275
SIN1-1	Si_xN_y	1.851	1.2×10^{10}	86

Resonators with large waveguides (type 1) have been built. The LORTOX recipe was used for the cladding material while the SION2 recipe was used for the core. The waveguides were defined by contact photolithography. The reactive ion etching was then used to transfer the pattern onto the core layer.

We have tested both the direct masking by photoresist and a more involved process with an intermediate step creating a Cr masking layer to define the waveguides. Both processes worked well. The RIE etching with CHF_3 of the Cr masked wafer resulted in a vertical wall profile as is shown in Figure 2.

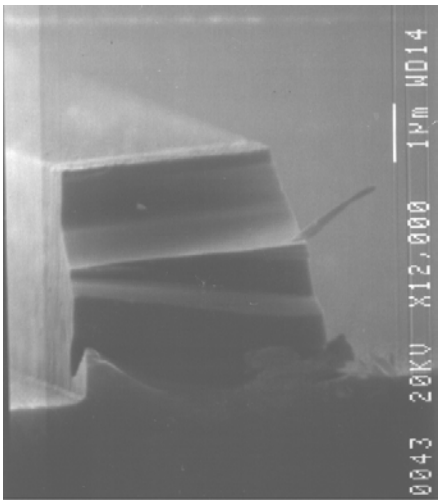

Figure 2. Waveguide etched using Cr mask.

The same etching recipe used on the wafer masked with the photoresist produced slightly slanted walls Both wall profiles are satisfactory.

However, we experience difficulty with the regions where waveguides are running close together, i.e. the ring to straight section coupling regions. As shown in Figure 3, the growth of the cladding material is non-conformal and causes air pockets between the waveguides.

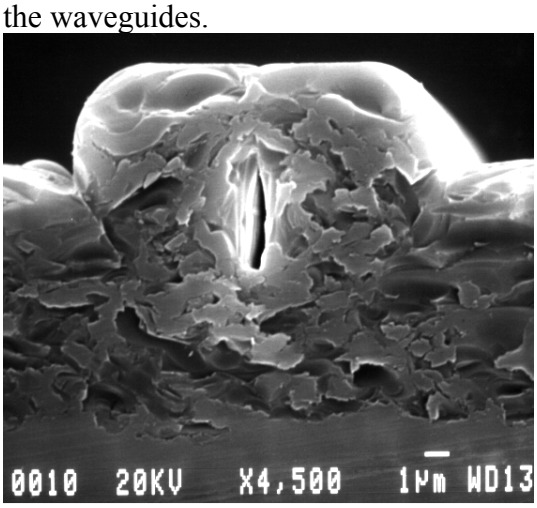

Figure 3. Notice the void in the center between the waveguides due to non-conformal growth.

Our calculations show that these air pockets reduce the coupling to unacceptably low levels. Methods for eliminating these pockets are well known. The preferred technique is to use boron-doped glass as the top cladding. This material can be reflown after deposition for conformal coating without voids.

We have also made a series of ring resonators with oblong modes that fit the mode of a semiconductor laser. These resonators will be useful in linewidth narrowing of semiconductor lasers. The LORTOX material core and SIN1-1 cladding materials were grown by PECVD; the processing sequence was similar to the one described above. The waveguide design has a shallow rib and therefore the overgrowth with the top cladding does not present difficulties encountered in the large waveguide case. These ring resonators are currently being tested at 1.55 μm. We have obtained pictures with an infrared camera of a ring resonator at resonance and off resonance (see fig. 4).

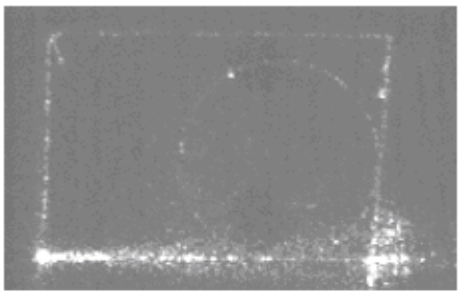

At resonance

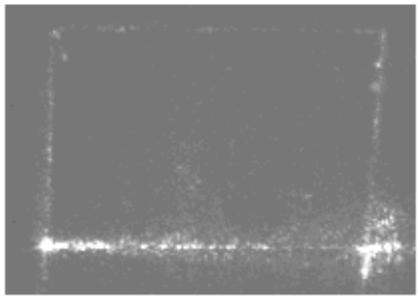

Off resonance

Figure 4. Infrared camera pictures of the ring resonator at resonance and off resonance.

The losses in these waveguides were measured using transmittance characteristics of the rings. As shown in Figure 6, the transmittance spectrum of a ring resonator exhibits periodic notch-like structures. Using the finesse (the ratio of the notch width to the periodicity) and the depth of notches, one can compute the loss in the ring. The spectrum in Figure 5 corresponds to a loss of 1.4 dB per turn or 1.5 dB/cm.

We have computed the possible laser linewidth narrowing, using such rings along the lines suggested in the original proposal. Chirp reduction factors of more than 40 are achievable (linewidth narrowing by more than a factor of 1600 is possible). This result is very encouraging, and we will pursue this technique for the semiconductor linewidth narrowing using other funds.

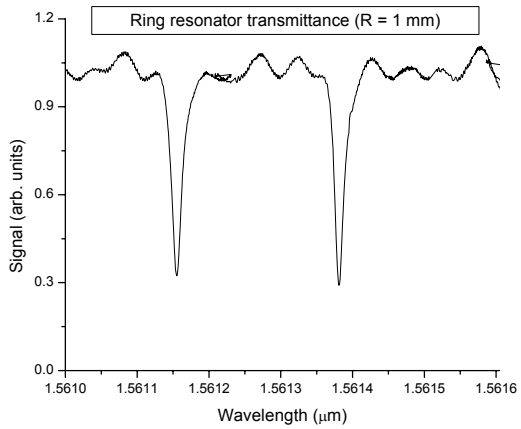

Figure 5. Transmittance spectrum of a ring resonator.

C. SIGNIFICANCE OF RESULTS

We developed ring resonators for space applications. In particular, the ring resonators for the semiconductor linewidth narrowing has been successfully produced.

D. FINANCIAL STATUS

The total funding for this task was $100,000, all of which has been expended.

E. PERSONNEL

No other personnel were involved.

F. PUBLICATIONS

None.

A MEMBRANE TRANSFER TECHNOLOGY FOR A CONTINUOUS MEMBRANE MEMS DEFORMABLE MIRROR

Interim Report

JPL Task 1016

Eui-Hyeok Yang, In Situ Technology and Experiments Systems Section (384)
Dean Wiberg, In Situ Technology and Experiments Systems Section (384)

A. OBJECTIVES

Future ultra-large, lightweight space telescopes envisioned by NASA have either segmented or inflatable primary mirrors [1]. Due to the optically imperfect surface figure of these mirrors, the primary optics would require an active compensation of large wavefront errors. A large-stroke deformable mirror is a key component for the wavefront compensation system for an astrophysical imaging instrument. Our ultimate goal is to develop deformable mirrors by a membrane transfer process. The membrane transfer technique will provide a critical technology complement for a deformable mirror meeting the requirements for the surface figure and the mechanical compliance.

Specifically under the proposed effort, the following was to be accomplished:

1) Transfer a compliant membrane with an area of 2500 mm^2 from one substrate to another to demonstrate the process.
2) Determine the surface quality of the transferred membrane.

The objective of this work is <u>to develop a membrane transfer technology</u> for the fabrication of a compact, low-cost, high-compliance, optical-quality continuous face-sheet deformable mirror for astrophysical imaging.

B. PROGRESS AND RESULTS

Wafer-scale single-crystal silicon membranes have been successfully transferred without using sacrificial layers such as adhesives or polymers.

A 10 μm thick single-crystal silicon membrane (4 in. diameter) was transferred in wafer-scale. The transfer process sequence is as follows: A Silicon-On-Insulator (SOI) wafer and a silicon wafer are used as the carrier and electrode wafers, respectively. A 0.5 μm thick oxide is thermally grown on both sides of the wafers. Then Ti/Pt/Au metal layers are deposited and patterned to form electrode arrays on the electrode wafer. The Cr/Pt/Au metal layers are deposited subsequently over the photoresist patterns on both wafers for the lift-off process. A 1 μm thick indium layer is then deposited on both wafers. Since the indium layer uniformly wets the Au layer, the Au acts as a "substrate" for hermetic bonding. This hermetic bonding process is a critical step for subsequent etch processes. Indium instantly oxidizes in air, and the oxidized

indium does not provide hermetic bonding. Thus, the indium deposition process is followed by the deposition of a 0.01 μm thick Au layer to prevent the indium surface from oxidizing. The deposited metal layers for bonding are patterned using a lift-off process. The carrier wafer is subsequently bonded to the electrode wafer. An Electronic Vision aligner and a thermo-compression bonder is used to align and bond two patterned wafers, respectively. The bonder chamber is pumped down to $1X10^{-5}$ Torr before bonding two wafers. A piston pressure of 4 kPa is applied at 156°C in a vacuum chamber to provide a complete hermetic sealing. The substrate of the SOI wafer is etched in a 25 wt % Tetramethylammonium hydroxide (TMAH) bath at 80°C until the buried oxide is exposed. A Teflon fixture is used to protect the backside of the bonded wafers as well as their bonded interface. The exposed oxide is then removed by using dilute hydrofluoric acid (49% HF) droplets after an O_2 plasma ashing. The wafer-scale silicon membrane transfer is completed at this stage.

Fig. 1 shows a photograph image of a transferred single-crystal silicon membrane. The surface profile of a transferred single-crystal silicon membrane was measured and compared with that of a typical silicon wafer.

Fig. 2 shows the surface figure of a wafer-scale transferred 10 μm thick single- crystal silicon membrane. The membrane was subsequently patterned and etched in order to remove the hermetic sealing for the surface figure measurement of a "standing" membrane. The peak-to-valley surface figure error of a membrane (area 1 mm^2) with indium posts spacing of 200 μm was 9 nm. This number (9 nm p-v) shows the "optical" surface quality of the transferred membrane, since the commercially available deformable mirrors provide $\lambda/20$ at $\lambda = 633$ nm [2].

The wafer-scale 4-inch diameter surface figure measurement has not been performed yet. The full aperture measurement of surface figure will be performed by using a Michelson Interferometer.

The wafer transfer technique demonstrated in this paper has the following benefits over those previously reported: 1) No post-assembly release process is required. (e.g. No sacrificial layer is used for the transfer purpose.) 2) The bonded interface is completely isolated from any acid, etchant, or solvent during the transfer process, ensuring a clean and uniform membrane surface. 3) It offers the capability of transferring multi-layer wafer-scale membranes onto actuators.

C. SIGNIFICANCE OF EXPECTED RESULTS

We have demonstrated a wafer-scale membrane transfer process technique by transferring a 10 μm thick single-crystal silicon membrane as a whole from a separate silicon substrate.

The membrane transfer technique, if successfully developed, will provide the critical technology complement for a compact deformable mirror technology meeting the requirements for the optical surface figure and the mechanical compliance. The specific advantage of the proposed technology is that an optical-quality membrane can be transferred onto various substrates/actuators with different volume and mass. Therefore the development of a MEMS-based deformable mirror in combination with various actuator technologies would be the next

step in order to provide a wide range of applications within the Space Science and Earth Science Enterprises.

D. FINANCIAL STATUS

The total funding for this task was $125,000, of which $16,000 has been expended. The remaining funding will be expended for further transfer and test experiments. Several membranes with different thickness will be transferred and tested. The transferred membranes will be characterized with a full aperture measurement, which allows for either interferometry or a wavefront sensing measurement.

E. PERSONNEL

No other personnel were involved.

F. PUBLICATIONS

E. H. Yang, "A Wafer Transfer Technology for MEMS Adaptive Optics," CfAO MEMS Workshop, CfAO, UC Berkeley, Feb. 2002.
(Other task results will be written up for publication soon.)

G. REFERENCES

[1] R. Dekany, S. Padin, E. H. Yang and M. Troy, "Advanced Segmented Silicon Space Telescopes (ASSiST)," SPIE International symposium on Astronomical Telescopes and Instrumentation, Adaptive Optical System Technologies II, 22-28 August 2002, Waikoloa, Hawaii, USA.
[2] M. A. Ealey and J. F. Washeba, "Continuous Face Sheet Low Voltage Deformable Mirrors," *Optical Eng.,* (29) p.1191, Oct. 1990.

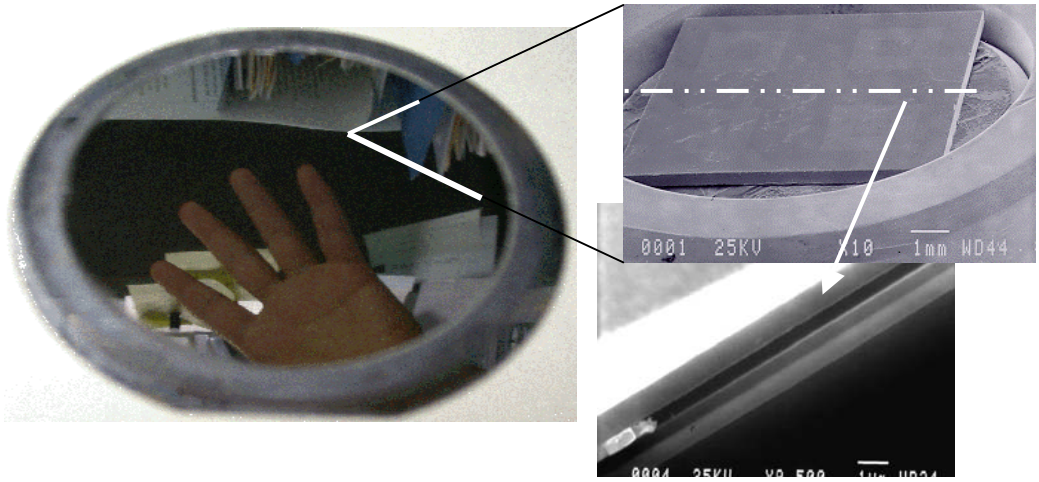

Fig.1 Transferred membrane with 4 inches in diameter.

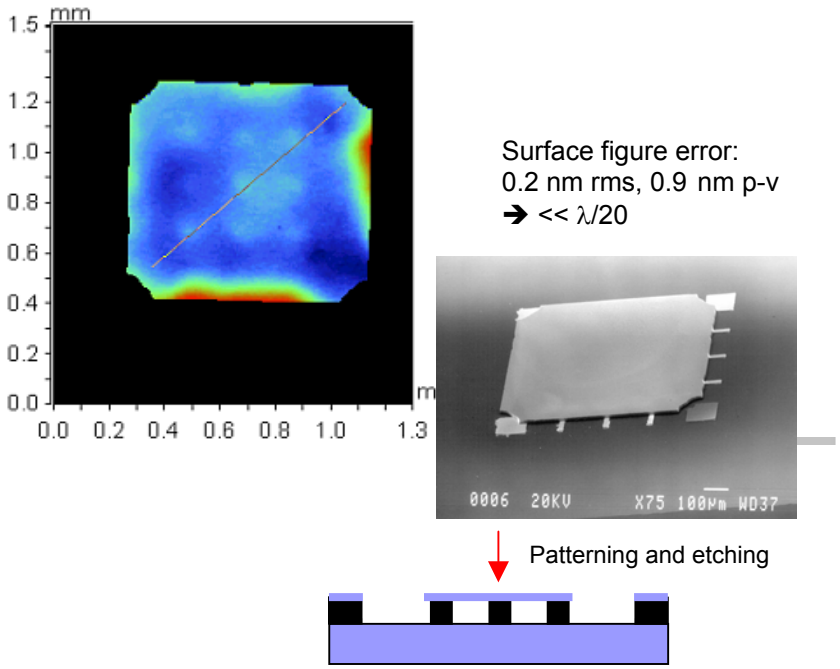

Fig. 2 Surface figure of a patterned single crystal silicon membrane (wafer-scale transferred and patterned). The surface figure error was 9 nm P-V for this sample.

ULTRA-LIGHTWEIGHT OPTICAL COLLECTOR USING IN-SPACE BUBBLE BLOWING AND METAL EVAPORATION TECHNOLOGIES

Final Report

JPL Task 1038

Yu Wang, (Section 387)

A. OBJECTIVES

An ultra-lightweight optical collector is very desirable for NASA's space missions. A collector can concentrate light to reduce the size of a spacecraft's solar cell panels, can be used for a big-aperture space telescope to acquire high resolution images, and can be used for big-diameter antennas to increase sensitivity and lower required power.

This task was aimed at studying the feasibility of a lightweight optical collector using in-space bubble blowing and metal evaporation technologies.

B. PROGRESS AND RESULTS

When we blow a soap bubble on earth, the soap bubble forms a very light sphere. But the size of the bubble is limited due to gravity. If we blow a bubble in space, the bubble can have an almost perfectly spherical shape and can grow very big, because there is no gravity. And such a spherical film is just what we need for optical collectors. Because space is a vacuum environment, we can then deposit metal coatings upon the spherical film to make an optical collector.

If we blow a free bubble in space, the bubble will have a spherical shape. Theoretical calculations show that the shape of the free bubble would change by applying an electrical field. Depending on the strength of the surface tension and the electrical field, the shape of the bubble can be either an ellipsoid or an elliptic paraboloid. The elliptic paraboloid is more desirable for space telescopes.

Several bubbles were blown using UV-curable epoxy. The epoxy was mixed with a commercially available surfactant and UV-curing agent, and then heated to eliminate gas bubbles formed during mixing. A small bubble was formed in a dish and then transferred to a ring support and pressurized to increase its size. Once exposed to UV, the epoxy cured and half the bubble was removed, leaving a spherical segment ready for metallization. These bubbles were then put in a vacuum chamber with a vacuum of $1x10^{-5}$, and coated with silver coating using thermal evaporation. Early depositions showed a lot of wrinkles around the edges of the coated bubbles. They indicated that different thermal expansion of the epoxy and the ring support was the problem. Later we reduced

the evaporation rate, the deposition temperature became lower, and a very smooth bubble light collector was fabricated (see figure below).

The bubble light collector has a diameter of about two inches. It shows a shiny smooth semi-spherical surface almost everywhere except around the edges. There are still some small wrinkles around the edges. In space, we don't need an edge support for the bubble. So if we blow a free bubble in space, we will be able to have a smooth bubble light collector without wrinkles.

To blow a bubble in space, we need to find the proper materials. The epoxy we used got boiled in vacuum, and it cannot be used in space. We have tried several materials, including liquid crystals, commercial glues, and several oils. Some of them could stay in vacuum more than 48 hours without noticeable evaporation loss. These materials can be used in a future bubble light collector.

C. SIGNIFICATION OF RESULTS

This task developed a prototype of a bubble light collector, a two-inch diameter bubble which was blown and deposited with silver coating. The bubble light collector showed a smooth surface.

The results indicate that this bubble light collector technology is feasible. This technology can be used as a light collector to reduce the size of solar cell panels and supply more electrical energy for a spacecraft, for big-aperture space telescopes to acquire high-resolution images, and for big-diameter antennas to increase the sensitivity and lower the required power.

D. FINANCIAL STATUS

The total funding for this task was $30,000, all of which has been expended.

E. PERSONNEL

Experimental work was done with the cooperation of Jennifer Dooley, Mark Dragovan, and Wally Scrivens.

F. PUBLICATIONS

A NTR was filed (NPO-30649), and will be published in *NASA Tech. Brief.*

ASTROBIOLOGY

MECHANISMS OF RESISTANCE TO HYDROGEN PEROXIDE IN MICROBES ISOLATED FROM A JPL SPACECRAFT ASSEMBLY FACILITY

Final Report

JPL Task 964

Kasthuri Venkateswaran, Biotechnology and Planetary Protection (3544)
Michael J. Kempf, Biotechnology and Planetary Protection (3544)

A. OBJECTIVES

Both NASA and CNES have been actively researching the use of hydrogen peroxide (H_2O_2) vapor as a chemical sterilant. The lack of carbon and relatively low temperature of application make it compatible with both life-detection experiments and general electronics. JPL's Planetary Protection Technologies Group has recently discovered that spores resistant to H_2O_2 can be readily found in spacecraft assembly facilities. Rather than redirect current sterilization efforts upon which considerable resources have been spent, we propose to study further the nature of the H_2O_2 resistance in these organisms to enable the purposeful modification of the existing approach with minimal cost and disruption. Low levels of resistance to this chemical treatment are generally associated with surface enzymes, in contrast to heat and radiation resistance, which are associated with specific molecules buried deep within the spore. By studying the biochemistry of high level H_2O_2 resistance and demonstrating its localization on the spore surface, benign strategies for inactivating this specific resistance can be investigated. At this stage in the development of the sterilization procedure, it may be possible to introduce a benign modification to the existing procedure.

- Hydrogen peroxide resistant strains, which are related to *Bacillus pumilus*, were repeatedly isolated from various locations in the JPL spacecraft assembly facility (SAF).
- These strains were found in both unclassified (entrance floors, anteroom, and air lock) and classified (class 100K) (floors, cabinet tops, and air) areas.
- The vegetative cells of 3 *B. pumilus* strains were resistant to vapor H_2O_2 whereas the *B. pumilus* type strain (ATCC 7061^T) was susceptible. In addition to the vapor H_2O_2, the vegetative cells of one of the SAF isolates (FO-036b) showed resistance to 5% liquid H_2O_2. Likewise, the purified spores of the FO-036b strain showed a great degree of resistance when compared to the spores of the *B. pumilus* type strain.
- Twenty-four proteins were isolated from purified spores and N-terminal amino acid sequences were determined. Some proteins that are unique to the hydrogen peroxide resistant spores were observed.

B. PROGRESS AND RESULTS

Task #1: Identification of hydrogen peroxide resistant microbes to the species level: A commercially available microbial identification system (BioLog Inc., Edward, CA) was used to identify the microbes. Fatty acid methyl ester (FAME) profiles were examined as described previously (Ringelberg *et al*., 1994). 16S rDNA sequence analysis was used to determine the phylogenetic affiliations of the microbes, as per protocols established by Ruimy *et al*. (1994). DNA-DNA hybridization was carried out as previously described (Satomi *et al*., 1997).

Based on the BioLog database, all 13 strains were characterized to the genus level and presumptively identified as *Bacillus* sp. FAME analysis identified these strains to the genus *Bacillus*. Among 7 strains identified to the species level, 3 strains were identified as *B. pumilus* (FO-033, FO-038, SAFN-001), 2 as *B. subtilis* (SAFN-027, SAFN-034) and one each as *B. amyloliquefaciens* (KL-052) and *B. thermoglucosidasius* (SAFN-036).

Variations in the 16S rDNA sequence similarities among 11 *B. pumilus* strains were negligible. This grouping was drawn on the basis of their proximity to the ATCC type strain (*B. pumilus* ATCC 7061^T). The 12 *B. pumilus* strains, including the type strain, were heterogeneous in their *gyrB* sequence (91 to 100% similarities) and appeared to form 4 clusters (data not shown). It is interesting to note that all of these strains were isolated from 3 different sampling periods and from various locations of a JPL-SAF (Building 179 High Bay-1). The speciation delineated by 16S rDNA sequence analysis could not differentiate *B. pumilus* at the species level. However, *gyrB* sequence analysis was useful in clustering the isolates into 2 groups. Strains isolated from clean-room air particles, floors, cabinet tops, anteroom, and the entrance room floor of the JPL-SAF formed one group, where the *gyrB* sequence similarities were over 98%. The 3 strains isolated from the air-lock of this facility, together with the type strain ATCC 7061^T, formed a second group. This second group showed only 92% similarity in their *gyrB* sequences with the strains of the first group, but these 3 strains were closely related to the ATCC type strain 7061^T (98% similarity).

Task #2: Comparison of the wild SAF strains vs. the *B. pumilus* type strain (ATCC 7061^T) for H_2O_2 resistance: Spores ($2x10^7$ per metal coupon) of FO-036b were seeded onto test strips of spacecraft qualified metals, such as Aluminum 6061 and Titanium 4Al-6V, and subjected to vapor H_2O_2 sterilization to check for spore survivability. The percentage of spores that survived after vapor H_2O_2 sterilization was determined by standard plate count assays. About 1% and 0.5% of the spores, on Aluminum 6061 and Titanium 4Al-6V, respectively, survived H_2O_2 sterilization (16 mg/L H_2O_2 vapor). The vegetative cells of *B. pumilus* (strains FO-033, FO-036b, FO-038) were also resistant to vapor H_2O_2 whereas the *B. pumilus* type strain (ATCC 7061^T) was susceptible. In addition to vapor H_2O_2, a liquid hydrogen peroxide protocol was used (Riesenman and Nicholson, 2000). Vegetative cells of 13 strains (2 ATCC strains [*B. pumilus* ATCC 7061^T, *B. pumilus* ATCC 27142] and 11 isolates [FO-033, FO-036b, FO-038, KL-052, SAFN-001, SAFN-027, SAFN-029, SAFN-034, SAFN-036, SAFN-037, and SAFR-032]) were subjected to 5% liquid hydrogen peroxide exposure. The only strain whose cells showed growth was FO-036b. Spores of 14 strains (2 *B. subtilis* strains [168 and PY79], 2 ATCC strains [*B. pumilus* ATCC 7061^T, *B. pumilus* ATCC 27142] and 10 SAF isolates [FO-033, FO-036b, FO-038, KL-052, SAFN-001, SAFN-027, SAFN-029, SAFN-036, SAFN-037, and SAFR-032]) were subjected to 60 minutes of exposure to 5% liquid hydrogen peroxide at room temperature. The *B. subtilis* spores showed 3-5 log reduction and the *B. pumilus* spores showed 5-6 log reduction. In contrast, the spores of the SAF isolates showed varying ranges between 0-5 log reduction. Spores of SAFR-032, SAFN-037, SAFN-001, FO-036b, FO-033, SAFN-027, and KL-052 all showed less than 2 log reduction after exposure to 5% liquid hydrogen peroxide. Spores of SAFN-029, SAFN-036, and FO-038 all showed greater than 3 log reduction after exposure to 5% liquid hydrogen peroxide. In addition, a quantitative liquid hydrogen peroxide resistance assay was performed on 5 strains. The percent survival of these strains was: 6.5% (SAFR-032), 8.8% (SAFN-037), 9.0% (FO-036b), 0.5% (KL-052), and 4.2% (*B. subtilis* 168).

Task #3: Sporulation of H_2O_2 resistant and susceptible microbes: We have successfully produced and purified spores from 19 out of 20 strains as per the Nicholson (2001) protocol. They are: *B. subtilis* (168, ATCC 6633, PY79); *B. pumilus* (ATCC 7061^T, ATCC 27142); *B. megaterium* (KL-197); *B. cereus* (JCM 1252); *B. thuringiensis* (IAM 12077); *B. nealsonii* (FO-092); and 10 of 11 SAF isolates (SAFR-032, SAFN-029, SAFN-037, SAFN-036, SAFN-001, FO-036b, FO-033, FO-038, SAFN-027, and KL-052). Phase contrast and electron microscopy were used to characterize the spore morphology of some of these spores. The spores were cross-sectioned further to learn the differences in the architecture of the spore coat layers. A wild strain from SAF (FO-036b) exhibited an "undulated inner spore coat" when compared to the smooth inner coat organization seen in a H_2O_2 susceptible strain (FO-092, not shown) and a UV radiation resistant strain (PY79).

Task #4: Nucleotide sequence of catalase gene: The nucleotide sequences of catalase genes (*katA*, *katB*, and *katE*) from 4 different *Bacillus* species were downloaded from public databases (http://www.ncbi.nlm.nih.gov/) and aligned to identify sequence similarities. The *B. subtilis katA* gene aligned with both the *B. subtilis* vegetative catalase gene and the *B. stearothermophilus* catalase genes. The *B. subtilis katB* and *katE* genes aligned with each other. The *B. stearothermophilus* catalase genes aligned to each other and *B. subtilis katA*, but not with the *B. subtilis katB*/*katE* genes. The *B. firmus* and *B. halodurans* catalase genes did not align with each other or any of the above catalase genes. Based on the alignments, it was determined that the *B. subtilis katA* gene would be the best template in order to design primers for the PCR amplification of the catalase gene(s) from *B. pumilus*.

One set of primers specific for the *katA* gene was designed. These primers were used to attempt to amplify the catalase gene(s) from the genomic DNA of *B. pumilus* ATCC 7061^T, *B. pumilus* ATCC 27142, and FO-036b. *B. subtilis* 168 chromosomal DNA was the template for the positive control PCR. The PCR products were purified by Qiagen column purification and cloned into the pCR4-TOPO plasmid (Invitrogen, Carlsbad, CA). The cloned product was 450-bp in length from *B. pumilus* ATCC 27142. The sequence reads of *B. pumilus* ATCC 7061^T and FO-036b were poor and no conclusive evidence was obtained. The translated amino acid sequences of *B. pumilus* ATCC 27142 were compared to the *B. subtilis* genome and the best hit was to a hypothetical protein, YugU, (66% identity over 129 residues) whose function is not known.

Task #5: Isolation of catalase-deficient mutants: As spores did not possess catalase, we tried to isolate the enzyme from the wild and type strains of *B. pumilus* vegetative cells. As reported in Task #4, we were able to clone this fragment only from ATCC 27142. Furthermore, we learned during the progress of the task that the catalase enzyme is involved in the vegetative cells, and proteins might be responsible for resistance to H_2O_2 in spores. Hence, the focus of the research shifted to develop a protocol to isolate the spore proteins. In addition to the isolation of proteins from spores, we further characterized the spore proteins.

Task #6: Development of a protocol to isolate the inner layer of the spore protein: Several protocols have been identified that will allow us to isolate the spore coat proteins. These protocols use various detergents, alkaline agents, and/or reducing agents and physical means (homogenization, French press) to extract the spore coat proteins (Nicholson and Setlow, 1990). In addition to the isolation of the spore coat, we developed analytical methods to successfully separate the proteins present in the sample for further analysis and characterization. We have

utilized a two-dimensional (2-D) gel electrophoresis system (BioRad, Hercules, CA) to analyze spore proteins from 3 different *Bacillus* species (Fig. 1).

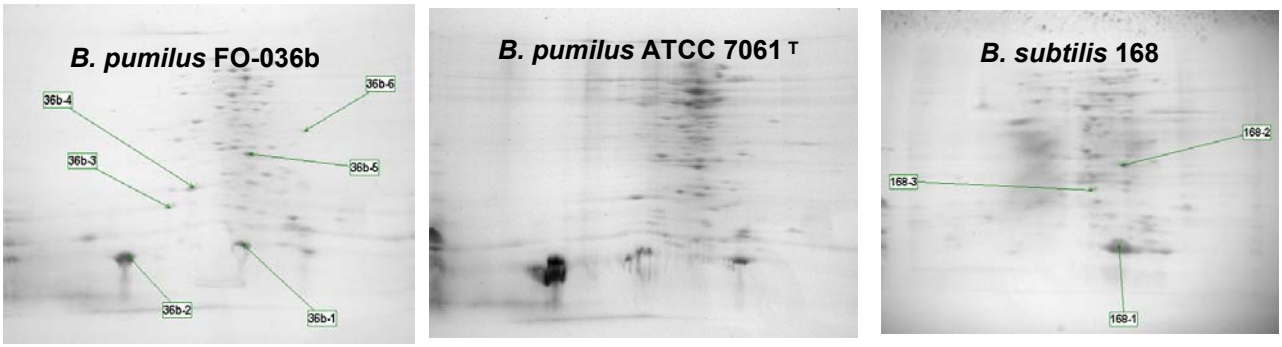

Fig. 1. Photomicrographs showing the 2-D gel electrophoresis results of the spore protein isolation experiments.

Proteins were isolated from purified spores of FO-036b, *B. pumilus* ATCC 7061^T, and *B. subtilis* 168 using a buffer containing urea, CHAPS, DTT, and ampholytes (BioRad, Hercules, CA). The isolated proteins were subjected to two-dimensional gel electrophoresis and analyzed. Several unique proteins that are found in hydrogen peroxide resistant species, but not in susceptible strains of the same species, were identified and purified. Twenty-three proteins from 3 strains (FO-036b, *B. pumilus* ATCC 7061^T, and *B. subtilis* 168) were picked, and the N-terminal amino acid sequences were determined at the Protein/Peptide Micro Analytical Laboratory at the California Institute of Technology. There were 3 proteins from *B. subtilis* 168, 4 proteins from *B. pumilus* ATCC 7061^T and 16 proteins from FO-036b. When compared to the *B. subtilis* 168 genome, 22 of 24 proteins and 7 of 24 proteins exhibited >60% and >90% amino acid identity, respectively. One protein (17 residues) of FO-036b spores did not show any homology to any of the proteins in the fully-sequenced *B. subtilis* 168 genome. The function of this protein in the resistant strain needs to be studied. It has been documented that small acid-soluble proteins (SASPs) are involved in various resistance properties such as dry heat, desiccation, hydrogen peroxide, UV and gamma radiation (Setlow, 1995). Among the identified proteins, the isolation of 2 proteins from FO-036b that have high similarity to the SASP β-subunit protein of *B. subtilis* 168 is interesting. Although another protein similar to the SASP β-subunit protein of FO-036b strain (~89%) was isolated from *B. pumilus* ATCC 7061^T, its expression levels in both the susceptible strain, *B. pumilus* ATCC 7061^T, and the hydrogen peroxide resistant strain, FO-036b, needs to be explored.

C. SIGNIFICANCE OF RESULTS

The results indicate that we have repeatedly isolated H_2O_2 resistant strains, which are related to a *B. pumilus* strain, FO-036b, from various locations of a JPL-SAF. These strains were found in both unclassified (entrance floors, anteroom, and air lock) and classified (class 100K)

(floors, cabinet tops, and air) areas (Kempf *et al*., 2001). The recurrence of a microbial species that is related to a hydrogen peroxide resistant microbe might have significant implications for the assembly of flight hardware at JPL. The isolation of unique proteins from the hydrogen peroxide resistant FO-036b strain that are not found in the susceptible type strain might relate to the resistance properties.

D. FINANCIAL STATUS

The total funding for this task was $150,000, all of which has been expended.

E. PERSONNEL

Greg Kuhlman assisted in performing the 2-D gel electrophoresis of the spore proteins and the protein sequencing.

F. PUBLICATIONS

1. K. Venkateswaran,, C. Echeverria, S. Chung, and C. Basic, "Characterization of Extremophiles Isolated From Spacecraft Assembly Facility," *Eos, Transactions, American Geophysical Union*, Vol. 81 (48), 2000, p. F199. San Francisco, CA.
2. M. J.Kempf, , F. Chen, M. S. Quigley, R. Kern, and K. Venkateswaran, "Recurrence of Hydrogen Peroxide Resistant Microbes From Spacecraft Assembly Facilities," *Proc. of the American Geophysical Union*, 2001, San Francisco, CA, Dec. 10-14.
3. M. J. Kempf,, G. M. Kuhlman, R. Kern, and K. Venkateswaran, "A Proteomics Approach to Analyze Hydrogen Peroxide Resistant *Bacillus pumilus* Spores Isolated From a Spacecraft Assembly Facility," American Society for Microbiology General Meeting, 2002, Salt Lake City, UT, May 19-23.
4. M. J. Kempf,, F. Chen, M. S. Quigley, M. Satomi, R. Kern, and K. Venkateswaran, "Recurrence of Hydrogen Peroxide Resistant Microbes From Spacecraft Assembly Facilities," *Environ. Microbiol.* (in preparation).
5. G.M. Kuhlman,, M. Kempf, and K. Venkateswaran, "Protein Characterization of Hydrogen Peroxide Resistant Spores Isolated From Spacecraft Assembly Facilities," *FEMS Microbiol. Ecol.* (in preparation).

G. REFERENCES

1. A. Driks, S. Roels, B. Beall, C. P. Moran, Jr., and R. Losick, "Subcellular Localization of Proteins Involved in the Assembly of the Spore Coat of *Bacillus subtilis,*" *Genes and Development*, 8, 1994, 234-244.
2. M. J. Kempf, F. Chen, M. S. Quigley, R. Kern, and K. Venkateswaran, "Recurrence of Hydrogen Peroxide Resistant Microbes from Spacecraft Assembly Facilities," American Geophysical Union, Dec. 10-14, 2001, San Francisco, CA.
3. W. L. Nicholson, and P. Setlow, "Sporulation, Germination, and Outgrowth," *Molecular Biological Methods for Bacillus*, John Wiley & Sons, Chichester, England, 1990, 391-450.

4. W. L. Nicholson, Personal communication, 2001.
5. P. J. Riesenman, and W. L. Nicholson, "Role of the Spore Coat Layers in *Bacillus subtilis* Resistance to Hydrogen Peroxide, Artificial UV-C, UV-B, and Solar Radiation," *Applied and Environmental Microbiology*, 66**,** 2000, 620-626.
6. D. B. Ringelberg, G. T. Townsend, K. A. DeWeerd, J. M. Suflita, and D. C. White, "Detection of the Anaerobic Dechlorinating Microorganism *Desulfomonile tiedjei* in Environmental Matrices by its Signature Lipopolysaccharide Branched-Long-Chain Hydroxy Fatty Acids," *FEMS Microbiology Ecology*, 14**,** 1994, 9-18.
7. R. Ruimy, V. Breittmayer, P. ElBaze, B. Lafay, O. Boussemart, M. Gauthier, and R. Christen, "Phylogenic Analysis and Assessment of the Genera *Vibrio, Photobacterium, Aeromonas,* and *Plesiomonas* Deduced From Small Subunit rRNA Sequences," *International Journal of Systemic Bacteriology*, 44, 1994, 416-426.
8. M. Satomi, B. Kimura, M. Mizoi, T. Sato, and T. Fujii, "*Tetragenococcus muriaticus* sp. nov., a New Moderately Halophilic Lactic Acid Bacterium Isolated From Fermented Squid Liver Sauce," *International Journal of Systemic Bacteriology*, 47, 1997, 832-836.
9. P. Setlow, "Mechanisms for the Prevention of Damage to DNA in Spores of *Bacillus* Species," *Annual Reviews of Microbiology* 49, 1995, 29-54.
10. E. Stackebrandt, and B. M. Goebel, "A Place for DNA-DNA Reassociation and 16S rRNA Sequence Analysis in the Present Species Definition in Bacteriology," *International Journal of Systemic Bacteriology*, 44, 1994, 846-849.
11. L. Wayne, D. J. Brenner, R. R. Colwell, P. A. D. Grimont, O. Kandler, M. I. Krichevsky, L. H. Moore, W. E. C. Moore, R. G. E. Murray, E. Stackebrandt, M. P. Starr, H. G. Truper, "International Committee on Systematic Bacteriology: Report of the Ad Hoc Committee on Reconciliation of Approaches to Bacterial Systematics," *International Journal of Systemic Bacteriology*, 37, 1987, 463-464.
12. P. Youngman, J. B. Perkins, and R. Losick, "Construction of a Cloning Site Near One End of Tn*917* Into Which Foreign DNA May Be Inserted Without Affecting Transposition in *Bacillus subtilis* or Expression of the Transposon-Borne *erm* Gene," *Plasmid*, 12, 1984, 1-9.

A NOVEL INVESTIGATION ON BIOTIC AND ABIOTIC MOLECULES IN AN ICE MATRIX UNDER ENERGETIC CONDITIONS

Final Report

JPL Task 978

Isik Kanik (Instrument Development and Spectroscopy Research Element-3264)

A. OBJECTIVES

The objective of this one-year proposal was to demonstrate the scientific utility of an experiment which will allow for a better understanding of the chemical makeup of the ice-covered surfaces of planetary bodies. This includes at least part of the surface of each satellite of the gas giants, with a primary focus on surface conditions approximating Europa. Since no experimental set up would be able to simulate the actual conditions entirely (i.e. high-radiation environment by energetic particles such as electrons, photons, and ions; chemical composition, etc.) which are present on the surfaces of these bodies, especially on Europa, we proposed to perform a series of simple experiments to better understand the chemical processes taking place on these surfaces in such intense radiation environments. The objective was to freeze different amino acids at various temperatures (10K and 90K) in an H_2O ice matrix and perform spectroscopic measurements (i.e. reflectance measurements) before and after we bombard the ice surface with energetic particles. The concentrations (~1 organic molecule for 10,000 H_2O molecules), which are probably several orders of magnitude higher than one would expect to find on planetary surfaces, should result in very little amino acid-amino acid interactions. At the same time, they are expected to yield enough intensities to be identified spectroscopically.

Two different spectroscopic methods, Laser Raman and UV/VIS reflectance spectroscopy, were planned to be utilized to monitor the alteration of organic molecules so that complete spectral coverage could be obtained. Laser Raman was chosen because of its known utility in several applications and because it has been identified as a prime candidate for the 2009 Mars Science Laboratory (MLS) mission. UV/VIS reflectance spectroscopy (in the 110 nm to 700 nm wavelength range) was chosen because of its inclusion as part of most current and future missions. Finally, the lifetimes of the amino acids were planned to be determined by calculating the incident influx of radiation on the sample, and comparing the altered and unaltered material over various time intervals.

B. PROGRESS AND RESULTS

As mentioned earlier, the experiment was designed to perform two different types of spectroscopic measurements: 1) UV/VIS/NIR and 2) laser Raman spectroscopy. Because this was a brand-new experimental setup, it required several months to design, purchase parts and then construct.

1) UV/VIS/NIR Experiments: We had obtained funding through the JPL EIC to purchase a monochromator and a CCD detector system. An Acton 0.39 meter, triple grating,

UV/VIS monochromator was purchased because of its ability to cover three wavelength ranges without breaking the vacuum. The Princeton Instruments CCD detector system was also purchased upon recommendation by an Acton design engineer to be used in conjunction with the monochromator. However, the CCD camera never worked correctly due to a faulty amplifier in the cryogenic part of the unit, and was sent to Princeton Instruments for repair. When the CCD was returned to us, we discovered that the CCD surface had become damaged in shipment, and thus the camera had to be returned to Princeton Instruments once again. This entire process came to a merciful conclusion in September of 2002, and the experiment instrumentation was finally in place. We have already completed the calibration process using a Hg vapor lamp (see Fig. 1). We are currently conducting experiments concerning the chemical evolution of the biotic and abiotic molecules in an ice matrix under energetic conditions, as was described in the original proposal

2) Laser Raman Experiments: While the UV/VIS apparatus was being constructed, we continued experiments on rock samples containing various amino acids with the portable laser Raman spectrometer (LRS) on loan to us from the University of Alabama at Birmingham. Fig 2 shows a spectrum of Phenylalanine as a single crystal taken with the LRS. One characteristic of the spectrometer was that while the wavelength of the features of phenylalanine crystal did not change, the relative intensities of them were dependent on the incident angle of the excitation laser. This was not expected, and caused concern for the ability of Raman to determine the quantitative amount of altered vs. unaltered material in the H_2O matrix during an experimental run. We obtained spectra of several other amino acids we had identified for use in the experiment, and the same effect was always observed.

To determine the effects of incident angle on mineralogy of samples, we obtained several dozen rock samples and attempted to determine the spectral properties of these samples. One of our objectives was to determine if there was functional dependence on incident angle when applied to rock samples. Figures 3 and 4 shows the Raman spectra of six of these samples. All the spectra were taken with 10 mW laser power and 10 sec scans. As expected, the spectra shows features clearly identifying the various rock samples. Furthermore, the relative intensities of these features were found to be independent of incident laser angle or specific spot location. To determine the ability to identify small concentrations of material, we attempted to do some Martian analog material (partially in conjunction with a Mars SCOUT proposal on which we were listed as Co-I's). We could unambiguously identify both crushed calcite and dolomite minerals when they were mixed with palagonite at the 10% level. Furthermore, we were able to identify calcite and dolomite in a mixture (Fig 5.)

Because we were getting outstanding mineralogical data from the LRS, we attempted to identify amino acids frozen in an H_2O matrix. Much to our surprise, no matter how we arranged the frozen mixture we never were able to obtain spectra of the amino acids. These attempts included a few % of both alanine and phenylalanine in both liquid and water ice. This was most likely due to the nature of H_2O and the incident laser wavelength. For example, in rock samples the incident radiation and the Raman excitation light come from the same spot on the surface, due to the opacity of the material. Therefore, focusing of the scattered Raman signal is not a problem. In water ice this is not the case, primarily due to the transparency of the material. Both the incident and excitation light can penetrate the sample, making detection of the Raman signal (which is on the order of 10^{-9} times less intense than the excitation signal) impossible.

C. SIGNIFICANCE OF RESULTS

The results of the LRS study are quite profound in terms of future use as an *in-situ* explorer. With minimal sample preparation, a small LRS can identify mineralogy in a very short time interval (usually less than a minute). This can happen even on different crushed minerals in a sand-type mixture if point counting is used. However, the identification of individual amino acids, especially in an ice matrix of some sort, is impossible. This has implications for an astrobiology-focused mission. If Raman spectroscopy is to be done for the goal of caching samples for later return to earth, the identification of Anthracite coal (See fig 4) with both graphitic and disordered carbon features might be all that is necessary to identify interesting samples (Schopf et al. 2001). However, individual organic components of a sample would need quite a bit of sample preparation before any data could be obtained from a sample. This would include doing surfaced enhanced Raman spectroscopy (SER), or pre-separation of material prior to identification.

Our experimental results regarding LRS measurements also resulted in our involvement in a $350 million JPL Mars SCOUT proposal which was recently submitted to NASA, A DRDF proposal submitted for FY03 funding, and a ASTEP proposal which will be submitted in May of 2003.

D. FINANCIAL STATUS

The total funding for this task was $145,000, all of which has been expended.

E. OTHER PERSONNEL

Dr. Luther Beegle (3264)
Dr. Sandor Trajmar (3264; on-call)
Prof. Thomas J. Wdowiak (UAB)
Prof. David Agresti (UAB
Prof. Perry Gerikines (UAB)
Dr. Charles Terrell (3264)
Dr. Yuk Yung (Caltech)

F. PUBLICATIONS AND PRESENTATIONS

[1] L.W. Beegle, I. Kanik and T. J. Wdowiak, "Laser Raman Spectroscopy of Mineralogical Samples From an Astrobiological Perspective," to be presented at the 34th Annual Lunar and Planetary Science Conference, Houston TX, March 2003.

G. REFERENCES

[1] J.W. Schopf, et al., *Nature* **416** 73, 2002

H. APPENDIX: FIGURES

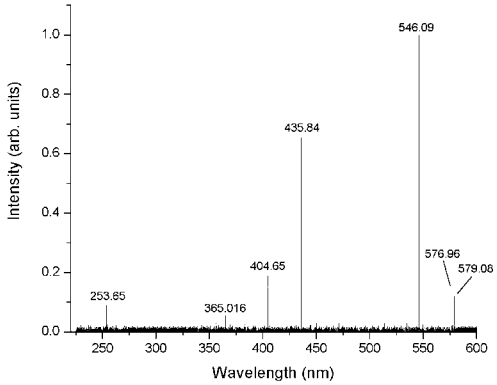

Fig. 1 Mercury lamp spectrum taken through one of the glass-windowed ports on the Ice Experiment chamber. Spectrometer slit width = 25 µm, 1200 gr/mm gratings, CCD exposure time = 0.1 s, CCD temperature = -20 ºC. Spectrum was normalized to the peak at 546.09 nm.

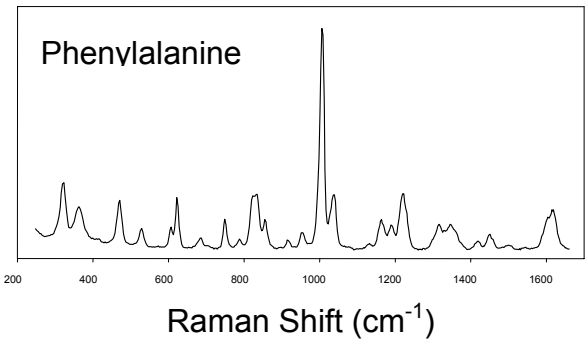

Fig 2 Phenylalanine take with the portable LRS. 10 mW laser operating power and a 10 sec. scan time.

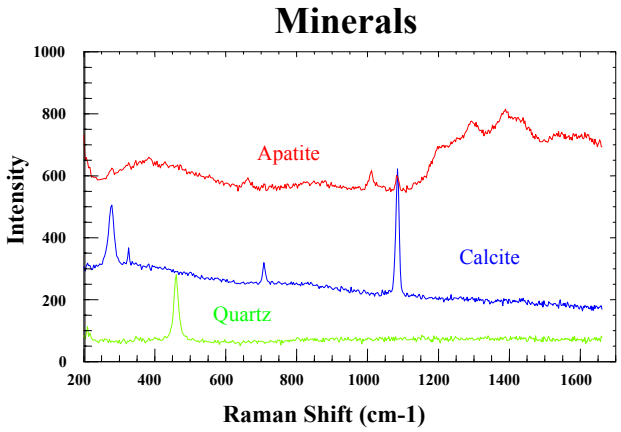

Fig 3 Laser Raman Spectra of three minerals, Apatite, Calcite and Quartz. Each spectra took 10 seconds of scan time on an unprepared surface.

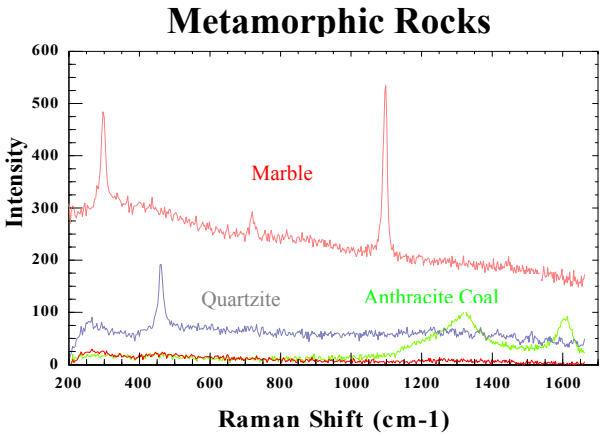

Fig 4 Laser Raman Spectra of three metamorphic rocks, Marble, Quartzite and Anthracite coal. Each spectra took 10 seconds of scan time on an unprepared surface.

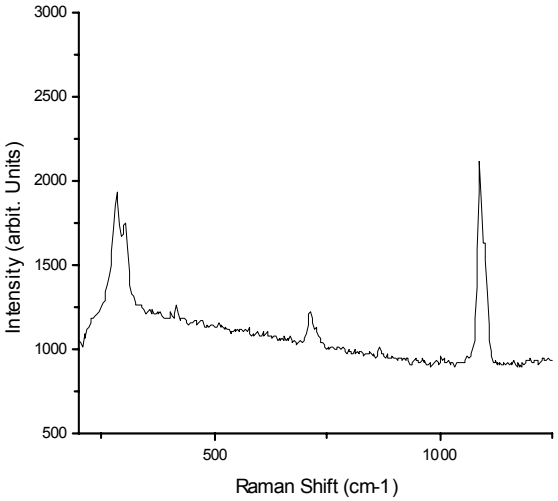

Fig 5 A laser Raman Spectra of a mixture of Calcite and Dolomite. The two minerals have a clearly distinguishable feature located at ~300 cm^{-1}

ORGANIC ENVIRONMENTS IN THE OUTER SOLAR SYSTEM

Final Report

JPL Task 1006

Patricia M. Beauchamp, JPL In-Situ Exploration and Sample Return Center of Excellence (303)
(Principal Investigator)
Jonathan I. Lunine, University of Arizona (University Lead Investigator)
Jesse L. Beauchamp, Department of Chemistry, California Institute of Technology
Dennis A. Dougherty, Department of Chemistry, California Institute of Technology
Mark Smith, Department of Chemistry, University of Arizona

A. OBJECTIVES

The aims of the project were (a) to set up simulations of the production of Titan tholins as raw material for the exploration of analysis techniques and ultimately (in follow-on projects) to examine the chemistry of the aqueous alteration of Titan organics, (b) to examine impact crater environments in which liquid water might form and become admixed with chiral molecules (by computer simulation) and (c) to develop sensitive and novel approaches to the identification and characterization of chiral molecules in organic phases.

B. PROGRESS AND RESULTS

Major results include:

1. Detailed NMR and mass spectrometric data on synthetic products of Titan organic chemistry
2. Detailed numerical hydrodynamic models of the formation of craters on Titan, with the consequent mixing of organic molecules and liquid water
3. First quantitative application of piezoelectric and fluorescence detection techniques for determination of enantiomeric composition and chiral molecules.

Tholin production and initial analysis - Tholins, the complex organic precipitates originating from Titan's stratospheric aerosol layers, form the feedstock for any significant complex organic chemistry at the surface level. We have recently obtained detailed NMR and mass spectral data on the *nonvolatile* tholin fractions generated by plasma sources, that sheds new light on these polymer mixtures. The apparatus for plasma-generated tholins has been modified to allow minimal plasma processing of nascent tholin aerosols produced in the low-temperature gas mixtures. In particular, surface exposure to energetic particles and species capable of tholin processing or contaminant participation in tholin generation is carefully minimized. In addition, this apparatus has been constructed in a way that allows for comparative

photolytic tholin generation using the output of VUV resonance discharge lamps of high light throughput, and for general selection of average photon energy through lamp selection and thus variance of the active species expected in the gaseous polymerization processes.

Our results suggest that these mixtures are entirely aliphatic, contain little aromatic component, and are comprised of predominantly saturated aliphatic hydrocarbon polymer containing significant free amino, imino and nitrile functionality. Surprisingly simple and regular patterns in the molecular weight distribution of the mixtures are observed. The major components are observed to cover only narrow ranges of C/N ratio with the level of unsaturation scaling with degree of fixed nitrogen. The full range and scope of structural functionality of these mixtures, the dependence upon temperature, pressure and atmospheric composition, and preliminary results on key reaction pathways and product distributions as pertinent to Titan's surface are being explored now as the project draws to a close.

Computer simulations of formation of liquid water in impact cratering on Titan - With collaborator N. Artemieva, we conducted three-dimensional hydrodynamical simulations of hypervelocity impacts into the crust of Titan to determine the fraction of liquid water generated, under the reasonable assumption that the crust is largely water ice, and to track the fate of the organic-rich layer that is thought to overlie the ice over much of the surface. Some of our results include: (i) impactors larger than a kilometer in diameter are only slightly affected by the atmosphere, while those well under that size are strongly decelerated and broken up before reaching the surface. (ii) impact of a 2 km diameter icy projectile into the crust at velocities of 7 km per second or higher, and angles of impact between 30° and 45°, generate about 2-5% melt by volume within the crater. (iii) while much of the organic surface layer is heavily shocked and ejected from the immediate region of the crater, a significant fraction located behind the oblique impact trajectory is only lightly shocked and is deposited in the liquid water at the crater base. Simple calculations suggest that the resulting aqueous organic phase may remain liquid for hundreds of years of longer, enough time for the synthesis of simple precursor molecules to the origin of life, such as amino acids. The results are in review in *Icarus.*

Chiral analysis techniques for evolved surface organic phases - <u>Piezoelectric sensors</u>: The quartz crystal microbalance (QCM) is an extremely sensitive mass sensor, capable of measuring mass changes in the nanogram range. QCM's are piezoelectric devices, typically fabricated of a thin plate of quartz, with metal (usually gold) electrodes affixed to each side of the plate. When driven by a simple circuit, the crystal oscillates at a specific resonant frequency. The frequency of oscillation of the crystal is dependent on the mass undergoing oscillation. By attaching a foreign mass to the crystal, the change in frequency accompanying the attachment of mass can be measured. This property of the QCM can be exploited to make chemical sensors by coating the crystal with a layer that selectively adsorbs certain molecules. When the sensor is then exposed to these compounds, its mass increases in proportion to the amount of analyte adsorbed (Janata, 1989; Ali, 1999; Liang, 2002).

We have developed enantioselective coatings for QCMs based on derivatized self-assembled monolayers. Enantioselective QCMs have been reported before (Bodenhofer et al, 1997); however, these devices used bulk coatings, and their response times were on the order of minutes. The scheme for the synthesis of one of these monolayers is shown in Fig. 1. This

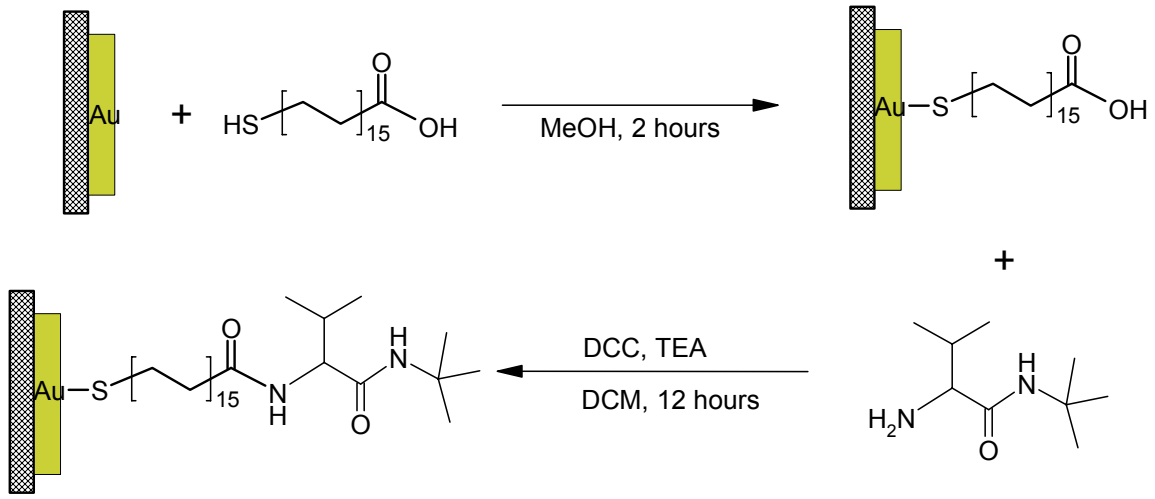

Figure 1. Synthesis of an L-valine t-butyl amide monolayer. L-valine t-butyl amide is coupled to a 16-mercaptohexadecanoic acid monolayer on gold to form a self-assembled monolayer (SAM)

monolayer is based on valine t-butyl amide as the chiral selector. This group has been used for years in chiral gas chromatography (as the Chirasil-Val stationary phase; Schreier, 1995), and has the ability to separate the enantiomers of a wide range of compounds. Fig. 2 shows the response of a crystal coated with this monolayer to the enantiomers of methyl lactate. Other experiments have developed monolayers from Boc-protected amino acids, and 3,5-dinitrobenzoyl-α-phenylglycine. The phenylglycine monolayer is expected to exhibit greater enantioselectivity than valine-based monolayers, and we are currently testing its response. Monolayer coatings show a fast response, good reversibility, and a clear enantioselectivity on exposure to analytes.

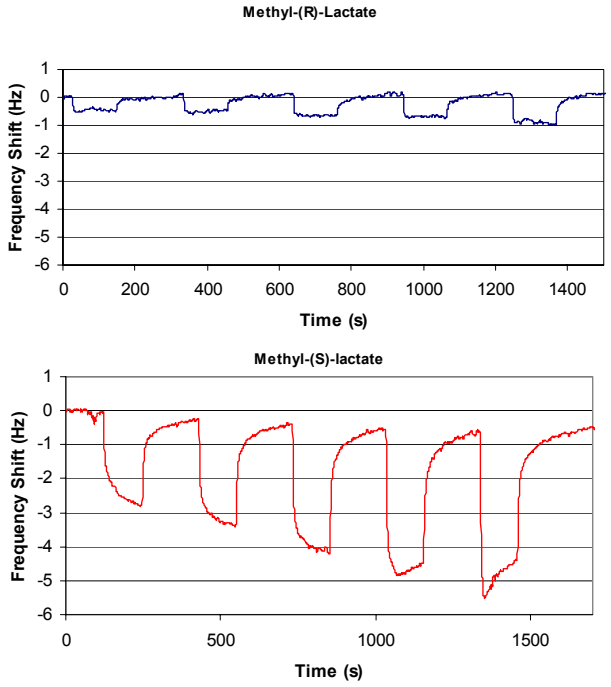

Figure 2. Response of a 15 MHz QCM to pulses of methyl lactate vapor. The sensor response to methyl-(S)-lactate is approximately 5 times greater than that of methyl-(R)-lactate. Concentrations are 16, 32, 64, 128,and 256 ppm for each.

In future work we intend to develop this technology for use as a gas chromatography detector capable of determining enantiomeric excess. The device in its final form would consist of two crystals with enantiomeric coatings. Monitoring the difference frequency between the crystals is then a measure of enantiomeric excess. Additional enantiomeric pairs would extend the range of the detector to a wider variety of analytes. We have already developed circuitry to extract the difference frequency and experimented with interfacing the QCMs to a gas chromatograph. Our initial results indicate that good temperature and gas flow control will be necessary to successfully develop a practical detection system.

We have also begun experiments with surface acoustic wave devices (SAW), piezoelectric mass sensors that operate on principles similar to QCMs. SAWs, however, operate at much higher frequencies, enabling much greater sensitivity, down to the picogram range (Levit, et al., 2002; Penza and Cassano, 2000). Our preliminary work confirms this degree of sensitivity. The enantioselective monolayers we have developed can also be applied to SAW devices, creating a more sensitive detector.

Fluorescence sensing: Our proposed fluorescence detection system was inspired by the work of Albert and Walt at Tufts University (Albert et al., 2001; Dikinson et al, 1999; Michael et al., 1998; White et al., 1996). The detector they describe is based on the differential adsorption of analyte vapors by porous, chemically-derivatized silica beads. A fluorescent, solvatochromic dye stains the beads. Solvatochromic dyes (Reichardt, 1994) undergo changes in fluorescence intensity as the polarity of their environment changes (as happens when analyte molecules are adsorbed). The beads are placed at the tip of an imaging optical fiber and excited with a Xe lamp. A CCD camera images the resulting fluorescence. By utilizing enantiomeric pairs of chirally derivatized beads, a gas-phase sensor for enantiomeric excess will be created. Such a system has a number of attractive features. The small bead size allows for a rapid response time, on the order of several hundred milliseconds. Each bead acts as an individual sensor, and imaging with a CCD allows the response of several hundred beads to be averaged, improving signal-to-noise.

Our initial work involved the synthesis of silica beads derivatized with chiral selectors, which we then stained with the solvatochromic dye Nile Red. These beads exhibited very large intensity shifts on exposure to solvent vapors. However, the beads tended to show diminishing responses after a few exposures to analytes, and did not exhibit significant selectivity with chiral analytes. Our next approach was to derivatize silica beads with a fluorescent, chiral valine selector (Fig. 3). Our approach differs from Walt's in that the fluorophore (in this case, the dansyl group (Haugland, 1998), an environmentally sensitive fluorophore) is covalently attached to the bead via the selector, instead of absorbed in the silica. We expect this to produce a more stable, robust sensor, and to increase the fluorescence response to analytes. The major difficulty with dansylated beads is that the excitation wavelength is in the UV, which causes some bleaching of the dye. We expect to overcome this difficulty with the use of longer wavelength UV from an LED. As well, we have experimented with simultaneously monitoring changes in fluorescence intensity and wavelength. Figure 4 shows changes in peak fluorescence wavelength as the beads are exposed to an analyte. By analyzing both intensity and wavelength changes, more specific responses to individual analytes are determined.

Chiral discrimination of gaseous analytes using optical transduction has been reported before, by a variety of techniques (Kieser et al., 2002; Bodenhofer et al., 1997). To our knowledge, chiral discrimination has not been reported using fluorescence sensing methodologies. We expect sensors based on this technique to be easier to implement in a space flight scenario, and more amenable to the creation of a sensory array comprising a range of different solvatochromic dyes.

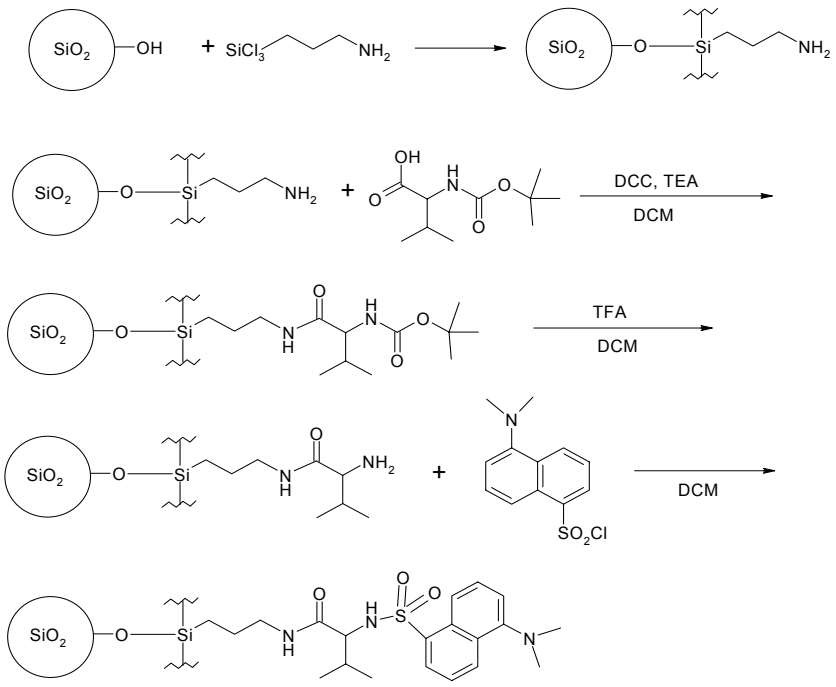

Figure 3. Derivatization of silica beads with a fluorescent chiral selector. The final step is the addition of the fluorescent dansyl

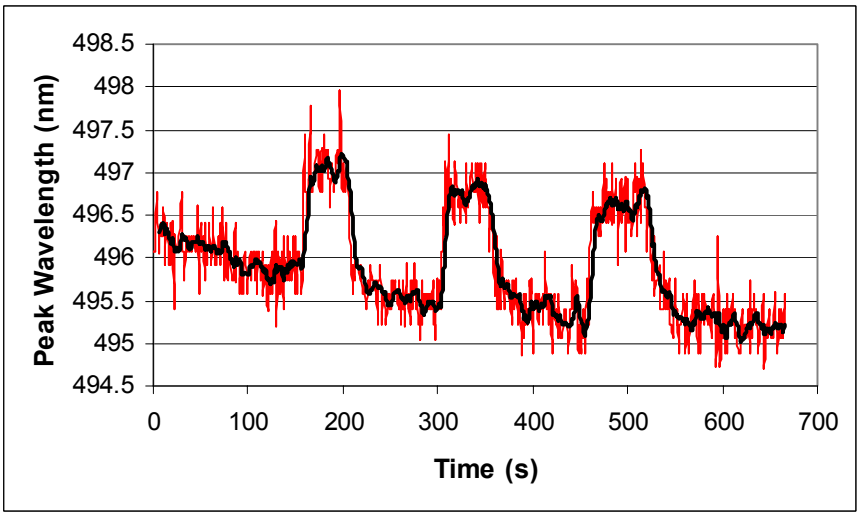

Figure 4. The response of dansyl valine-derivatized silica beads to methyl lactate vapor. The wavelength maximum of fluorescence shifts as the beads absorb methyl lactate. The black line is a 10 point running average.

C. SIGNIFICANCE OF RESULTS

The known organic environments in the solar system other than the Earth are located in the outer solar system. Those with astrobiological interest or potential are Europa, Titan and comets. Europa may contain organic compounds in a subcrustal liquid water environment, but this assumption will not be tested until after 2010. Titan is the focus of the present effort because (a) organic compounds are present on Titan's surface, protected from damaging particle and UV radiation by a thick atmosphere and (b) we should have a global spectroscopic inventory of organic molecules on the surface of Titan beginning in 2004 from Cassini-Huygens. Understanding the surface conditions of Titan from the view of chemical sources and continuing chemical dynamics is paramount to both analysis of forthcoming data from the Cassini mission and development of future probes to study extraterrestrial prebiological chemistry. The results obtained in this work are the first steps in understanding the chemistry of Titan's surface and in defining a set of instruments that could elucidate the chemical species present in a follow-on mission which would land on Titan.

D. FINANCIAL STATUS

The total funding for this task was $200,000, all of which has been expended.

E. PERSONNEL

Chris Welch, Merck Corporation,
Francois Raulin, LISA/University

F. PUBLICATIONS

(1) N. Artemieva and J. I. Lunine, "Cratering on Titan: Impact Melt, Ejecta, and the Fate of Surface Organics," *Icarus,* submitted 2002.
(2) Ryan R. Julian, Robert Hodyss, Brian Kinnear, Martin F. Jarrold, and J.L. Beauchamp, "Nanocrystalline Aggregation of Serine Detected by Electrospray Ionization Mass Spectrometry: Origin of the Stable Homochiral Gas Phase Serine Octamer," *J. Phys. Chem. B*, **106**, 1219-1228 (2002).
(3) Robert Hodyss and J. L. Beauchamp, "Quartz Crystal Microbalance Detector for Direct Enantiomeric Analysis of Chiral Molecules," *Anal. Chem*., in preparation.
(4) P. Beauchamp, J. I. Lunine, J. Beauchamp, D. Dougherty, C. Welch, M. Smith, "The Potential for Chemical Evolution on Titan," *CD-ROM Proceedings of the 2002 IEEE Aerospace Conference*, Big Sky, MT; March 9-16, 2002

Papers Presented

(1) P. Beauchamp *et al*, "Detection and Characterization in Planetary Environments of Chemistry at the Threshold of Life," *Origins of Life Gordon Conference*, Ventura, CA 2002
(2) P. Beauchamp, "From the Present to the Future of Mass Spectrometry in Space: Novel In Situ Measurements," *ASMS 17th Asilomar Conf. on Mass Spectrometry,* October 2001

(3) J. L. Lunine, "Titan and the Origin of Life," *AGU*, Dec 02
(4) J. L. Lunine, "Signs of Life," *COSPAR*, Houston Oct 02
(5) J. L. Lunine, "Other Targets for Astrobiology: From Titan to Extrasolar Giant Planets," *AAS*, Wash. DC, Jan 02.
(6) Mass Spectrometry: Solving Fundamental Problems in the Solar System, *ASMS*, Asilomar, Oct.01

G. REFERENCES

K.J. Albert, D.R.Walt, , D.S. Gill, and T.C. Pearce, "Optical Multibead Arrays for Simple and Complex Odor Discrimination," *Anal. Chem.*, 73, 2501-2508, 2001.

Z. Ali, "Acoustic Wave Mass Sensors," *Journal of Thermal Analysis and Calorimetry,* 55, 397-412, 1999.

N. Artemievaand J.I. Lunine, "Cratering on Titan: Impact Melt, Ejecta, and the Fate of Surface Organics," *Icarus*, submitted 2002.

E. Bayer, "Chiral Recognition of Natural-Products on Optically-Active Polysiloxanes," *Z. Naturforsch. B*, 38, 1281-1291, 1983.

K. Bodenhöfer, A. Hierlemann, J. Seemann, G. Gauglitz, B. Koppenhoefer, W. Göpel, "Chiral Discrimination Using Piezoelectric and Optical Gas Sensors," *Nature*, 387, 577-580, 1997.

T.A. Dikinson, K.L. Michael, J.S. Kauer, and D.R. Walt, "Convergent, Self-Encoded Bead Sensor Arrays in the Design of an Artificial Nose," *Anal. Chem.*, 71, 2192-2198, 1999.

R.P. Haugland, "Molecular Probes," *Handbook of Fluorescent Probes and Research Chemicals*, p. 40-41, Eugene, OR, 1998.

J. Janata, *Principles of Chemical Sensors* (Plenum Press, New York, 1989).

Birgit Kieser, Christopher Fietzek, Roswitha Schmidt, Georg Belge, Udo Weimar, Volker Schurig, Gunter Gauglitz, "Use of a Modified Cyclodextrin Host for the Enantioselective Detection of a Halogenated Diether as Chiral Guest Via Optical and Electrical Transducers," *Anal. Chem*.,74, 3005-3012, 2002.

Natalia Levit, Dmitry Pestov, Gary Tepper, "High Surface Area Polymer Coatings for SAW-Based Chemical Sensor Applications, *Sensors and Actuators, B: Chemical,* B82, 241-249,2002

Chengdu Liang, Ching-Yao Yuan, Robert J. Warmack, Craig E. Barnes, Sheng Dai, "Ionic Liquids: A New Class of Sensing Materials for Detection of Organic Vapors Based on the Use of a Quartz Crystal Microbalance," *Anal. Chem*., 74, 2172-2176, 2002.

K.L. Michael, L.C. Taylor, S.L. Schultz, and D.R. Walt. "Randomly Ordered Addressable High Density Optical Sensor Arrays", *Anal. Chem.*, 70, 1242-1248, 1998.

M. Penza, G. Cassano, "Relative Humidity Sensing by PVA-Coated Dual Resonator SAW Oscillator," *Sensors and Actuators, B: Chemical,* B68, 300-306, 2000.

Christian Reichardt, "Solvatochromic Dyes as Solvent Polarity Indicators", *Chem. Rev.*, 94, 2319-2358, 1994.

P. Schreier, et al. *Analysis of Chiral Organic Molecules,* (Walter de Gruyter, New York, 1995)

J. White, J.S. Kauer, T.A. Dikinson, and D.R. Walt, "Rapid Analyte Recognition in a Device Based on Optical Sensors and the Olfactory System", *Anal. Chem.*, 68, 2191-2202, 1996.

NANOFLUIDIC LAB-ON-A-CHIP FOR BIOMOLECULE DETECTION

Interim Report

JPL Task 1010

Sabrina Feldman*, Danielle Svehla[+], Frank Grunthaner, Jason Feldman, *In situ* Technology and Experiments Systems Section (384)
Joseph Wang, New Mexico State University (NMSU)
*now collaborating from the University of Puget Sound, [+]corresponding author

A. OBJECTIVES

We proposed to develop a nanofluidic lab-on-a-chip chromatographic system that may potentially provide detailed information on the geochemical and biological history of soil, ice, and water samples by identifying and quantifying a broad range of polar and non-polar organic compounds. This study has followed three task areas identified in the first year task plan: 1) design and fabrication of a nanofluidic chromatographic column based on the principles of size exclusion chromatography; 2) assembly of characterization equipment, including a microfluidic fluid handling system capable of ultra-low fluid flow rates, a Zeiss microscope, and an Ocean Optics spectrometer; and 3) design and testing of an amperometric electrochemical detector for fatty acids that can be integrated with the output of the nanofluidic chromatographic channel.

B. PROGRESS AND RESULTS

Task 1: In conventional size exclusion chromatography (SEC), molecules are separated based on their transit time through a size exclusion network formed by closely packed small (~10μm) silica or polymer beads with uniform nanopores. We have designed a nanofluidic size exclusion chromatograph (nSEC) consisting of a column containing size-exclusion gaps defined in the z-direction, analogous to SEC's nanopores, over a matrix of microchannels in the x-y plane, similar to the interstices between the beads in traditional SEC (Fig. 1). Several geometrical variations of this design have been fabricated in order to determine the optimal channel separation geometry. We have developed a model for the nSEC column which predicts that the analyte will be efficiently separated based on molecular size by differential diffusion into the planar size-exclusion gap. Figure 2 shows a modeled chromatogram, similar to that obtained by conventional SEC, of the separation of an analyte mixture of nanobeads in the nSEC.

Our device fabrication process has evolved from the original strategy based on the nanochannel fabrication technologies of Harold Craighead's group at Cornell University [1] in order to overcome several fabrication challenges. Optimization of each etching step and its associated pattern definition and removal processes, including both photolithography and metalization, has required multiple runs for fine adjustment of several operating parameters specific to each process step and material in order to obtain a robust, reproducible technology. We have successfully ion milled 100nm tall support posts (for definition of the size exclusion gap) in silicon, and used reactive ion etching to create the channel matrix (Fig. 3). The following fabrication steps resulting in a sealed device are on schedule to be completed by the end of the FY02 award: growth of a ~1-2nm thermal oxide layer over the entire wafer to create a chemically uniform surface (critical for eliminating analyte/surface interactions), water-jet drilling of interface ports, and anodically bonding a cover glass to form the device roof.

Task 2: Essential to the success of obtaining interpretable qualitative and quantitative data from chromatographic separations is the ability to generate and precisely control ultra-low fluid flow. We have designed and are implementing a custom fluid-handling system (Fig. 4) capable of continuous reliable ultra-low fluid flow rates. Initial fluidic tests are scheduled to begin under the FY02 award. For characterization of the fluidic flow through the nSEC, the appropriate fluorescent microscopy components have been assembled in order to detect a series of different-sized fluorescently labeled nanospheres, which are to be flown through the column.

Task 3: Prof. Wang and his group at NMSU have developed several electrochemical detection methodologies suitable for detection of many biological molecules. A novel contactless conductivity technique using aluminum film electrodes deposited on the outside of a PMMA fluidic channel detected ions in a solution at μM concentrations (Fig. 5). The response was reproducible and linear over a broad range (20μM – 7mM) at an operating voltage of 5 V. Additionally, NMSU has developed techniques for amperometric detection of amino acids, peptides, and organic peroxides, which in themselves are relevant detection capabilities, but also provide groundwork for detecting other nonelectroactive analytes, such as fatty acids. Current efforts focus on labelling techniques involved for fatty acid detection in connection with the fundamental benchtop chemistry for amperometric detection. The necessary combination of redox markers and electrode materials is on schedule to be determined under the FY02 award.

C. SIGNIFICANCE OF RESULTS AND EXPECTED RESULTS

The novel contactless conductivity measurement demonstrated by NMSU obviates many problems (e.g. fouling, unwanted reactions) associated with the electrode-solution contact, offers isolation of the detection system from high separation fields (used in capillary electrophoresis), does not compromise the separation efficiency, and greatly simplifies the detector fabrication. With further optimization to lower detection limits, the contactless approach will enhance the power and scope of microfluidic chemical analyzers.

Few experimental studies have been conducted to study fluid flow in the nanoregime, and to our knowledge no one has developed a microscale size exclusion chromatograph. Successful separations in the nSEC determined by the size exclusion gap, which is expected to range from ~10 to 100nm, offers the opportunity to study the effects of geometry, fluid velocity, and surface interactions on the nanoscale. Our ability to directly manipulate and control nanoscale features in the separation column should allow significantly greater control of the size exclusion process compared to conventional SEC columns. It may also result in the separation of a greater number of bands with narrower individual bands than can be achieved with conventional SEC.

If successful, the nSEC could eventually be used to detect of a wide variety of organic macromolecules and non-polar molecules that cannot be separated by capillary electrophoresis or other microfluidic/miniature separation methods. Our particular development effort is focused on optimizing the nSEC for the analysis of lipid compounds and their breakdown products including fatty acids, high-molecular-weight lipid polymers, and crude oils. Subsurface oils, for which conventional SEC is a well-established standard terrestrial technique, and fatty acids, to which successful SEC analysis has been applied [2], are of particular astrobiological interest. Fatty acids are the building blocks for lipid bilayer membranes found in all terrestrial cellular organisms, are extremely stable over geological time scales, and are not expected to decompose under the conditions found in subsurface soil or ice. Biologically-derived fatty acids on Earth can be determined by their preference for an even number of carbon atoms with concentrations peaking around 14 to 22 atoms. In contrast, nonbiological fatty acid samples potentially found on

other planetary bodies are not expected to show a similar preference or pattern. On Earth, the largest identifiable trace of past life is generally thought to be subsurface oil deposits [3]. Similarities between the Earth and Mars at the time of formation suggest large deposits of oil beneath the Martian surface. Due to the lack of plate tectonic signatures, less volcanic activity, unlikely burial of ancient rocks by sedimentation, and lower subsurface temperatures and pressures, hydrocarbon deposits formed on Mars billions of years ago are likely to have survived near the surface. Subsurface oil on Mars would thus be an excellent place to look for evidence of past life and perhaps for extant life, as oil would provide unoxidized carbon fuel.

The nSEC system with electrochemical detection is suitable for potential *in situ* instrumentation for planetary missions as it is expected to have a minimum number of components, perform a minimum number of discrete operations, be robust and capable of withstanding space environments, and have low mass and low power requirements.

D. FINANCIAL STATUS

The total funding for this task was $320,000, of which $250,000 has been expended.

E. PERSONNEL

Partha Shakkottai (353) has been instrumental in modeling the nSEC column. Linda del Castillo (345) and Victor White (384) have fabricated the nSEC devices. Martin Pumera (NMSU) has had a major role in development of the electrochemical detection techniques.

F. PUBLICATIONS

[1] M. Pumera, J. Wang, F. Opekar, I. Jelinek, J. Feldman, H. Löwe, and S. Hardt, "A Contactless Conductivity Detector for Microchip Capillary Electrophoresis," *Anal. Chem.,* 74, 1968 (2002).

[2] J. Wang, A. Escarpa, M. Pumera, J. Feldman, "Capillary Electrophoresis-Electrochemistry Microfluidic System for the Determination of Organic Peroxides," *J. Chromatogr. A*, 952, 249 (2002).

[3] D. Svehla, S. Feldman, J. Feldman, F. Grunthaner, P. Shakkottai, L. del Castillo, and V. White, "Nano-fabricated Size Exclusion Chromatograph," *Proc μTAS 2002 Symp.*, in press (2002).

[4] J. Wang, G. Chen, and M. Pumera, "Microchip Separation and Electrochemical Detection of Amino Acids Following Precolumn Derivatization with Naphthalene-2,3-dicarboxyaldehyde," *Electroanalysis*, in press (2003).

[5] J. Wang, and M. Pumera, "Nonaqueous Microchip Capillary Electrophoresis," submitted.

G. REFERENCES

[1] S.W. Turner, A.M. Perez, A. Lopez, and H.G. Craighead, "Monolithic Nanofluid Sieving Structures for DNA Manipulation" *J. Vac. Sci. Technol. B*, 16, 3835 (1998).

[2] C.M. Dobarganes, and G. Marquez-Ruiz, *Advances in Lipid Methodology Two* (ed. W.W. Christie), Dundee: Oily Press, 1993, pp. 113-137.

[3] J.F. McGowan, "Oil and Natural Gas on Mars," *Proceedings of SPIE-Instruments, Methods, and Missions for Astrobiology III*, 4137, 63 (2000).

H. APPENDIX: *FIGURES*

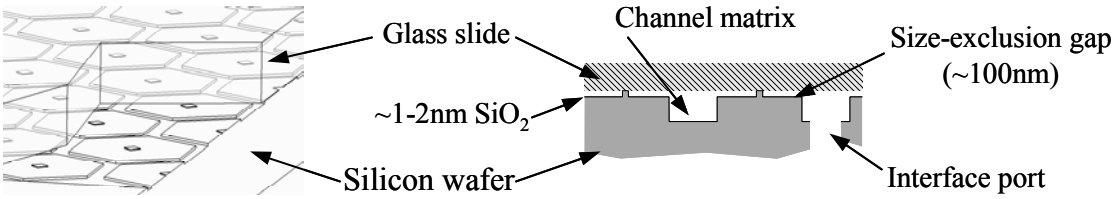

Figure 1: 3-D and cross-sectional views of nSEC schematic

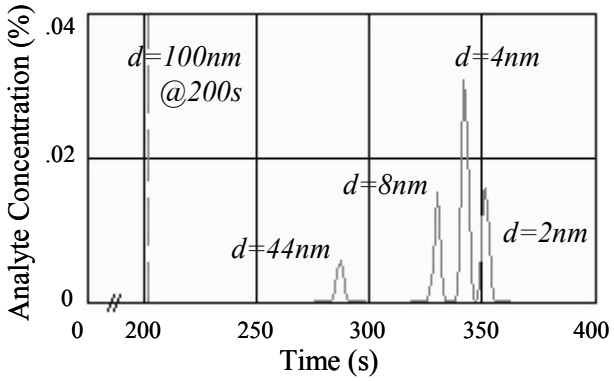

Figure 2: Chromatogram of modeled nSEC separation

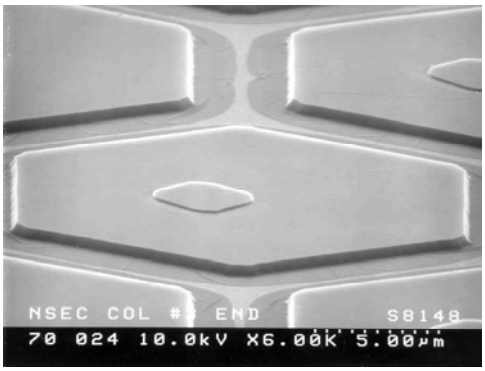

Figure 3: nSEC channel matrix and 100nm tall support posts

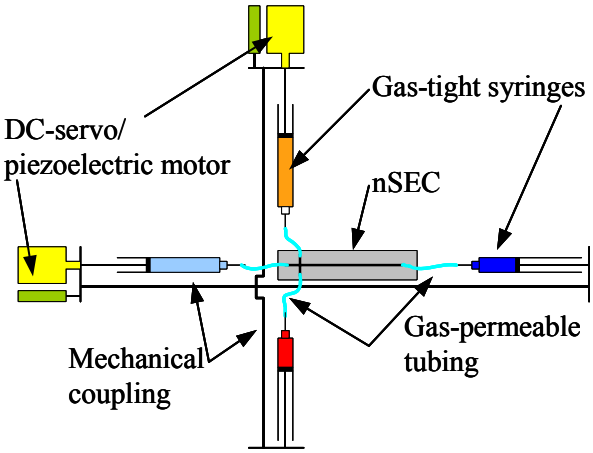

Figure 4: Schematic of continuous ultra-low fluid flow (sub-pL/s – µL/s) pump system: two sets of mechanically coupled syringes driven by a closed-loop DC-servo/piezo stack actuator. Gas in the system is evacuated via the gas-permeable tubing.

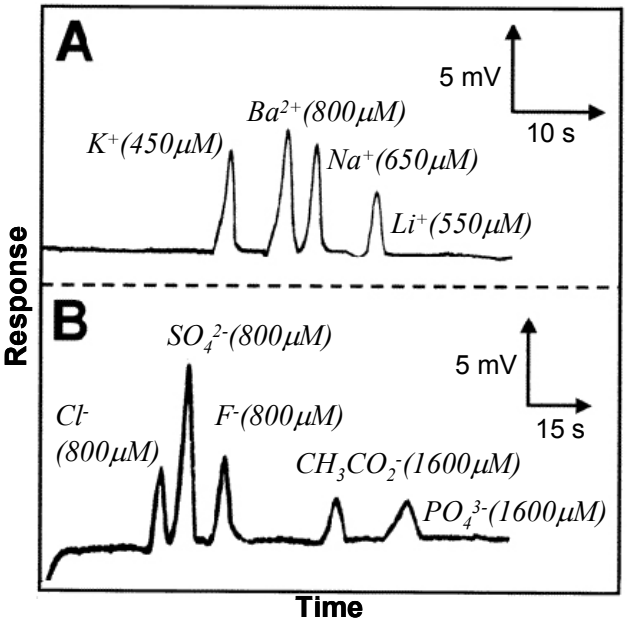

Figure 5: Electorgrams of cation (A) and anion (B) solutions using contactless conductivity detection for capillary electrophoresis separations.

NOVEL NON-DESTRUCTIVE MICROWAVE EXTRACTION OF ORGANIC MOLECULES FROM ROCK AND SOIL SAMPLES

Interim Report

JPL Task 1022

Luther W. Beegle, Instrument Development and Spectroscopy Research Element (3264)
Isik Kanik, Instrument Development and Spectroscopy Research Element (3264)
Nasser Budraa, Instrument Development and Spectroscopy Research Element (3264)

A. OBJECTIVES

Accurate *in-situ* analysis of chemical compounds of astrobiological importance from planetary rocks and soils is strongly dependent on the ability to extract appropriate materials from such samples. In studying the chemical composition of any planetary sample, the most scientifically interesting part of that sample might be inside of it, underneath a protective outer surface. Presently, volatile extraction is limited to the sampling of the surface of a rock or soil from conductive heating or laser ablation. However, in-situ analysis of rock or soil samples for organic molecules would be significantly enhanced by sampling the rock interior, not just its surface.

Cryptoendolithic microorganisms have been demonstrated to survive in the very hostile dry valleys of Antarctic deserts. They accomplish this by finding protected environments inside of rocks where they grow between the rock crystals (Friedman 1982). Protected by a few cm of rock from UV radiation and harsh temperatures of their external environment, they flourish in an environment that may be analogous to ones which may have existed on the Martian surface. This makes rock interiors a prime spot to look for trace elements and microfossils as evidence of extinct Martian life.

The conventional conductive heating method is perhaps the most straightforward of techniques presently available for use by a landed spacecraft. However, it has three major shortcomings: inefficient heating, slow response time and high power loss. Similarly, laser ablation to extract volatiles from soil/rock samples is found to be inefficient since heating of the sample is limited to a small surface area and a very small penetration depth. Therefore, we propose to use microwave energy to extract compounds of interest (such as organic molecules) from the interior of soil and rocks samples. We present this technique (named the Microwave Enhanced Extraction Technique (*MEET*)) as a precision tool to selectively remove compounds of interest by volatilization. This process is useful in delivering controlled heating to the interior of samples, where temperatures can range from just above room temperature (~30ºC) to well over 1000º C. This technique simply offers the best chance to extract specimens from deep inside Martian soil and rock samples. Because microwave energy is deposited directly into the entire sample without the mediation of conductive heating, the microwave heating process is very efficient without an unnecessary power loss, the sample reaches its vaporization point very rapidly (Barnabas et al. 1995), and the extraction process is very energy-efficient (Lopez-Avila et al. 1994). For example, it was reported that extraction of pesticides from soil using less than 1 min of microwave radiation is comparable to more than 1.5 hr of traditional heating, and the

quality of the extracts were vastly superior to that obtained by those methods (Granzler et al. 1986).

The objective of this proposal is to demonstrate the feasibility of the MEET technique to sublimate trapped atmospheric gases, chemical species and <u>especially</u> organic molecules in soils that could help elucidate questions on Martian abiotic and biotic chemical evolution. Furthermore, we will explore the utility of changing the frequency of radiation, attempting to raise the temperature of different species one at a time, and vaporizing them so they can be introduced into a mass spectrometer. Some preliminary experiments in a frequency-tuning approach have already been carried out here at JPL, where pure amino acid samples in a microwave cavity have been shown to sublimate at different frequencies. As shown in Fig 1., ~ 10 mg of proline (115 amu) sublimated within a few seconds at a frequency of 2.393 GHz while ~ 10 mg of alanine (89 amu) sublimated at 2.407 GHz (*<u>both with <8 watts of total power</u>*). By frequency tuning other chemicals present, the host matrix will be minimally heated, reducing the amount of heat energy needed.

The proposed proof-of-concept laboratory study will focus on a) the utility of selectively extracting molecules of interest by choosing a discrete microwave wavelength that only sublimates certain compounds while ignoring the rest, and b) exploring and comparing different MEET procedures (with and without solvent added to the sample of interest). This work will dramatically decrease the power and mechanical complexity of sample introduction into a variety of instruments likely to be included on an in-situ astrobiological mission to Mars. Follow up funding from the NASA PIDDP and/or ASTID programs will be sought.

B. PROGRESS AND RESULTS

The experimental setup required use of a fume hood to be able to properly vent the organic material after it had been sublimated, and the laboratory in 183-623 did not have an installed fume hood. Therefore progress on this work has consisted of getting a fume hood installed. This took approximately six months to finish due to a variety of reasons. The hood was approved by the JPL safety office at the end of September 2002, and the experimental apparatus was set up and now is fully operational. Preliminary data from two amino acids, Proline and Alanine, were taken as shown in Fig. 1.

We expect to obtain data from other amino acids as well by the end of October, 2002. This work will be the basis of a planned ASTID proposal for follow-up funding.

C. SIGNIFICANCE OF RESULTS

Work in progress.

D. FINANCIAL STATUS

The total funding for this task was $40,000, of which $20,000 has been expended.

E. PERSONNEL

No other personnel were involved.

F. PUBLICATIONS

N. Budraa, I. Kanik, and L. W. Beegle, "Microwave Heating of Astrobiologically Interesting Samples,"To be submitted, 34th LPSC science conference in Houston TX, March 2003.

G. REFERENCES

None.

H. APPENDIX

Novel Non-Destructive Microwave Extraction of Organic Molecules From Rock and Soil Samples

Fig 1. Pressure vs. microwave cavity frequency for two amino acids, Proline (*left*) and Alanine (*right*), in the same microwave cavity along with structural diagrams.

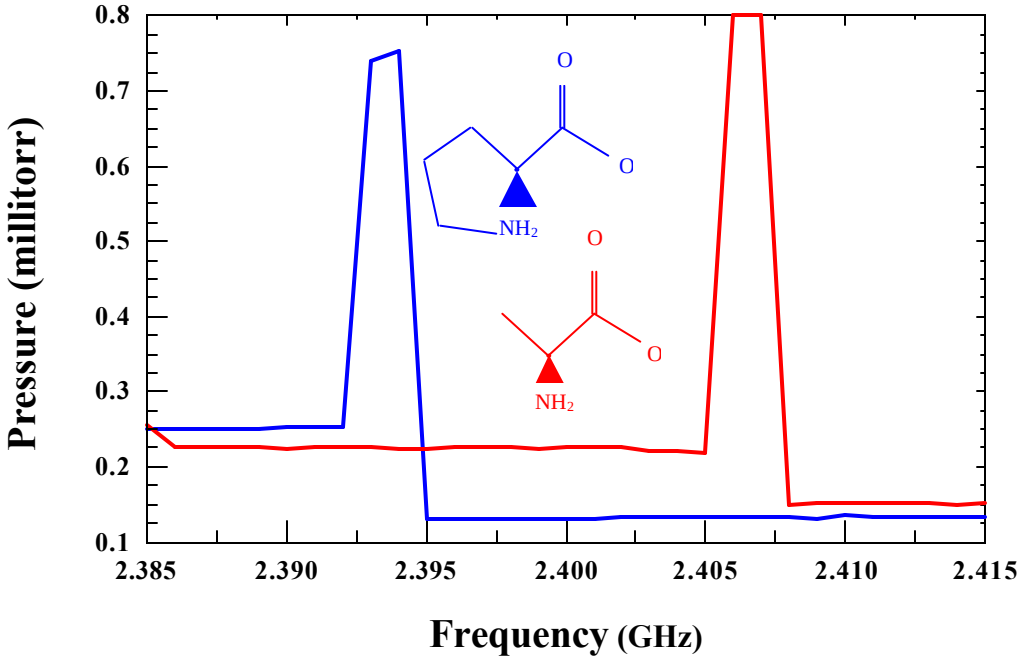

AUTOMATION AND CONTROL

PASSIVE ATTITUDE CONTROL OF A SPIN-STABILIZED SPACECRAFT BY SOLAR RADIATION PRESSURE ON CANTED VANES

Final Report

JPL Task 919

Thomas R. Spilker, Mission & Systems Architecture Section (311)

A. OBJECTIVES

The objective of this task is to determine the feasibility of an alternate attitude control system, based on solar radiation pressure on simple vanes fixed to a spin-stabilized spacecraft, that uses no consumable resources and thus offers potentially unlimited mission lifetimes. Efforts to reduce the mass or extend the lifetime of some space flight missions hinge on the mass of attitude determination and control systems, and the amount of attitude control propellant the spacecraft can carry. This has been a roadblock for envisioned missions involving multiple small, simple spacecraft in heliocentric or sun-synchronous Earth orbit that might have such science objectives as near-side and far-side solar activity monitoring, heliospheric monitoring, etc. Freeing such missions of the cost, mass, and consumables constraints of standard attitude control methods would make them economically much more attractive to NASA and industry.

B. PROGRESS AND RESULTS

My analysis, which is now complete, used fundamental principles of physics (geometric optics and mechanics) to calculate forces applied by sunlight to a system of vanes fixed to a spinning spacecraft as illustrated in Figures 1 and 2, and the response of the spacecraft to those forces and the resulting torques. Major conclusions include:

(1) The method works. A wide range of vane configurations yield torques that precess the spacecraft's spin axis toward sunpointing. Although unable to move the axis to exactly sun-pointing, a vane system can produce a precession rate matching heliocentric angular rates with only a few degrees offset from sun-pointing. The proper torques arise primarily from photons absorbed by the vanes, so "black" vanes are desired. The sizing relation for the vanes on a given spacecraft is

$$A r_v = \frac{2R^2 L n_{sun}}{S_c \sin\kappa \tan\delta}$$

where A is the total (one-sided) surface area of the vanes, r_v is the distance from the vanes' centroids to the spacecraft spin axis, R is heliocentric radius, L is the magnitude of the spacecraft's spin angular momentum, n_{sun} is the spacecraft's angular rate of orbital motion around the sun, S_c is the solar light pressure on a perfectly absorbing surface normal to the sun direction at 1 AU (~4.6 x 10^{-6} Nt/m^2), κ is the "cant angle" of the vanes, and δ is the desired spin

axis' equilibrium angular offset from sun-pointing, as illustrated in Figure 3; this equation is valid for $\kappa + \delta < p/2$. For example, a 10 kg spacecraft ("Tuna can" shaped, ~40 cm diam.) in a 1 AU heliocentric orbit, spinning at 3 RPM, would need four 15 cm x 15 cm vanes, centered 40 cm from the spin axis, to maintain the spin axis within 20° of sun-pointing. For solar cells on the sunlit face of the spacecraft, that offset yields a cosine loss of ~6%. Increasing the vane size to 22 cm x 22 cm decreases the equilibrium solar offset angle to 10°.

(2) The torques that precess the spin axis act to slowly despin the spacecraft.

(3) Parasitic torques arising from the non-zero reflectivity of real vanes also act to despin the spacecraft. For small (a few degrees) pointing offsets, the magnitudes of these torques are larger than those in (2) above.

(4) There are multiple methods, involving no use of spacecraft-provided energy or consumables, to counter the despin torques mentioned above. These methods rely on smaller, specularly-reflecting "spin-up" vanes.

(5) For a fixed spacecraft geometry, total vane area scales as mass to the 4/3 power while spacecraft area scales as mass to the 2/3 power: as mass increases, the relative vane size increases. Eventually the vanes become sufficiently large that their mass is comparable to the spacecraft mass, and present packaging problems in small launch vehicle fairings.

C. SIGNIFICANCE OF RESULTS

The results of this task show that it is possible to maintain a small (up to tens of kg, maybe up to 100 kg), spin-stabilized spacecraft in a quasi-sun-pointing attitude for an indefinite period using a lightweight system of vanes. This enables a class of small, low-cost, long-lived spacecraft that, for example, monitor the Sun and heliosphere. A flotilla of such small spacecraft could be launched from a single small launch vehicle and deployed such that the flotilla spreads in a nearly one-AU heliocentric orbit ahead of or behind Earth's position. Eventually these long-lived spacecraft would form a loose ring around the sun, viewing it from many positions. The many spacecraft could establish a data relay network (possibly autonomous?), relaying data from spacecraft to spacecraft toward Earth until the one nearest Earth performs the final downlink.

D. FINANCIAL STATUS

The total funding for this task was $25,000, of which $11,000 has been expended.

E. PERSONNEL

No other personnel were involved.

F. PUBLICATIONS

None. I did not want to publish anything that might interfere with patentability.

G. REFERENCES

None. All work began with fundamental physics.

H. APPENDIX: *FIGURES*

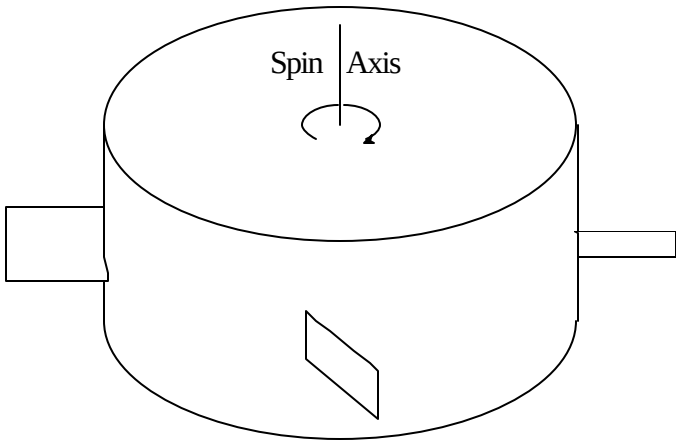

Figure 1: Gross System Geometry. This oblique view shows three vanes of an example four-vane system. The spacecraft is modeled as a short "tuna can" cylinder.

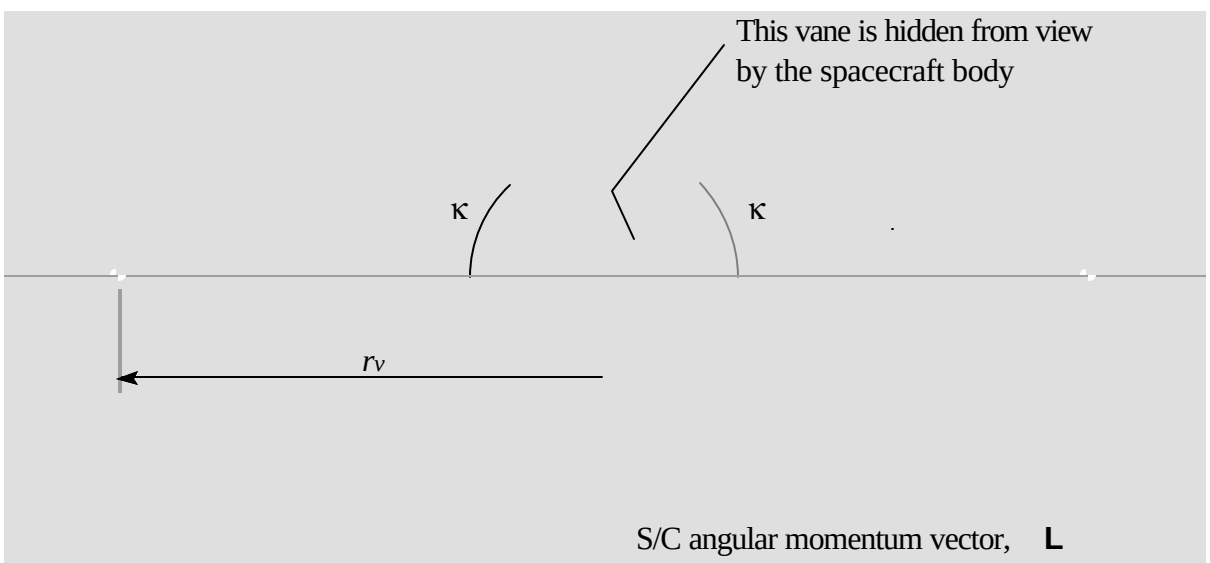

Figure 2: Vane Specifications. This side view illustrates the vane "cant angle" κ, and the distance from the spin axis to the vanes' centroids.

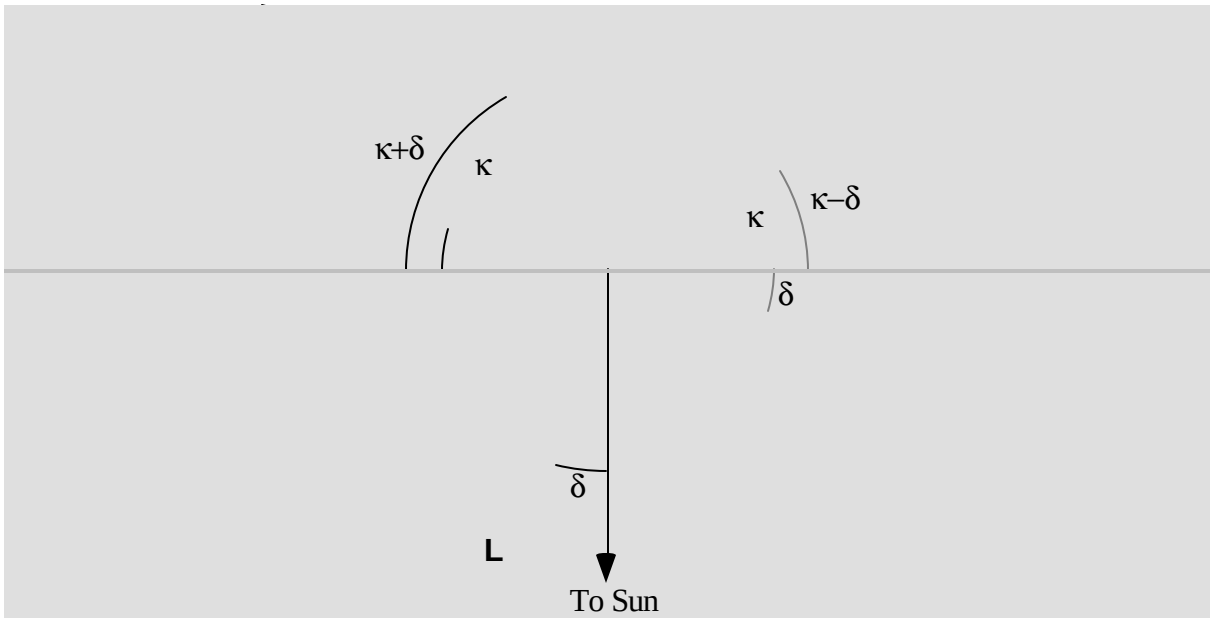

Figure 3: Off-Sun Pointing. This side view shows the effect of off-sun pointing. Note that the hidden vane (dashed line in the center) offers a larger projected area to the sun than the near-side vane, yielding higher solar light pressure on a vane in that position and thus an unbalanced torque. This unbalanced torque precesses the L vector toward sun-pointing.

A NOVEL APPROACH TO PLANETARY PRECISION LANDING USING PARAFOILS

Final Report

JPL Task 961

Marco B. Quadrelli, Autonomy and Control Section (345)
Fred Y. Hadaegh, Autonomy and Control Section (345)

A. OBJECTIVES

In this research, we have addressed the problem of how to achieve precision landing, in an autonomous manner, through an actively-controlled parafoil. By precision landing, we mean the capability of steering the vehicle to a pre-specified target area on the ground. The mechanization to achieve this maneuverability is provided by a parafoil, i.e. a high-glide parachute characterized by airfoil-type canopy cross-sections and wing-type plan forms, which can actively be steered to control the trajectory. Previous flight tests done at NASA Dryden (1991-1996) have established the feasibility of autonomous precision landing on Earth by means of GPS and a commercially-available ram-air parachute. This research leverages on this past achievement, and addresses the fundamental issues involved in using an actively-controlled parafoil and an image-in-the-loop architecture to land the spacecraft on a specific planetary surface location.

The objectives of the task were:

1) To obtain a detailed model of the parafoil dynamics and of the system dynamics in terminal descent.
2) To obtain sensor/actuator models ready to be used in control design.
3) To synthesize a feedback/switching controller showing some robustness to lateral wind gusts and enabling landing on the target with high precision.
4) To demonstrate the concept by simulation.

However, during the course of the investigation, we realized that it would have been more appropriate to look at the fundamental issues rather than focusing on a point design problem. Therefore, based on the fact that a parafoil-assisted descent needs first to come to terms with an unknown atmosphere, we focused our work on developing an atmospheric density estimator.

B. PROGRESS AND RESULTS

Significant progress has been made on achieving the first and second objectives. We now have a working dynamic model (Fig. 1 and Fig. 2) for simulations of the probe/parafoil system during descent in wind. Models of Mars' atmosphere used for the PathFinder and MER simulations have been used, as well as simpler models derived for our balloon modeling work in the Mars Aerobot Validation Program for Earth, Venus, and Titan. The dynamic model of the system includes a rigid body model of the probe/parafoil vehicle in a flat Earth/planet approximation, a model of the apparent mass forces and torques acting on the inflated parafoil (which is a predominant effect in parafoil dynamics), a model of the aerodynamic coefficients of

the canopy, the suspension lines, and load as well. The aerodynamic coefficients of the parafoil are those of a typical sports jumper application [Ref. 1].

A sensor suite is also modeled, and consists of an accelerometer, a star tracker, and a three-axis gyro mounted on the body of the probe. A more complex model has also been developed which also features a gimbaled camera mounted on the probe, actuated via a two-axis gimbal. The pulley-actuator model is represented by a first-order process, which takes into account the symmetric and asymmetric line pull with some characteristic lag. The dynamic model is of sufficient generality as to accommodate other prospective devices for controlled planetary descent, namely rotafoils, or Stokes decelerators, provided their aerodynamic characteristics are known in the form of wind-tunnel-derived aerodynamic coefficients. Figure 1 shows the initial geometry of the system, as well as a typical descent profile with maneuvers such as: pull lines symmetrically to achieve a sink rate, operate a turn to the right (or to the left) via an asymmetric pull of the lines, and finally perform a flare to touch-down in proximity of the target. Figure 2 shows the elements present in the model and some details of the simulation environment, and Figure 3 (left) shows the profile of lift-to-drag ratio required to perform the maneuvers of Figure 1, as well as (right) the discrepancy in descent trajectory when a 3m/s lateral wind acts steadily during the descent. This simulation shows the dramatic effect that wind can have, and hints at the appropriate control philosophy that is required, which will be the subject of future work.

Figure 4 (left) shows the excellent performance of the on-board, discrete-time, model-based, density estimator, which relies on body-fixed accelerometer measurements only. The filter state equation is $\dot{r} = -b\,h\,r$ where ρ is the current density, β the height scale factor, and h the current height along the local vertical, and the measurement equation is given by $y = Hx + M^{-1}C_0$ where H is the measurement sensitivity matrix, M is the mass matrix, and C_0 the density-independent part of the equations of motion (of the form $M\ddot{q} = C_0 + r\,C_1$). We assume that the knowledge of the aerodynamic and geometric parameters is exact, although methods for their estimation are available. Figure 4 (right) depicts the functional phase of the descent to be considered in a more thorough study. The envisioned control architecture is based on an optical guidance scheme [Ref. 2]. The essentials of this architecture rely on a measure of the coordinates on the planetary geoid where the landing site is located. These coordinates are given in terms of longitude, latitude, and planetocentric radius. More simply, with the flat planet model we have developed, they are given in terms of (x,y,z) inertial coordinates. The control logic includes a feedback architecture to compensate for deviations from the intended flight path originated by wind gusts, a feed-forward logic which generates the programmed descent path and provides a reference for the feedback controller, and a switching logic to enable/disable the precision landing architecture when the system is in proximity of the target.

C. SIGNIFICANCE OF RESULTS

This task developed a dynamic-aerodynamic-control-estimation model of a fully-actuated parafoil controlling the descent of a space probe in a Mars-like planetary atmosphere. Based on the promising results allowed by the model developed in this task, our future work will focus on more robust estimation and control schemes, which will guide the vehicle to land autonomously at a specified target point. The findings from this investigation will apply to missions to Mars, Titan, and other planets with an atmosphere. The preliminary results obtained so far indicate that

precision control of these types of vehicles can be achieved, provided that enough control authority and enough knowledge of the atmospheric parameters (density, wind magnitude and direction) are available.

D. FINANCIAL STATUS

The total funding for this task was $81,000, of which $71,000 was expended.

E. PERSONNEL

No other personnel were involved.

F. PUBLICATIONS

[1] M. B. Quadrelli, J. M. Cameron, V. V. Kerzhanovic, "Modeling, Simulation, and Control of Parachute/Balloon Flight Systems for Mars Exploration," presented as paper 2001-2026 at the 16th AIAA Aerodynamic Decelerator Systems Technology Conference 21-24 May 2001, in Boston, MA, also submitted for publication to the Journal of Guidance, Control, and Dynamics.

[2] A Microsoft PowerPoint presentation entitled "A Novel Approach to Planetary Precision Landing Using Parafoils" has been distributed to the participants of the EDL Workshop in the Embassy Suites, Arcadia, on March 26, 2002.

[2] Three papers derived from this DRDF work: "Precision Landing with Parafoils: Dynamics and Control," "Precision Landing with Parafoils: Atmospheric Density Estimation," and "Precision Landing with Parafoils: Wind Estimation" are in preparation.

[3] A proposal entitled "Robust Reentry Aeromaneuvering with Actively Controlled Ballutes," extending our idea into the hypersonic, rarefied flow regime, has been submitted to the FY'03 RTD call for proposals.

[4] A proposal entitled "Ribbon Assisted Lift/Drag Modulation and Heat Mitigation during Hypersonic Reentry," also extending our idea into the hypersonic, rarefied flow regime, has been submitted to the FY'03 DRDF.

G. REFERENCES

[1] W. Gockel, "Computer-Based Modeling and Analysis of a Parafoil-Load Vehicle," 14th AIAA Aerodynamic Decelerator Systems Technology Seminar, San Francisco, June 1997.

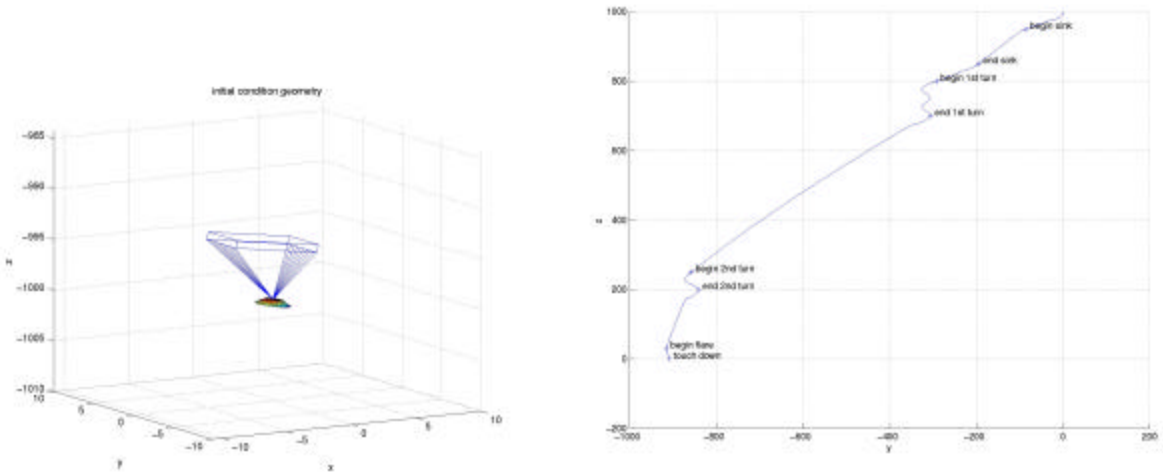

Figure 1. Geometry of problem (Left). The typical phases of a reentry trajectory (Right).

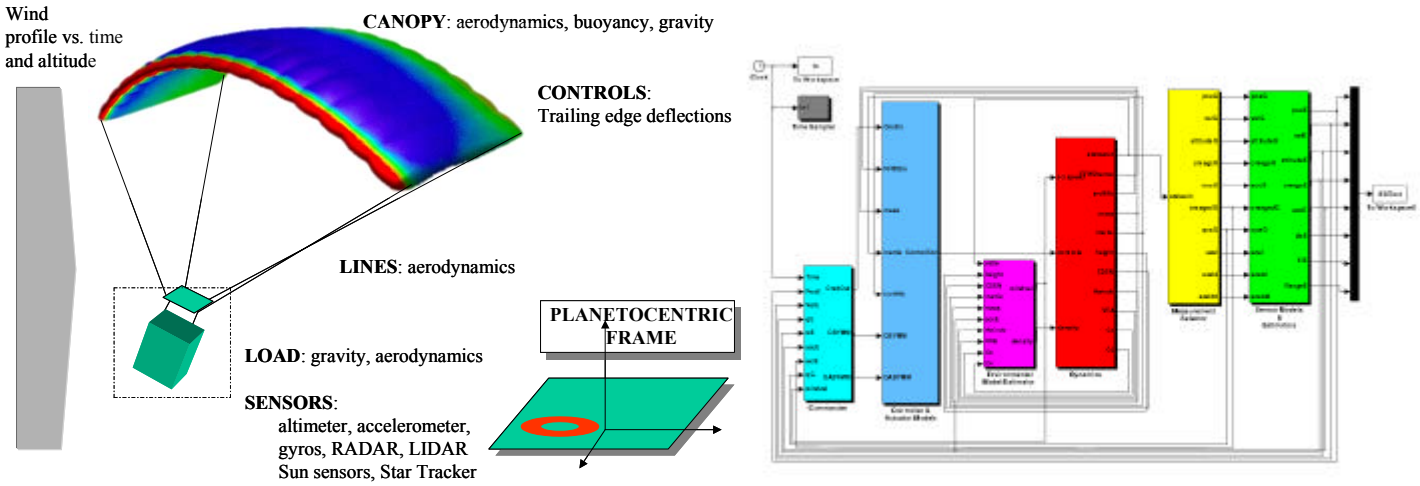

Figure 2. Details of the dynamics model (Left). Matlab/Simulink simulation model (Right).

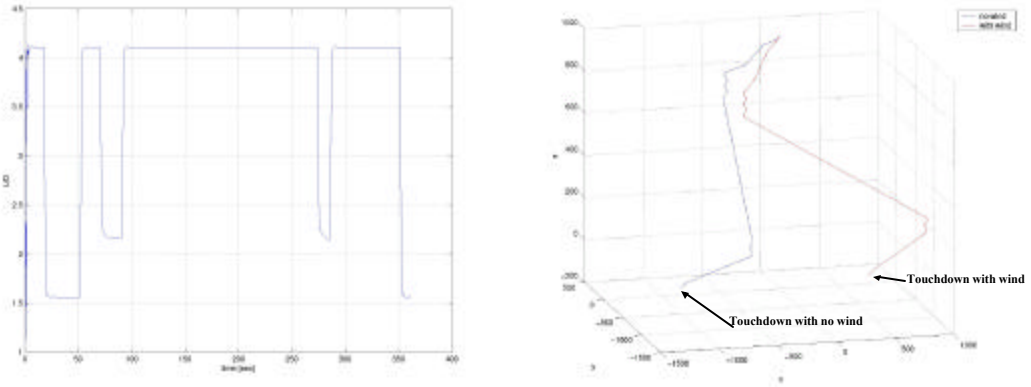

Figure 3. A typical lift-to-drag profile during descent (Left). Discrepancy in descent trajectories with and without wind (linear profile with altitude) present (Right).

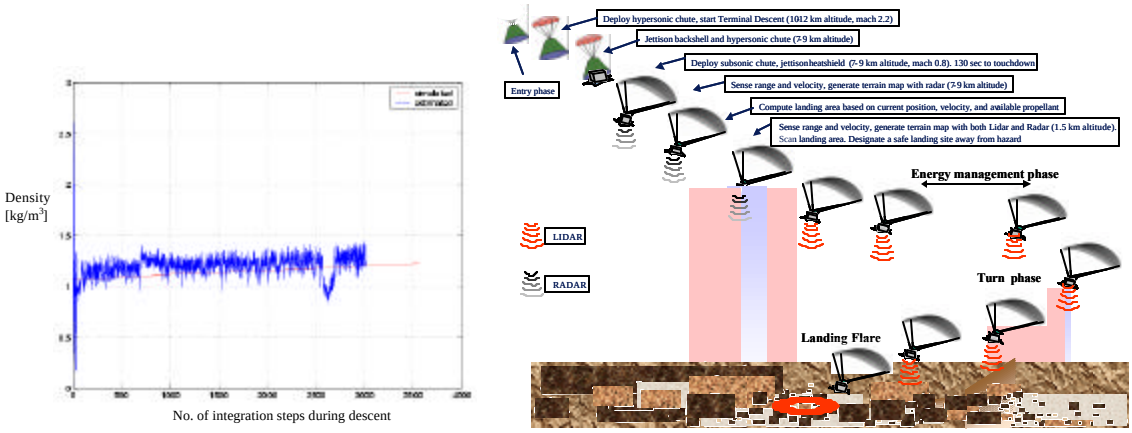

Figure 4. Simulated (red) vs. estimated (blue) density during descent (left). Functional description of parafoil-assisted descent phase (right).

INFLATABLE STRUCTURES

A NEW TYPE OF SELF-RIGIDIZABLE SPACE INFLATABLE STRUCTURE

Interim Report

JPL Task 966

Michael Lou, Mechanical System Engineering and Research Division (350)
Houfei Fang, Thermal and Propulsion Engineering Section (353)

A. OBJECTIVES

This research effort focuses on the development of a new type of self-rigidizable inflatable structure, called the spring-tap-reinforced (STR) aluminum laminate boom, for applications to space missions that require in-space deployment of large ultra-lightweight membrane structures.

Space-inflatable structures technology is an emerging technology that can revolutionize the design of large space-deployable systems. Many currently planned NASA missions need to use space inflatable/rigidizable structures to meet stringent launch volume and mass goals. This is especially true for missions of which the flight systems have large in-orbit configurations. Compared to mechanically-deployed structures that are traditionally used on these missions, space inflatable/rigidizable structures have many advantages, including lower mass, smaller launch volume, simpler design, higher deployment reliability, and lower life-cycle cost. In the past several years, NASA has been actively developing inflatable structures and has made significant progresses in this important technology area. However, space rigidization remains a significant obstacle that prevents inflatable structures from being implemented in near-term flight missions. Successful development of the self-rigidizable STR aluminum laminate boom can potentially meet this urgent technology challenge.

B. PROGRESS AND RESULTS

We completed in the past year the formulation and analysis of the baseline design of the STR aluminum laminate boom. Several sample booms of the baseline design, with a diameter of 3 inches and a nominal length of 5 meters, were fabricated. Figures 1 through 3 show a baseline STR boom in the stowed, deployed, and test configurations, respectively. Actual measurements of the sample booms indicated that the average weight of each boom, including two end caps, is 1.25 kg. The sample booms were subjected to a series of buckling and modal tests. The test results were used to correlate with the corresponding analytical predictions. A comparison of the dynamic analysis and test results is shown in Table 1.

During the fabrication and testing of the baseline STR booms, we observed that structural integrity of a deployed boom deteriorates over time. An investigation into this observation discovered that after the internal pressure used to deploy the boom is vented out, the aluminum laminate skin of the boom wall will undergoes stress relaxation. When the stress relaxation reaches a certain degree, the boom's cross-section will change from a circular shape to a near-square shape that has the four longitudinal spring tapes at its four corners. It was experimentally

proven that a boom with such a distorted cross section would have a substantially lower load-carrying capability. To remedy this deficiency of the baseline boom, we decided to add circumferential rings to the boom, such that the shape stability of its cross sections can be maintained (see Figure 4). The following requirements were established for the design of the circumferential rings:

1) They must be able to be flattened such that the boom can be rolled up for stowage.
2) They must be able to autonomously assume and maintain a circular shape after the boom is deployed by inflation pressure.
3) They must have sufficient stiffness in the hoop direction of the boom to resist shape changes in cross-sections of the boom.
4) They must be lightweight and not require any complicated mechanisms for deployment.

Several ring design concepts, including an extensive search of suitable materials, were developed, analyzed, and tested. The final selection is the design shown in Figures 5 and 6. This ring consists of two semi-circular halves that are connected by two hinges. The ring halves are made of high-modulus spring steel strips and the hinge material is Kevlar. Figure 7 shows the rings being installed onto the inner wall of a boom. Finite-element analyses of the modified STR boom design (i.e., the design with reinforcing rings) were performed to optimize the ring dimensions, as well as the distance between the rings. It was determined from the analysis results that a distance of 10 inches will give sufficient structural support in the hoop direction and yield an acceptable weight increase.

Three sample booms of the modified STR boom design were fabricated. Structural tests of these sample booms are currently in progress. Preliminary dynamic test results confirmed that although the modified booms are slightly heavier (1.4 kg each) than the baseline boom, their fundamental frequencies have noticeably increased (see Table 2).

We will complete the ongoing test program of the modified STR boom and perform additional structural analyses to optimize selected design features of the boom. These include the hinge design and material as well as the design of the ring/boom interfaces. We will also document for publication in open literature the design, analysis, and test results produced by this DRDF research effort.

C. SIGNIFICANCE OF RESULTS

The modification of adding circumferential rings to the STR boom design greatly improves the boom's long-term configuration stability and structural integrity. The circumferentially-reinforced boom can also carry lateral and bending loads. Preliminary analysis results indicated that the modified STR booms, even keeping the same diameter of 3 inches, could have a working length of over eight meters and, thus, a much wider range of applications. For example, the longer STR booms can potentially enable the development of a 5- to 7-meter-aperture Ka-band inflatable reflectarray antenna currently being planned by the JPL Interplanetary Network Directorate (IND).

D. FINANCIAL STATUS

The total fund for this task was$100,000, of which $$62,000 has been expended.

E. PERSONNEL

Professor Lih-Min Hsia of California State University at Los Angeles (CSULA), as well as his students Ubalso O. Quijano, Giovany A. Pelaez, and Elvis P. Garay, contributed to this effort.

F. PUBLICATIONS

1. H. Fang, M. Lou, J. Huang, L. Hsia, and G. Kerdanyan, "An Inflatable/Rigidizable Ka-Band Reflectarray Antenna", AIAA 2002-1706, *Proceedings of the 43rd AIAA/ASME/ASCE/AHS/ASC Structures, Structural Dynamics, and Materials Conference and Exhibit,* Denver, Colorado, 22-25 April 2002.
2. H. Fang, M. Lou, J. Huang, L. Hsia, and G. Kerdanyan, "Design and Development of an Inflatable Reflectarray Antenna," *The IPN Progress Report,* Issue 42-149, May 2002. http://ipnpr.jpl.nasa.gov/
3. H. Fang, M. Lou, J. Huang, "Inflatable/Self-Rigidizable Reflectarray Antenna," *JPL IND News,* Issue 16, September 2002.
4. M. Lou, H. Fang, and L. Hsia, "Development of A New Type of Space Inflatable/Rigidizable Booms," accepted for publication by the *AIAA Journal of Spacecraft and Rockets.*

G. FIGURES AND TABLES

Fig. 1 A 5-meter STR boom stowed on a six-inch-diameter mandrel

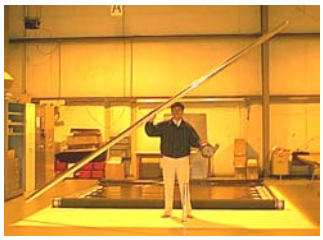

Fig. 2 A fully deployed five-meter STR boom

Fig. 3 Setup for buckling and dynamic tests

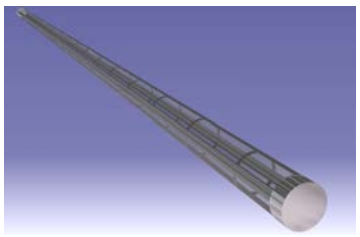

Figure 4. STR boom with circumferential rings

Fig. 5. A two semi-circular halves ring made with high-modulus spring steel strip

Fig. 6 A partially-flattened circumferential ring

Figure 7. Circumferential rings being installed onto the boom

Table 1. Comparison of dynamic test and analysis results of the baseline STR boom

	1st frequency	2nd frequency	3rd frequency
Test	1.46 Hz	11.30 Hz	34.31 Hz
Analysis	1.47 Hz	11.54 Hz	34.21 Hz
Differences	0.7%	1.3%	0.3%

Table 2. Dynamic test results of the modified STR boom

Boom #	1st frequency	2nd frequency	3rd frequency
1	1.63	11.25	32.38
2	1.63	11.00	31.56
3	1.63	11.19	32.44

TITAN BALLOON BUOYANCY CONTROL ANALYSIS AND DEMONSTRATION

Interim Report

JPL Task 969

Jack A. Jones, Science and Technology Development Section (354)
Andre Yavrouian, Thermal and Propulsion Engineering Section (353)
Ralph Lorenz, University of Arizona, Lunar and Planetary Laboratory

A. OBJECTIVES

Titan, the largest moon of Saturn, is the only moon in our solar system with a significant atmosphere, and it happens to be ideally suited for balloon exploration. The nitrogen atmosphere has a pressure a bit higher than Earth's, and it is much colder at -180ºC (Reference 1). This makes the density of the atmosphere four times as much as that of Earth, and thus helium balloons can carry four times as much payload. Titan is believed to have large solid land masses and cold, liquid hydrocarbon oceans. The goal of this program is to design, fabricate, and test a buoyancy- controlled balloon system for Titan that will allow complete atmospheric mobility below the methane ice cloud level (10 km altitude) and that can travel about the solid surfaces and liquid seas.

B. PROGRESS AND RESULTS

A number of balloon buoyancy and mobility systems have been considered, and the design with the most flexibility to accomplish all mobility-related science objectives has been determined to be a blimp modified with a large floatation wheel (Figure 1) that can land and operate on cryogenic solid surfaces or liquid seas (Reference 2).

One possible mission scenario is shown in Figure 2. After entry into Titan's atmosphere, a parachute would pull out a deflated blimp. While falling, the blimp would be filled with helium or hydrogen, and would gently descend to the surface due to a slightly positive weight. The Aerover could then reascend using propeller power or by heating the blimp cavity with waste heat from a radioisotope thermal generator (RTG). The blimp could make repeated descents to the surface through direct commands from Earth or by autonomously seeking certain targets, such as biosignatures or heat sources. Although the surface winds are anticipated to be only about 0.5 m/sec (1.1 mph), at 10-km altitude the winds are strong enough to allow complete circumnavigation of the moon every one-to-two weeks. The Aerover would essentially be "orbiting" Titan well below the upper, obscuring clouds and could, for the first time, allow detailed imaging of the moon, which appears only as an orange disk from space.

Initial testing of Aerover concepts has begun with materials research and scale-model Aerover mobility tests. The first Aerover model tested was a commercially-available one-meter blimp that was modified to allow surface mobility (floatation/landing wheel added), with heat-activated altitude control (black patch added to absorb external radiant heat). The model exhibited excellent control both in the air and on solid surfaces. Altitude variations were fully controllable by engine fan thrusts, by radiant heat input (ascent), and convective cooling (descent).

A larger, six-meter commercially-available blimp has since been purchased and has been modified for testing as a Titan Aerover (Figure 3). A landing floatation wheel has been added that will allow the blimp to land on solid land or lakes. The engines are rotatable to allow powered ascent. A series of internal, lightweight heating coils has been added, representing waste heat additions inside the blimp, and a thermal model of the system has been created. The measured buoyancy change has closely matched those analytically predicted (Figure 4). All future outdoor mobility test results will be compared with theory to ascertain accurate mobility and thermal models. A number of power vs. velocity measurements have already been made, as well as power vs. thrust measurements. These values have been compared with various numerical models and are discussed in the next section.

Another area of Aerover research that was explored is that of the Aerover envelope material. Although there are many polymer materials that can function well at cryogenic temperatures (Mylar, Kapton, Kevlar, PBO, etc.), it was previously unknown how to make a non-porous, strong, envelope whose gores could be sealed to survive Titan's 80-93 K temperatures. A breakthrough last year by Taconic Corporation, however, has demonstrated that a tough PBO fabric weave can be coated with Teflon and aluminized to create a lightweight, non-porous tough envelope, whose gores can be sealed with a Teflon precursor. The primary thrust for the near-term future work will be with autonomous mobility and demonstration of heat-activated buoyancy control.

C. SIGNIFICANCE OF RESULTS

There are several primary areas of significance for the results thus far. The first is that a combined aerobot/rover, or Aerover, appears to be the best means to explore the atmosphere, solid surfaces, and liquid oceans of Saturn's moon, Titan. The second is that power measurements made on a 6-m blimp have confirmed a novel, empirical correlation (Reference 3) made by this task's science advisor, Professor Ralph Lorenz. Based on these calculations, we now know that approximately 90 watts of power (out of 110 watts available) are required to propel our 12.5 meter long, 200 kg Titan Aerover at a speed of 1.0 m/sec, which is adequately above the 0.5 m/sec anticipated surface wind speeds at Titan. We have also calculated that this speed can be increased for the same power if the propellers are more efficiently designed. A third significant result is that a breakthrough materials advance has been made with the creation of a rugged, lightweight fabric material (Teflon-coated PBO) that can survive the cryogenic temperatures on the Titan surface. The fourth, and most recent, significant result is that our thermal models are accurately predicting buoyancy change as a function of waste heat input to the blimp (Figure 4). Due to Titan's low gravity, low temperature, and dense atmosphere, the lift created by adding 200 watts of heat inside the 12.5-m blimp is about 0.6 kg while the blimp is

floating in a stationary position above Titan. This should allow vibration-free science and imaging while traveling with the relatively high winds at 10 km altitude above the Titan surface.

D. FINANCIAL STATUS

The total funding for this task was $100,000, all of which has been expended.

E. PERSONNEL

Other personnel contracted for this study include Tim Lachenmeier, President of Global Solutions for Science and Learning, as well as Professor James DeLaurier of the University of Toronto's Institute for Aerospace Studies.

F. PUBLICATIONS

[1] Jack A. Jones, "Titan Amphibious Aerover," AIAA Space 2000 Conference, Long Beach, CA. September 19-21, 2000.

[2] Jack A. Jones, "Inflatable Robotics for Planetary Applications," 6th International Symposium on Artificial Intelligence, Robotics, and Automation in Space", i-SAIRAS, Montreal, Canada, June 19-21, 2001.

[3] Jack A. Jones and Ralph Lorenz, "Titan Aerover All-Terrain Vehicle," Space Technology and Applications International Forum (STAIF-2002), Albuquerque, NM, February, 2002.

[4] Jeffery L. Hall et al, "Titan Airship Explorer," IEEE Aerospace 2002 Conference, Big Sky Montana, March 2002.

[5] Ralph D. Lorenz, "Flight Power Scaling of Airplanes, Airships, and Helicopters Applications to Planetary Exploration," *Journal of Aircraft*, Vol. 38, No. 2, March-April 2001.

[6] Jack A. Jones, "Aerover Development at JPL/NASA," *SPIE Unmanned Ground Vehicle Technology Video Session*, Orlando, Fl, 2002, JPL Video #2002_01_02.

[7] JPL Titan Aerover URL (updated July 2001): http://www.jpl.nasa.gov/adv_tech/balloons/outer.htm

G. REFERENCES

[1] Ralph Lorenz, "2000 Post-Cassini Exploration of Titan: Science Rationale and Mission Concepts," *Journal of the British Interplanetary Society*, Vol. 53, pp. 218-234, 2000.

[2] Jack A. Jones and Ralph D. Lorenz, "Titan Aerover All-Terrain Vehicle," Space Technology and Applications International Forum (STAIF-2002), Albuquerque, NM, February, 2002.

[3] Ralph D. Lorenz, "Flight Power Scaling of Airplanes, Airships, and Helicopters: Application to Planetary Exploration," *Journal of Aircraft*, Vol. 38, No. 2, March-April 2001.

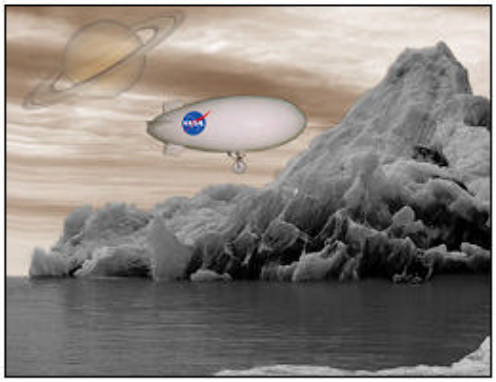

Figure 1. Titan Aerover

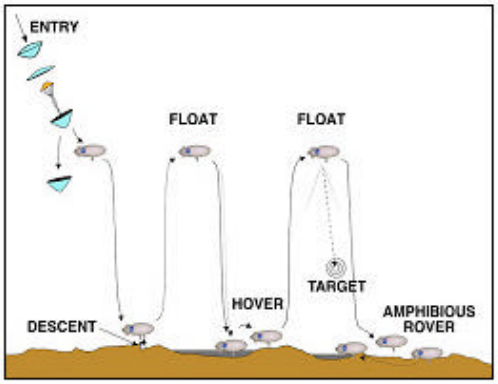

Figure 2. Mission Sequence

Figure 3. Titan Aerover Tests

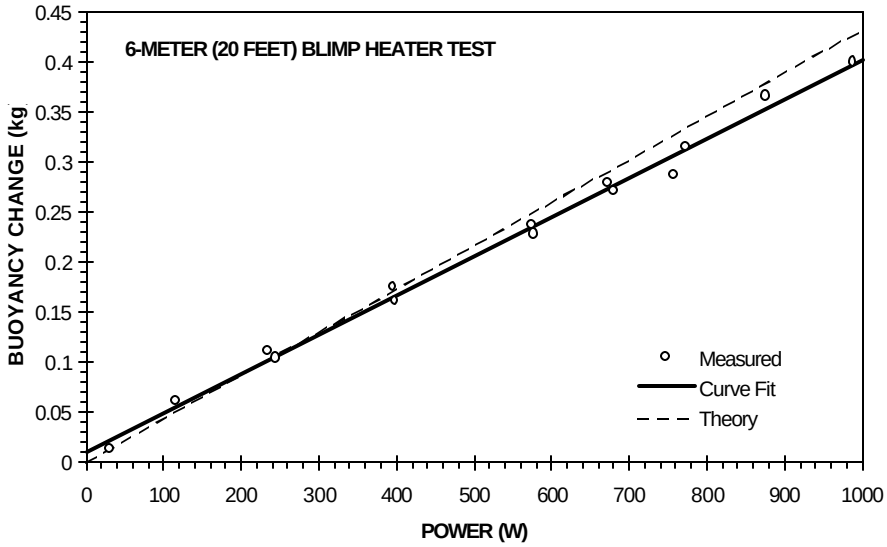

Figure 4. Buoyancy Change vs Blimp Heat Input

INFORMATION SYSTEMS

QUANTUM INTERFEROMETRY

Final Report

JPL Task 1035

Jonathan P. Dowling, Exploration Systems Autonomy Section (367)

A. OBJECTIVES

In recent years, it has been theoretically demonstrated that quantum photon entanglement has the potential to revolutionize the entire field of optical interferometry by providing many orders of magnitude improvement in interferometer sensitivity [1]. The quantum-entangled photon interferometer approach is very general and applies to many types of interferometers. In particular, without non-local entanglement, a generic classical interferometer has a statistical-sampling shot-noise limited sensitivity that scales like 1/Sqrt[N] (one over square root of N), where N is the number of particles (photons, electrons, atoms, neutrons) passing through the interferometer per unit time. However, if carefully prepared quantum correlations are engineered between the particles, then the interferometer sensitivity improves by a factor of Sqrt[N] to scale like 1/N, which is the limit imposed by the Heisenberg Uncertainty Principle. In addition to these developments, we have also recently shown that optical quantum entanglement effects can be used in interferometric photolithography [2]. This application brings about a breakthrough in lithographic resolution by overcoming the diffraction limit, allowing features to be etched that are several factors smaller than the optical wavelength. Of course, how to prepare the desired quantum correlation is the key issue in quantum interferometry, which is the goal of this proposal.

B. PROGRESS AND RESULTS

1. Science Data

During this period of time, we have designed optical devices that are useful in quantum interferometry. We developed a method to generate maximal path-entanglement with a definite photon number, which is the desired quantum correlation for enhanced resolution in interferometric photolithography and Heisenberg-limited interferometry, as well as applications to quantum networks. The breakdown is shown below:

(1) In our recent work, it has been shown that the Rayleigh diffraction limit in optical lithography can be circumvented by the use of path-entangled photon number states [2]. Subsequently, a proof-of-principle experiment was demonstrated by using two-photon entanglement [3]. However, for more than three photons, optical generation of such a quantum correlation was not known except by using unrealistically large optical nonlinearity. We developed a method of making such quantum states by using so-called

projective measurements. Projective measurement is a process of determining the quantum state of a system by measuring some part of the system, which turned out to be an essential tool in quantum information processing [4]. Our method is unique in that only simple linear optical devices are required, and provides the first experimentally realizable scheme for this purpose. Our result has been recently published in *Physical Review A Rapid Communications.* We further developed a generalization of this scheme for an arbitrarily large photon-number, for which our result has been published in *Physical Review A.* These papers have also been selected for the *Virtual Journal of Quantum Information,* and also the *Virtual Journal of Nanoscale Science and Technology.*

(2) Heisenberg-limited measurement protocols can be useful in measurement precision over classical protocols. While the sensitivity of the conventional interferometers is limited by 1/Sqrt[N] (shot-noise limit) where N is the involved particle flux, the Heisenberg-limited interferometry provides that the sensitivity of the device scales as 1/N, yielding a huge increase of the sensitivity of the phase measurement. Such measurements can be implemented using optical Mach-Zehnder interferometers [1], atomic clocks [5], as well as quantum logic gates [6]. We characterized the common features of quantum enhancement in various kinds of interferometers, and established the concept of quantum Rosetta stone based on the equivalence between them. We have also shown that a particular quantum correlation between the two input ports of the interferometer can be made efficiently with the technique of projective measurements, and the Heisenberg limit can be achieved without using sophisticated final detection schemes previously reported. The result has been accepted for publication in a special issue of *Journal of Modern Optics.* We are currently pursuing application of our method to entanglement of massive particles for atom interferometers.

2. Other Results

a. The results of the work motivated exciting new ideas in various research fields that deal with creating nonlinearity by projective measurement technique. In particular, we have developed a special kind of single-photon quantum nondemolition (QND) device that signals the presence of a single photon with no absorption [7]. Furthermore, we designed an expanded protocol to perform polarization-preserving QND detections of a single photon. This result was filed for NASA New Technology Reports [NPO 30551 (2002)], and submitted for publication in *Physical Review Letters.*

b. In collaboration with Prof. Gerald J. Milburn at the University of Queensland, Australia, we presented an invited paper to Philosophical Transaction of the Royal Society on perspectives of the 21st century quantum technologies based on quantum interferometry.

c. We have also analyzed quantum optical networks for quantum cryptography and distributed quantum computing.

C. SIGNIFICANCE OF RESULTS

This task developed a new method of preparing desired quantum correlations for quantum interferometry and interferometric lithography. The effect of quantum interferometry can translate into a tremendous science pay-off for NASA-JPL missions. For example, one application of this new effect is to fiber optical gyroscopes for deep-space inertial guidance and tests of General Relativity (Gravity Probe B). Another application is to ground and orbiting optical interferometers for gravity wave detection: Laser Interferometer Gravity Observatory (LIGO) and the European Laser Interferometer Space Antenna (LISA), respectively. Other applications are to Satellite-to-Satellite laser Interferometry (SSI), proposed for the next generation Gravity Recovery And Climate Experiment (GRACE II). In particular, quantum correlations employed in SSI could improve the orbital sensitivity to gravity enough to give unprecedented accuracy in measuring Earth gravitational anomalies from space with a resolution of 1 km or less. Such sensitivity could be used for orbital oil prospecting or measuring water content of aquifers.

The application of quantum interferometry in photolithography has tremendous commercial potential in the computer chip and semiconductor industries by allowing sub-100 nm fabrication resolution at low cost. In addition to writing features much smaller than the wavelength, it is also possible to read that information with this resolution. In both lithography and microscopy, the conventional classical road to finer resolution is to actually reduce the wavelength. But it is very hard and expensive to make imaging elements at UV and X-ray scales. In addition, such high-frequency photons pack quite a punch and damage the object to be imaged or written on. Employing quantum entanglement may completely overcome such a bottleneck.

D. FINANCIAL STATUS

The total funding for this task was $100,000, all of which has been expended.

E. PERSONNEL

Dr. Deborah Jackson, Section 367
Dr. Pieter Kok, Resident Research Associate at JPL under National Research Council Associateship Program.
Dr. Hwang Lee, Resident Research Associate at JPL under National Research Council Associateship Program.

F. PUBLICATIONS

[1] Hwang Lee, Pieter Kok, Nicolas Cerf, and Jonathan P. Dowling, "Linear Optics and Projective Measurements Alone Suffice to Create Large-Photon-Number Path Entanglement," *Phys. Rev. A* 65, 030101(R) (2002).

[2] Pieter Kok, Hwang Lee, and Jonathan P. Dowling, "Creation of Large Photon-Number Path Entanglement Conditioned on Photo-Detection," *Phys. Rev. A* 65, 052104 (2002).

[3] Hwang Lee, Pieter Kok, and Jonathan P. Dowling, "A Quantum Rosetta Stone for Interferometry," (in press) *Journal of Modern Optics* (2002), quant-ph/0202133.

[4] Pieter Kok, Hwang Lee, and Jonathan P. Dowling, "Single-Photon Quantum Nondemolition Devices Constructed with Linear Optics and Projective Measurements," (submitted to) *Physical Review Letters* (2002), quant-ph/0202046.

[5] Jonathan P. Dowling and Gerald J. Milburn, "Quantum Technologies: The Second Quantum Revolution," (in press) *Philosophical Transactions of the Royal Society* (London, 2002), quant-ph/0206091.

[6] Pieter Kok, Hwang Lee, and Jonathan P. Dowling, "Novel Interferometric Quantum Nondemolition Device for Single-Photon Detection," *NASA New Technology Reports*, NPO-30551 (2002).

G. REFERENCES

[1] Jonathan P. Dowling, "Correlated Input-Port, Matter-Wave Interferometer: Quantum Noise Limits to Atom-Laser Gyroscope," *Phys. Rev. A* 57, 4736 (1998).

[2] Agedi N. Boto, Pieter Kok, Daniel S. Abrams, Samuel L. Braunstein, Colin P. Williams, and Jonathan P. Dowling, "Quantum Interferometric Optical Lithography: Exploiting Entanglement to Beat the Diffraction Limit," *Phys. Rev. Lett.* 85, 2733 (2000).

[3] Milena D'Angelo, Maria V. Chekhova, and Ynhua Shih, "Two-Photon Diffraction and Quantum Lithography," *Phys. Rev. Lett.* 87, 013602 (2001).

[4] E. Knill, R. Laflamme, and G.J. Milburn, "A Scheme for Efficient Quantum Computation with Linear Optics," *Nature* 409, 46 (2001).

[5] J.J. Bollinger, W.M. Itano, D.J. Wineland, and D.J. Heinzen, "Optimal Frequency Measurements with Maximally Correlated States," *Phys. Rev. A* 54, R4649 (1996).

[6] Authur Ekert, "Quantum Interferometers as Quantum Computers," *Physica Scripta* T76, 218 (1998).

[7] G. Nogues, A. Rauschenbeutel, S. Osnaghi, M. Brune, J.M. Raimond, and S. Haroche, "Seeing a Single Photon Without Destroying It," *Nature* 400, 239 (1999).

MATERIALS

SHAPE MEMORY ALLOY THERMAL SWITCH

Final Report

JPL Task 973

Virginia Gordon Ford, Mechanical Engineering Section, (352P)
Georg Siebes, Thermal and Propulsion Engineering Section, (3536)
Eric Sunada, Thermal and Propulsion Engineering Section, (3536)
Sean Haggart, Mechanical Engineering Section, (352)

A. OBJECTIVES

In the year 2000, a DRDF study demonstrated that the shape memory alloy effect could be used to modulate conductivity through a bolted joint to passively provide thermal isolation when a component is cold, and to thermally conduct when a component is hot. The objective of the DRDF study of the year 2001 was to further refine this device to improve its temperature range performance, to amplify the conductivity modulation effect, and to further characterize the device.

B. PROGRESS AND RESULTS

Alloy Selection - Temperature range of performance for shape memory alloy (SMA) is controlled by the alloy used and the stress within the part. A survey of vendors resulted in determining two alloys within the range of desired performance that were affordable, were available, and could be two-way trained within a lead-time that satisfied the testing schedule. Alloy D had unstressed properties to reach full martensitic condition at -278°C and full austenitic condition at 0°C. Alloy X had unstressed properties to reach full martensitic condition at -538°C and full austenitic condition at -158°C. A goal of this study was to select an alloy that would fully develop a flight-level stress in the bolt upon warming to room temperature. By selecting alloys with full austenitic condition temperatures lower than room temperature, the SMA washers have 208°C to 358°C to generate strain that will produce stress within the bolt.

Hardware Modification - Modifications from the first test configuration were made to improve the conductivity modulation effect. The modifications were to add a spring to lift the variable-temperature component off of the cold component when the SMA shrinks; to add insulating washers beneath the head of the bolt, beneath the nut of the bolt, and beneath the spring; and to coat the bottom of the switch body with low-emissivity gold. Figure 1 shows the configuration that was tested. An additional change was to contain each instance of the switch in a body that could be easily assembled to the variable-temperature component.

Testing - A test fixture was assembled that included three variable-temperature base plates with four thermal switches attaching each base plate to one single cold plate. Heaters

totaling about 102 ohms of resistance were attached to each base plate. The thermal switches for each base plate were of three configurations (one type for each base plate) differing by thickness of SMA washers and alloy type for the SMA washers. The three configurations were: Alloy D stacked 0.4" high, Alloy D stacked 0.6" high, and Alloy X stacked 0.6" high. Thermal couples were taped on either side of the thermal switches to enable measurement of conduction through each thermal switch joint.

The test fixture was installed into a vacuum chamber with the cold plate clamped to a nitrogen-cooled heat exchanger. The heat exchanger was cooled to –608°C. Power was applied to the heaters, and the temperature was allowed to stabilize. Once the changes in temperatures were less than 0.18°C every 5 minutes, the current, voltage, and temperature readings were recorded. This data was used to calculate conductance, and was plotted versus temperature. The data is presented in Figure 2, Test Data -- Complete. As can be seen, the data of both the Alloy D, 0.6" SMA increasing temperature case and decreasing temperature case are not well behaved. This could be a result of poor thermal couple attachment or performance. Removing those cases from the data yields the graph shown in Figure 2, Test Data -- Reduced.

C. SIGNIFICANCE OF RESULTS

The test results do not show the effect that was anticipated. The SMA washer made of Alloy X should have reached a full extension sooner than the Alloy D washers, but showed consistently worse conduction performance. The cause of the anomalous readings for the 0.6" Alloy D case needs to be explored. In addition, the SMA washers do not appear to have reached their full extension, since the increasing temperature curves do not appear to be leveling off.

These results indicate that the test setup needs to be carefully examined before proceeding further. The thermal couple attachments, blanketing, and workmanship of the test needs to be evaluated. In addition, further testing is needed that brings the temperature of the SMA washer up to its full extension limit.

D. FINANCIAL STATUS

The total funding for this task was $77,000, all of which has been expended.

E. PERSONNEL

No other personnel were involved.

Figure 1. Thermal Switch Configuration

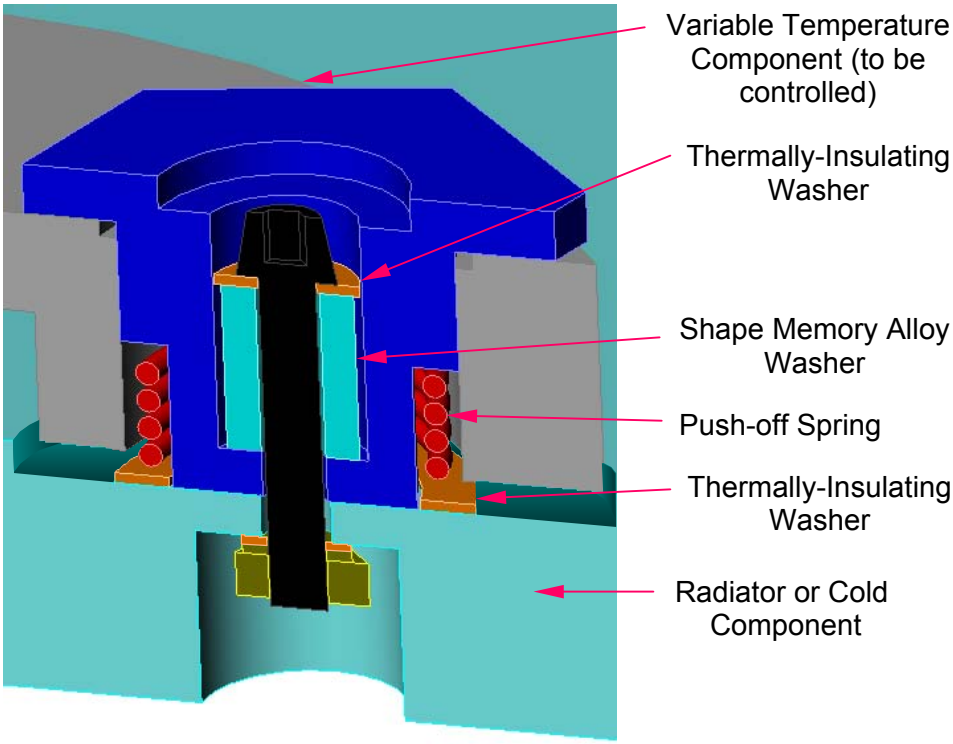

Figure 2.

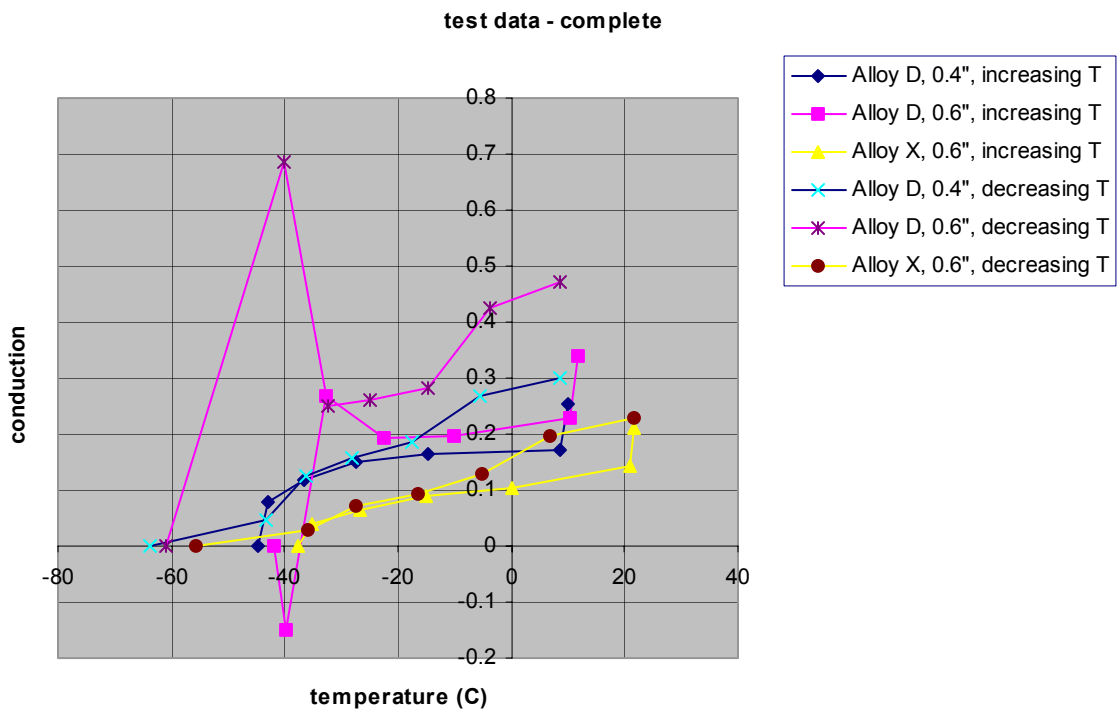

Figure 3.

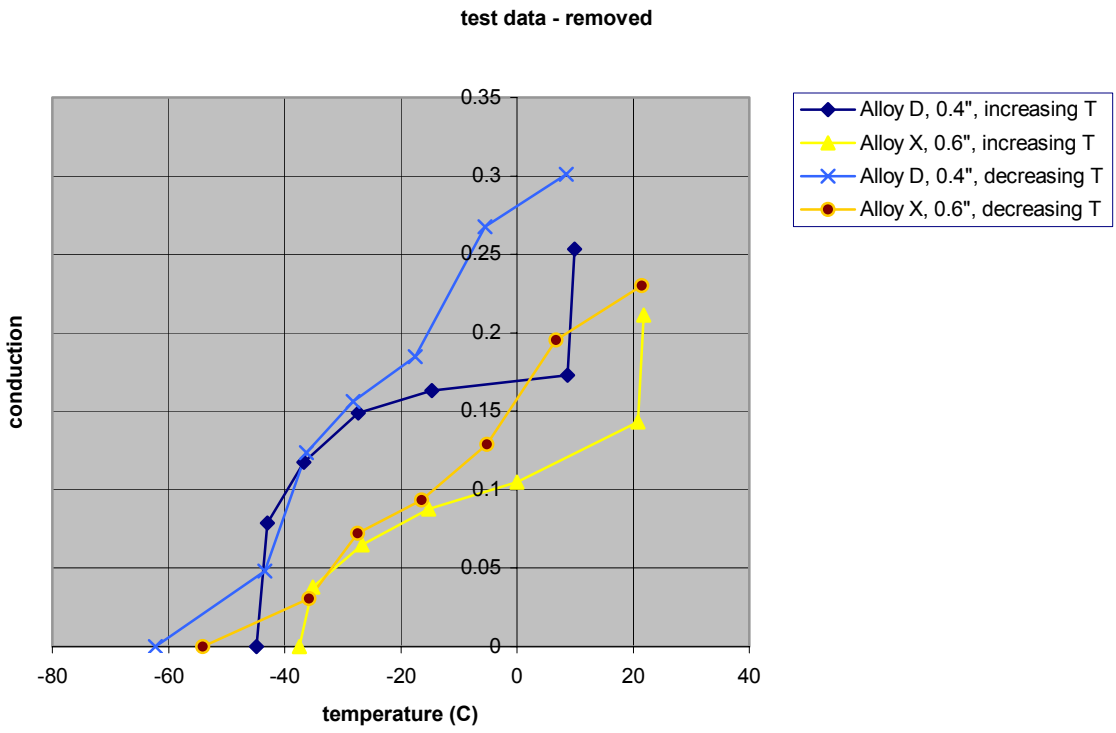
test data - removed
conduction
temperature (C)
0.35
0.3
0.25
0.2
0.15
0.1
0.05
0
-80
-60
-40
-20
0
20
40
Alloy D, 0.4", increasing T
Alloy X, 0.6", increasing T
Alloy D, 0.4", decreasing T
Alloy X, 0.6", decreasing T

MICRO/NANO DEVICES

NANOTUBE ENGINEERING

Final Report

JPL Task 935

Brian Hunt, Michael Hoenk, Flavio Noca, In Situ Technology and Experiments Systems (384)
Prof. Jimmy Xu, Brown University
Prof. Axel Scherer, Caltech

A. OBJECTIVES

Carbon nanotubes exhibit a variety of unique properties, which make them well suited for state-of-the-art sensor applications of interest to NASA. This effort focused on nanotube growth and device processing development aimed at nanotube device applications, including a novel biomimetic acoustic sensor modeled after the rod-like stereocilia arrays that provide the hearing mechanism for all mammals. The major objectives of this work were to develop the growth and processing techniques for producing uniform carbon nanotube arrays, and to utilize these arrays to demonstrate the basic concept of acoustic sensing with artificial stereocilia. The baseline process for producing uniform nanotube arrays utilized alumina nanopores as a template for growth of hexagonally ordered arrays, but complementary processes for fabrication of arrays with more complex ordering were also developed.

B. PROGRESS AND RESULTS

1. Alumina pore array development

It has been known for decades that anodic oxidation of aluminum results in the formation of long, straight nanopores with diameters less than 100 nm, and aspect ratios that can exceed 500:1. More recently it has been found that careful control of the anodization process can produce highly ordered arrays of nanopores. Both Brown University and Caltech contributed to optimization of the alumina nanopore process under this program. The alumina nanopore structures can be used as templates for growth of carbon nanotubes (CNT) by electrodepositing Co in the bottom of the nanopores and using chemical vapor deposition (CVD) with acetylene. Prof. Xu's group at Brown has used this process to grow high quality multiwall carbon nanotubes in the pores. Following nanotube growth, the alumina matrix is etched back using a mixture of phosphoric and chromic acid or Ar ion milling to expose the ends of the nanotubes as shown in Figure 1a) for an ion-etched sample. The exposed nanotubes in Fig.1a) are less than 200 nm long. However, the biomimetic acoustic sensor and other applications of interest require tubes greater than ~500 nm in length. Wet etching of the alumina can produce longer exposed nanotubes, but it has been found that nanotubes with large aspect ratios tend to clump and stick in this process as shown in Fig. 1b). Recently, Prof. Xu's group has found that they can significantly reduce the nanotube sticking problem by adding suitable dispersants to the wet etching solution as indicated in Fig. 1 c). This is a very promising result that Prof. Xu will pursue in collaboration with this team under new funding from DARPA aimed at demonstration of CNT high-Q mechanical oscillators.

2. Nanotube growth and array processing

As part of this program, we developed a nanotube growth process at JPL which uses plasma-enhanced (PE) CVD in an ethylene/hydrogen atmosphere to produce carbon nanotubes at temperatures ranging from 410-750°C. The nanotube growth is selectively nucleated on a variety of thin metal catalysts, including a new Ti/Ni bilayer developed in our group. Figure 2a) illustrates the dense vertically-aligned arrays that are produced on the metal catalyst films using the ethylene CVD process at 635°C. However, closer inspection of the nanotubes reveals that the tubes show local bending, which is a sign of defect incorporation during growth. This finding motivated the development of a high temperature CVD process using a new tube-furnace-based system capable of growth above 1000°C. Figure 2c) shows a recent example of CNT growth using methane CVD in this system at 900°C. In this case, it was found that an un-patterned sub-nm Fe catalyst layer produced a sparse array of straight, freestanding vertical and off-vertical nanotubes. The important points to note are that the tubes are very straight, which indicates a low defect density, and that the tubes are sticking up from the substrate surface. This geometry is ideal for our acoustic sensor application as well as other CNT-based devices.

Because the nanotubes grow only on areas of the substrate with catalyst material present, it should be possible to produce ordered arrays of such freestanding nanotubes by patterning arrays of catalyst dots with diameters on the order of 20-30 nm using electron beam lithography (EBL) or alternate techniques. The e-beam approach has the advantage of flexibility in pattern design, but is also pushing the resolution limits of EBL and is expensive to implement. Figure 3 shows a number of catalyst patterns defined using the new JEOL EBL system in the Microdevices laboratory at JPL. Fig. 3a) shows Fe catalyst dots ~50 nm in diameter, while Fig. 3b) and 3c) are images of 30 nm pores patterned by EBL and RIE and then partially filled with Fe catalyst layers. We have grown carbon nanotubes from samples similar to that shown in Fig. 3a) using our low temperature PECVD process, but these nanotubes exhibited the type of defective growth seen in Fig. 2b). Higher temperature nanotube growth using methane at 900°C was attempted with the pore catalyst samples of Fig. 3b) and 3c), but was not successful in the initial runs. We believe the growth did not occur because the Fe catalyst thickness must be re-optimized for the pore geometry. This optimization will be pursued under new programs from NASA Code R and DARPA. We also started investigations of a much different approach for patterning catalyst dot arrays, which utilizes self-organizing block copolymers (Bronikowski and Hunt, NTR, 2001). The great advantage of the block copolymer approach is that it should be able to quickly and efficiently define large areas of ordered nanotubes for a variety of practical applications. This process has been used to pattern 10-30 nm Mo dots for nanotube growth. The growth studies are proceeding with the new funding sources mentioned, as well as under a DRDF focused on this approach (M. Bronikowski, 2002).

3. Development of acoustic readout techniques of nanotube arrays

Experiments were started to determine the acoustic response of dense nanotube arrays such as those shown in Figure 2a). The main approach to date has utilized an Environmental Scanning Electron Microscope (ESEM) to directly visualize the response of the nanotube arrays to an acoustic input provided by flowing gas. The results indicate that the sparser arrays generated by the nanopore or EBL approaches will be essential for high performance acoustic

sensors. We have obtained ASTID funding to continue development of the CNT acoustic sensors (Noca).

C. SIGNIFICANCE OF RESULTS

This task has developed improved techniques for nanotube array fabrication, including improvements in the anodized alumina nanopore process, demonstration of nm scale catalysts defined by electron beam lithography, and a new process using self-assembling block copolymer arrays. The funding for this program also enabled the development of a CMOS-compatible plasma-enhanced CVD process and an improved high temperature CVD process for growth of low-defect-density freestanding nanotubes. The techniques developed here for production of uniform nanotube arrays are expected to be useful for a variety of applications above and beyond the biomimetic acoustic sensor, including biomolecular separation (e.g. DNA sequencing), biomolecular sensing, and mechanical signal processing. The progress made in this seed effort and in complementary programs has already led to follow-on funding from DARPA in a new program aimed at using carbon nanotubes for high-Q resonators for signal processing applications ($2.3M over 3 years, starting 10/01). We have also obtained new funding from the ASTID program for nanotube-based acoustic sensors ($230K, 1 year), and the NASA Code R BioNano program for development of carbon and Si nanowire biosensors ($1.3M over 3 years).

D. FINANCIAL STATUS

The total funding for this task was $110,000, all of which has been expended.

E. PERSONNEL

In addition to the people listed on the title page, other personnel active in this effort include Mike Bronikowski, Dan Choi, Bob Kowalczyk, and Roger Williams.

F. PUBLICATIONS AND PRESENTATIONS

[1] B.D. Hunt, F. Noca, M. Hoenk, “Carbon Nanotube Actuators And Force Sensors,” NASA NTR, NPO-21153. (9/00), Patent application, 1/02.

[2] B.D. Hunt, D. Choi, M. Hoenk, R. Kowalczyk, F. Noca, “Pattern-Aligned Carbon Nanotube Growth,” NASA NTR, NPO-30205 (3/01), Patent application 4/02.

[3] B.D. Hunt, F. Noca, M. Hoenk, “A Carbon Nanotube Tunable High-Q Resonator And Spectrum Analyzer,” NASA NTR, NPO-30206 (3/01), Patent application 4/02.

[4] D. Hoppe, B.D. Hunt, M. Hoenk, F. Noca, J. Xu, “Waveguide-Embedded Carbon Nanotube Array RF Filter and RF Filter Bank,” NASA New Technology Report, NPO-30207 (3/01), Patent application 4/02.

[5] M. Bronikowski and B.D. Hunt, “Regular arrays of carbon nanotubes produced using templates from nano-structured block-copolymeric materials,” NASA New Technology Report, NPO-30240 (5/01).

[6] F. Noca et al., "Nanotube-Based Sensors and Systems for Outer Planetary Exploration," Outer Planetary Exploration Workshop, Houston, 2/21/00.

[7] M. Hoenk et al., "Carbon-Nanotube-Based Sensors and Systems," Nanospace 2001, Galveston, TX, March 13-16, 2001.
[8] *Invited: M. Bronikowski, "Carbon nanotube growth by HiPCO process," APS March Meeting, 3/01, Seattle.
[9] B.D. Hunt et al., "Nanomechanical Resonators Based on Carbon Nanotubes," Nanoscale/ Molecular Mechanics Meeting, Maui, Hawaii, 5/02.

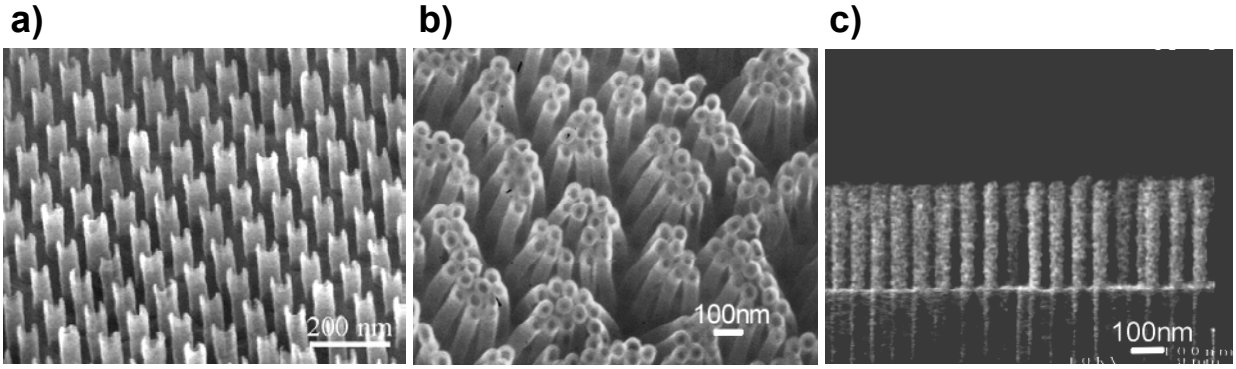

Fig.1 SEM images of exposed CNT arrays produced by etching back the alumina nanopore template. a) Nanotubes ~200 nm long exposed by ion milling. b) Sticking tubes after conventional wet etch of alumina. c) Non-sticking 500 nm long exposed tubes produced with dispersant added to etch solution. Here the tubes have a 25 nm Au/Pt coating (J. Xu et al., Brown U.).

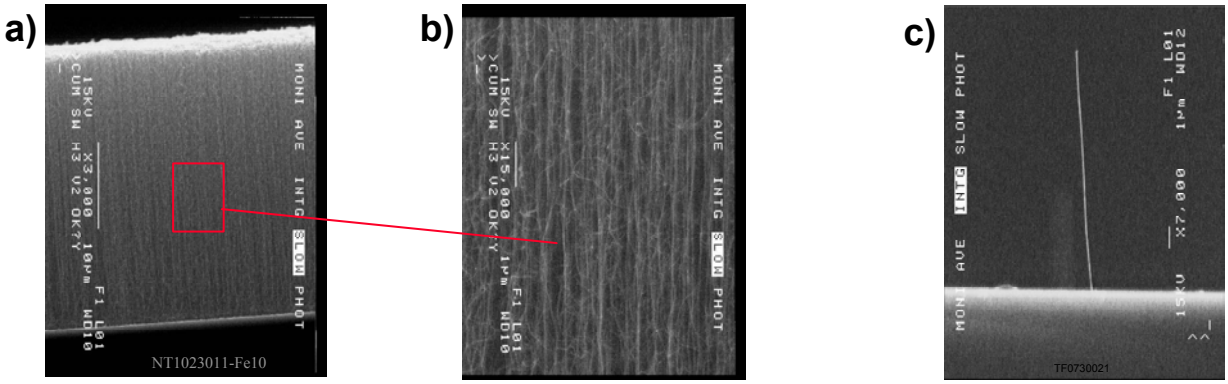

Figure 2. Nanotube growth on thin Fe catalysts using CVD. a) PECVD growth at 635°C with ethylene: low magnification SEM image showing dense growth of ~30µm long CNT. b) Higher magnification view showing local bending of nanotubes due to defect incorporation during this low temperature growth. c) SEM micrograph showing side view of a single, straight, *freestanding vertical nanotube* produced by 900°C methane CVD with a sub-nm Fe catalyst layer.

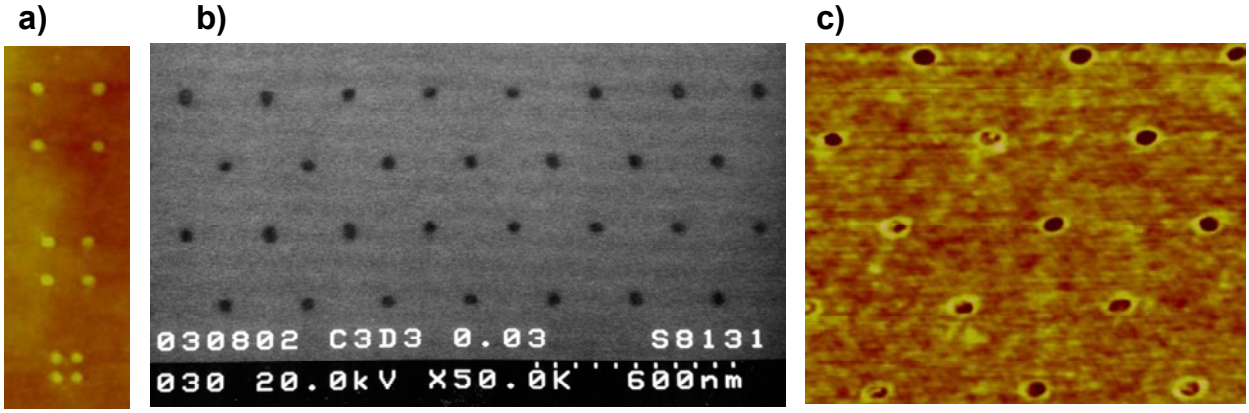

Figure 3. Catalyst patterns defined by electron beam lithography. a) AFM image of 8 nm thick Fe dots, ~50 nm in diameter, patterned by liftoff; b) SEM picture of 30 nm diameter pores, 10 nm deep with 2 nm thick Fe layers in the holes, patterned by reactive ion etching of SiO_2, followed by deposition and liftoff of Fe; c) AFM image of Fe-containing pores.

INFRARED DETECTORS BASED ON SELF-ORGANIZED CARBON NANOTUBE ARRAYS

Final Report

JPL Task 939

David Z. Ting, Sumith V. Bandara, Sarath D. Gunapala,
John K. Liu, and Sir B. Rafol, Section 384

A. OBJECTIVES

The objective of this study is to explore the possibility of using carbon nanotubes for infrared detector applications. The unique structural and electronic properties of carbon nanotubes (CNTs) have generated great interest in using this new class of material for a wide range of device applications. Electrically, depending on the structure, CNTs can be either semiconducting or metallic, and can behave as quantum wires. Although the technology for fabricating CNTs in macroscopic quantities has been developed previously, the material produced tended to be entangled (spaghetti-like), and was difficult to process. Recently, our collaborators at Brown University (Prof. Jimmy Xu's group) have been able to produce **arrays of highly-ordered carbon nanotubes** fabricated on **nano-channel alumina (NCA)** plates. Unlike nanotubes fabricated by other means, which tended to be entangled bundles or random matrices of CNTs with varying dimensions, samples produced by the new technique are highly-ordered, large-area, two-dimensional arrays of densely-packed CNTs with unprecedented uniformity in diameter, length and orientation. These dense (10^{11} cm^{-2}) arrays contain nanotubes

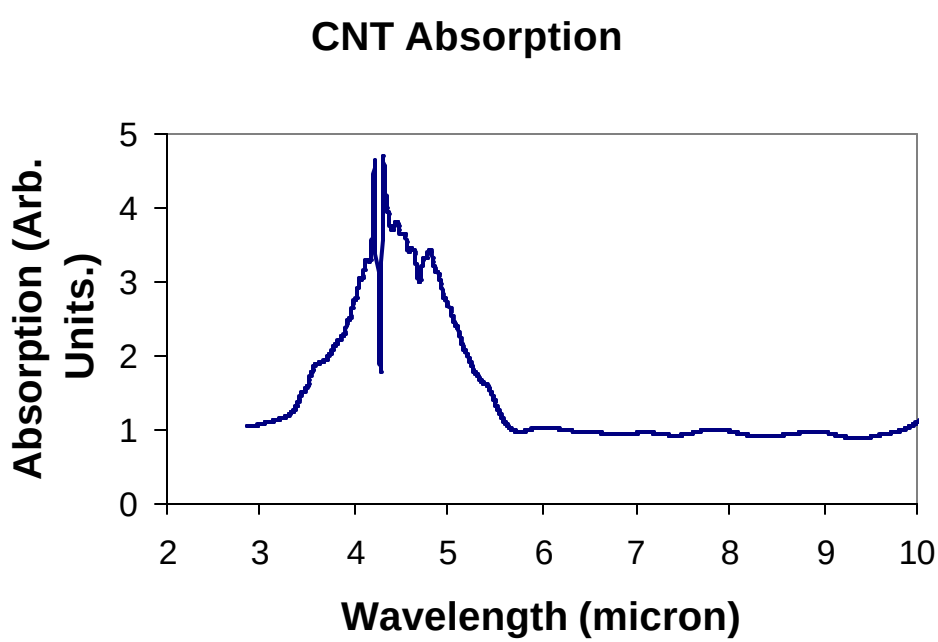

Figure 1. Infrared absorption characteristics of ordered carbon nanotubes grown on nano-channel alumina template.

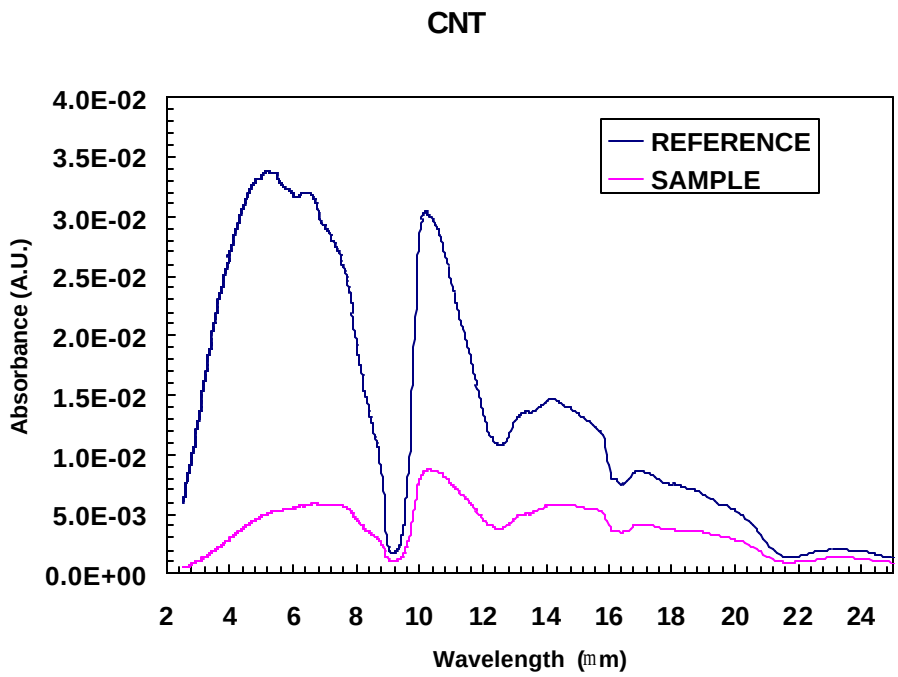

Figure 2. Infrared absorption characteristics of aligned carbon nanotubes grown at JPL on silicon substrate.

with selectable diameter sizes ranging from 10 to 350 nm, and lengths of up to 100 µm. The inter-tube spacing in the CNT arrays can be made to be as small as 30 nm. In contrast, the smallest achievable feature size using the much more expensive and time-consuming process of electron-beam lithography is 100 nm. This breakthrough material growth technology has made carbon nanotubes amenable to planar processing, and brought device applications to within reach. For this study in particular, we intend to test CNT arrays for infrared detector applications.

B. PROGRESS AND RESULTS

We have measured the infrared response of carbon nanotube samples obtained from Prof. Jimmy Xu's group at Brown University. These samples were grown on nano-channel alumina templates which, in turn, were grown on aluminum substrates which are opaque in infrared. The aluminum substrates must be removed before infrared response can be measured in the Fourier Transform Infrared spectrometer. This process requires considerable care in order that the carbon nanotubes themselves are not damaged during the process. The sample shows peak response in the 3 to 5 micron wavelength regime, but drops off at longer wavelengths (see Figure 1). We believe the drop-off in infrared response may be due to the reflection characteristics of the alumina template.

The unfavorable characteristics associated with the aluminum substrate processing and alumina template reflections led us to look for alternative solutions. We were able to obtain samples of dense, aligned carbon nanotubes grown on silicon substrate from Michael Hoenk, Michael Bronikowski, and Brian Hunt at JPL. Silicon substrates are infrared-transparent and greatly simplify sample preparation. Infrared response is shown in Fig. 2. The response seems to be over a broad spectrum and extends to 20 microns. Good absorption quantum efficiency, shown in Fig. 3, is observed over a wide spectral range.

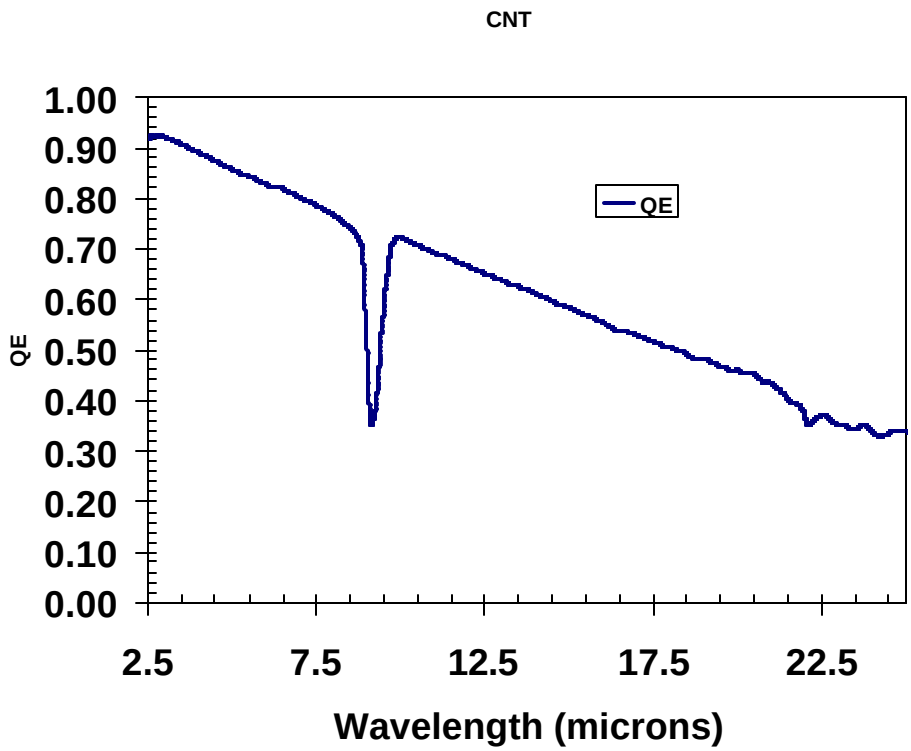

Figure 3. Absorption quantum efficiency of aligned carbon nanotubes grown on silicon substrate.

C. SIGNIFICANCE OF RESULTS

The results indicate that for infrared absorption applications, aligned carbon nanotubes grown on silicon substrates are probably better candidates than those grown on nano-channel alumina templates. Further advances in carbon nanotube growth techniques allowing the control of tube size would make them more favorable for infrared applications.

D. FINANCIAL STATUS

The total funding for this task was $25,000, all of which has been expended.

E. PERSONNEL

Prof. Jimmy Xu of Brown University supplied us with arrays of highly-ordered carbon nanotubes fabricated on nano-channel alumina (NCA) plates. Michael Hoenk, Michael Bronikowski, and Brian Hunt from JPL supplied the samples of aligned carbon nanotubes grown on silicon substrate.

F. PUBLICATIONS

None

G. REFERENCES

[1] J. Li, C. Papadopoulos, M. Moskovits and J. M. Xu, "Highly-ordered carbon nanotube arrays for electronics applications," *Appl. Phys. Lett.* 75, 367 (1999).

NANOTUBE ACTUATORS AND OSCILLATORS

Final Report

JPL Task 960

Brian D. Hunt, Michael Hoenk, Flavio Noca,
Dan Choi, Bob Kowalczyk, Space Microsensors Technology (384)
Prof. Michael Roukes, Dr. Jim Hone, Caltech

A. OBJECTIVES

Nanoscale structures are becoming increasingly important to NASA because they provide the basis for instruments and spacecraft with dramatically reduced power and mass, and enhanced capabilities. Practical nanotechnology-based applications will require nanoscale sensors and actuators for characterization and manipulation on the molecular scale. Nanoscale mechanical structures also enable the fabrication of high-quality-factor (Q) mechanical resonators with high mechanical responsivity. Such devices can form very low-loss, low-phase-noise oscillators for filters, local oscillators, and other signal-processing applications. Carbon nanotubes exhibit a number of unique properties which make them well-suited for nanoscale sensors, actuators, and oscillators. In particular, carbon nanotubes have high mechanical strength and enable direct electromechanical transduction, because nanotube length depends on charge injection. The present effort has been focused on the fabrication and testing of prototype nanotube actuators and oscillators relevant to future NASA sensors, actuators, and computers. The major objectives of this work are summarized below.

B. PROGRESS AND RESULTS

1) Development of growth and processing techniques to control nanotube location and orientation

Practical applications of carbon nanotube-based actuators and oscillators depend on the development of growth and processing methods for control of nanotube placement and orientation. These techniques are also critical for a wide variety of other nanotube applications, including nanotube electronic systems. This subtask was aimed at development of novel techniques for controlling nanotube growth, both perpendicular to and in the plane of the substrate. The nanotube growth was done by chemical vapor deposition (CVD) using ethylene or methane at temperatures ranging from 410°C to above 900°C [1]. We have studied a variety of catalyst layers including Ti/Ni bilayers, Fe, and inorganic-based spin-on catalyst coatings. Since catalyst particle size controls the nanotube diameter and growth rate, we have recently investigated chemical synthesis techniques for production of uniform iron oxide nanoparticles. Figure 1 shows a TEM micrograph of a sample from the first Fe_2O_3 synthesis run, indicating crystalline nanoparticles with good uniformity. The initial methane growth runs with the iron oxide nanoparticles exhibit many long straight nanotubes, demonstrating that this basic process is a good approach. An example of a straight lateral nanotube, grown from chemically-synthesized nanoparticles, will be presented below. We have also studied vertical CNT growth on nanoscale catalyst dots pat-

terned by e-beam lithography (EBL) or other techniques under a related program [1]. In addition, we have found that unpatterned sub-nm Fe layers lead to the growth of isolated near-vertical nanotubes, as will be seen in the next section. One technique for control of nanotube growth in the plane of the substrate was suggested by the observation that the nanotubes grow perpendicular to the local substrate surface. This indicates that a structure like that shown in Fig. 2a), in which a catalyst layer is capped by a refractory metal overlayer, should act to direct nanotube growth across a patterned trench. The refractory metal cap layer serves to prevent vertical nanotube growth, and also acts as an integrated metal electrode. Our initial experiments with this approach used an ethylene plasma-enhanced CVD process with Nb cap layers and Fe catalyst films. Typical results for this process are shown in Figure 2b), which is a top view of a somewhat defective nanotube bridging a 3μm-wide trench ion milled into a Nb/Fe/SiO_2 trilayer. More recently, we have discovered that much higher-quality CNT bridges can be produced using higher temperature methane growth, as will be seen in subtask 3.

2) Demonstration of a nanotube actuator based on a bimorph geometry

Because carbon nanotubes change length as a function of charge injection [2], a bimorph geometry structure (Figure 3a) can be used as a nanoscale actuator and force sensor. The basic idea is to grow single nanotubes on closely-spaced catalyst patterns with separate electrodes going to each tube. During growth, it is likely that the adjacent tubes will become attached along their sidewalls due to van der Waals attraction, as shown in the figure. Because the conductance perpendicular to the tube sidewalls is very low, this geometry should allow a significant differential voltage across the tube pair, which will result in one tube shrinking along its length, while the other tube expands lengthwise. The differential length changes produce a lateral motion of the paired tip ends as shown in Fig. 3a. Conversely, motion of the tube ends will generate a signal, so the device can act as a force sensor. We have recently taken a major step towards fabrication of a nanotube bimorph as shown in Fig. 3b. In this case, a sparse array of vertical CNTs was produced on a sub-nm layer of iron catalyst. The CNT density was high enough that bimorph configurations like that shown in the figure were quite common. While these structures do not include electrodes at this point, this is a very important demonstration of a key element of the proposed bimorph fabrication process. Future work on the nanotube bimorph will be funded by a new Code R BioNano program.

3) Demonstration and characterization of a nanotube oscillator

The primary oscillator geometry studied here was a nanotube bridge, suspended over a trench, with electrical contacts to both ends. Such a mechanical oscillator can operate with much higher-quality factors than conventional electronic resonators, and can have resonant frequencies in the GHz range for readily-achievable bridge lengths. Because the tube length depends on injected charge [2], a capacitively-coupled dc bias can be used to control the stress and resonant frequency of the suspended tube. To produce the required CNT bridge structures, we investigated high temperature CNT growth in methane, using the iron oxide nanoparticle catalysts of Figure 1 (in addition to the approach shown earlier in Fig. 2). Figure 4 is an SEM micrograph of a straight, high-quality nanotube bridge crossing a 100nm-wide SiO_2 trench patterned by e-beam lithography and wet etching. The calculated mechanical resonant frequency for this nanotube bridge *is close to 10 GHz*. This is a very important and promising initial result. To make this

into a useful device structure, metal electrodes will have to be incorporated. This will occur under a new DARPA program on nanotube-based mechanical resonators, which was awarded, in part, on the basis of progress in this DRDF seed effort. The work on this subtask has resulted in two New Technology Reports listed below.

C. SIGNIFICANCE OF RESULTS

This effort developed basic fabrication processes needed for production of nanotube-based actuators and oscillators. Carbon nanotube-based actuators and oscillators promise to enable a number of important JPL applications, ranging from molecular-scale characterization and manipulation, to ultra-low-loss mechanical filters and local oscillators for communications and radar, to rad-hard, low-power mechanical signal processors. This program has demonstrated prototype nanotube actuators and oscillators and provides the foundation for a wide variety of future NASA sensors, actuators, and computers. Furthermore, this collaborative effort with Prof. Michael Roukes' group at Caltech has helped strengthen JPL-Caltech ties in the important area of nanotechnology. The progress made in this seed effort and in complementary programs has led to follow-on funding from DARPA in a new program aimed at using carbon nanotubes for high-Q resonators for signal processing applications ("High-Q Mechanical Resonator Arrays Based on Carbon Nanotubes", $2.3M over 3 years, starting 10/01). It has also contributed to the winning of new funding from the ASTID program for nanotube-based acoustic sensors ($230K, 1 year), and the NASA Code R BioNano program for development of carbon and Si nanowire biosensors ($1.3M over 3 years).

D. FINANCIAL STATUS

The total funding for this task was $150,000, all of which has been expended.

E. PERSONNEL

In addition to the people listed on the title page, other personnel active in this effort include Eric Wong, Mike Bronikowski, and Dan Choi.

F. PUBLICATIONS AND PRESENTATIONS

[1] B.D. Hunt, F. Noca, M. Hoenk "Carbon Nanotube Actuators And Force Sensors," NASA NTR, NPO-21153. (9/00), Patent application, 1/02.

[2] B.D. Hunt, D. Choi, M. Hoenk, R. Kowalczyk, F. Noca, "Pattern-Aligned Carbon Nanotube Growth," NASA NTR, NPO-30205 (3/01), Patent applic. 4/02.

[3] B.D. Hunt, F. Noca, M. Hoenk, "A Carbon Nanotube Tunable High-Q Resonator And Spectrum Analyzer," NASA NTR, NPO-30206 (3/01), Patent applic. 4/02.

[4] D. Hoppe, B.D. Hunt, M. Hoenk, F. Noca, J. Xu, "Waveguide-Embedded Carbon Nanotube Array RF Filter and RF Filter Bank," NASA New Technology Report, NPO-30207 (3/01), Patent application 4/02.

[5] M. Bronikowski and B.D. Hunt, "Regular Arrays of Carbon Nanotubes Produced Using Templates from Nano-Structured Block-Copolymeric Materials," NASA New Technology Report, NPO-30240 (5/01).

[6] F. Noca et al. "Nanotube-Based Sensors and Systems for Outer Planetary Exploration," Outer Planetary Exploration Workshop, Houston, 2/21/00.

[7] M. Hoenk et al. "Carbon-Nanotube-Based Sensors and Systems," Nanospace 2001, Galveston, TX, March 13-16, 2001.

[8] *Invited: M. Bronikowski, "Carbon Nanotube Growth by HiPCO Process," APS March Meeting, 3/01, Seattle.

[9] B.D. Hunt et al. “Nanomechanical Resonators Based on Carbon Nanotubes,” Nanoscale/ Molecular Mechanics Meeting, Maui, Hawaii, 5/02.

G. REFERENCES

[1] B.D. Hunt et al., DRDF Annual Report on “Nanotube Engineering” (100656-00935, 10/02).

[2] R.H. Baughman, et al., “Carbon Nanotube Actuators,” *Science,* 284, 1340 (1999).

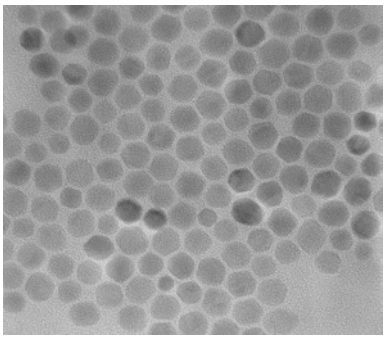

Figure 1. TEM micrograph of synthetic Fe_2O_3 nanoparticles with an average size of ~ 15 nm.

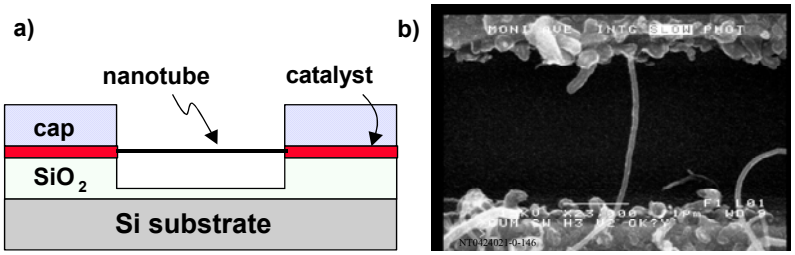

Figure 2. a) Side view schematic illustrating lateral nanotube growth from catalyst layer capped by a non-catalytic refractory metal overlayer. b) Top view of 3 µm lateral nanotube grown with ethylene PECVD process and capped catalyst structure.

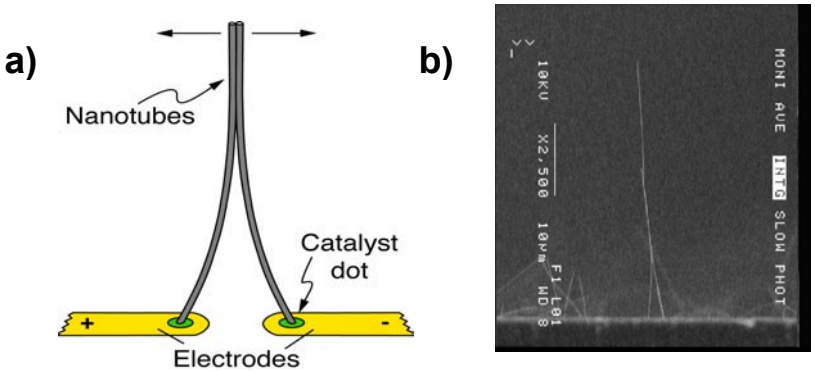

Figure 3. a) CNT bimorph force sensor and actuator. Motion of the tube ends generates a voltage, and conversely, charge injection results in deflection. b) SEM side-view micrograph of nanotube bimorph grown on sub-nm Fe catalyst layer.

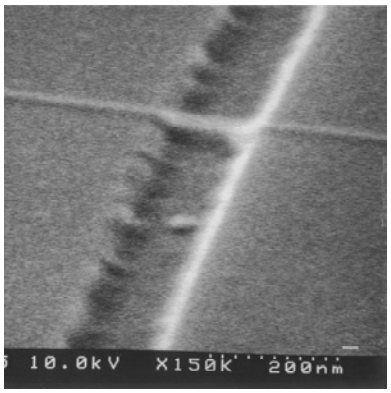

Figure 4. High quality nanotube produced by 900°C methane growth with Fe_2O_3 nanoparticles, spanning a ~100nm-wide SiO_2 trench patterned by e-beam lithography and wet etching.

CARBON NANOTUBE FIELD EMITTERS FOR MINIATURE MASS SPECTROMETERS AND NANOKLYSTRONS

Interim Report

JPL Task 1018

Harish M. Manohara, Microwave Experiment Systems and Technology Section (386)
Peter H. Siegel, Microwave Experiment Systems and Technology Section (386)
Michael Hoenk, Section 384
Murray Darrach, Section 323
Ali Husain, California Institute of Technology
James Hone, California Institute of Technology
Michael Roukes, California Institute of Technology
Axel Scherer, California Institute of Technology

A. OBJECTIVES

This is a seed proposal to develop ordered, grid-integrated carbon nanotube (CNT) field-emission arrays for use as ionizers in miniature mass spectrometers and as a cold cathode in the nanoklystron, a microminiature source of terahertz radiation. Both of these devices are essential components for future lightweight, low-cost, robotic space missions.

Objectives of this proposal are to 1) fabricate dense, unidirectional carbon nanotubes with monolithic integrated grids, 2) test the field emission characteristics of these nanotubes in a generic emission test system, built using this grant, which can also be used for assembling and packaging nanotubes with micro devices, and 3) demonstrate the use of these new emitters in prototype compact gas ionizers and nanoklystrons. The proposal represents a multidisciplinary effort spanning four different research groups at JPL and Caltech, drawing from and merging their combined strengths and device needs.

B. PROGRESS AND RESULTS

Significant progress has been made in achieving the goals initially set out. Table 1 below compares the original task implementation plan with the tasks accomplished so far (■ indicates the originally-planned milestone period, and ■ indicates the accomplished milestones in this reporting period). From the table, it is clear that the project is well on course in this reporting period (that is, the first six months), making progress faster than initially expected. We have finished first field emission tests of single-walled nanotubes (SWNTs) fabricated at Caltech (see Figure 1), and multi-walled nanotubes (MWNTs) fabricated at JPL (see Figure 2).

***Table 1**. Status of the project with respect to the original task implementation plan*

Tasks	First 6 Months	Second 6 Months	Third 6 Months
SWNT and MWNT growth on plain and patterned substrates			
Field emission test system construction			
Fabrication of stand-alone grids for initial testing			
First field emission tests			
Integration of grid on SWNTs and MWNTs			
Second field emission tests			
Possible assembly of nanotubes into a Nanoklystron prototype			
Designing of field emission source for miniature gas ionizers			

1. Science Data

Figure 3 shows a sketch of the measurement setup that was used for field emission testing. Figures 4 shows cumulative field emission graphs for all the samples. Field emission phenomenon is defined by the Fowler-Nordheim equation: $ln\ (I / V^2) = ln\ (a) - b / V$, where I is the emission current (in A), V is the biasing voltage (in V), a and b are the F-N parameters, which qualify the field emission characteristics of a given sample. Figure 5 shows comparative Fowler-Nordheim (F-N) plots for all the samples. Linearity of the curves proves field emission. By fitting the F-N curves, parameters a and b of the F-N equation have been calculated. The individual results breakdown is given below (Note: Threshold voltage mentioned below is tube density dependent, as it gives a macroscopic value of the total measured current over the entire emission area).

(1) SWNT (Caltech): Tube diameter ~ 5 nm; threshold voltage for 1 mA/cm^2 emission density ~ 18 V/μm; maximum measured current density ~7.4 mA/cm^2 @ 30.7 V/μm; F-N parameters, $a = 4.11\times10^{-6}$, $b = 3054$.

(2) MWNT (JPL) sample 1: Tube diameter ~ 50 nm; threshold voltage for 1 mA/cm^2 emission density ~ 2.3 V/μm; maximum measured current density ~25.5 mA/cm^2 @ 3.6 V/μm; F-N parameters, $a = 3.44\times10^{-6}$, $b = 3349$.

(3) MWNT (JPL) sample 2: Tube diameter ~ 50 nm; threshold voltage for 1 mA/cm^2 emission density ~ 3.8 V/μm; maximum measured current density ~32.3 mA/cm^2 @ 6.25 V/μm; F-N parameters, $a = 1.98\times10^{-6}$, $b = 5257$.

2. Other Results

As planned in the original proposal, a multipurpose ultra-high vacuum (UHV) chamber was constructed for field emission testing as well as for the nanoklystron device assembly and testing. Figure 6 shows a photograph of the test chamber, which is currently being used for field emission testing.

C. SIGNIFICANCE OF RESULTS

This task is in the process of developing high-current-density, low-threshold-voltage field emission sources for a nanoklystron (a novel source of terahertz radiation) and a miniature mass spectrometer (to chemically analyze complex environments and safeguard astronaut health through environmental monitoring). Both of these instruments are of great significance for future NASA missions.

The results indicate that low-emission threshold voltage is already possible and can be further improved by adding extraction grids. Also, the measured current density is already suitable for preliminary tests with the miniature mass spectrometer. However, the emission density is still less than that required to realize a high-power-output nanoklystron. But adding focusing grids and improving the planarity of emission tips is anticipated to help achieve this goal.

D. FINANCIAL STATUS

The total funding for this task was $156,500, of which $78,230 has been expended.

E. PERSONNEL

Wei Lien Dang (SURF student from Caltech)

F. PUBLICATIONS

[1] H. Manohara, P.H. Siegel, C. Marrese, B. Chang, J. Xu, "Fabrication and Emitter Measurements for Nanoklystron: A Novel THz Micro-Tube Source," Third IEEE International Vacuum Electronics Conference - IVEC 2002, Monterey, CA, April 23-25 (2002)

G. APPENDIX: *FIGURES*

Figure 1. SWNTs from Caltech

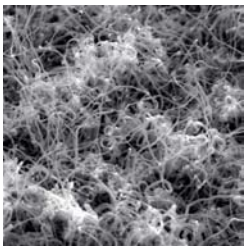

Figure 2. MWNTs from JPL

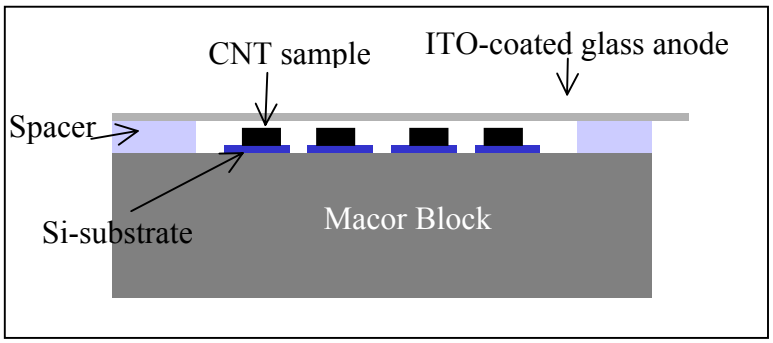

Figure 3. Field emission measurement setup

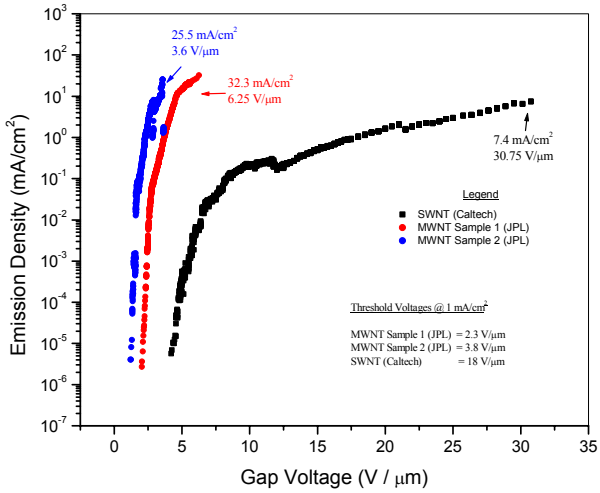

Figure 4. Normalized field emission curves for SWNTs and MWNTs

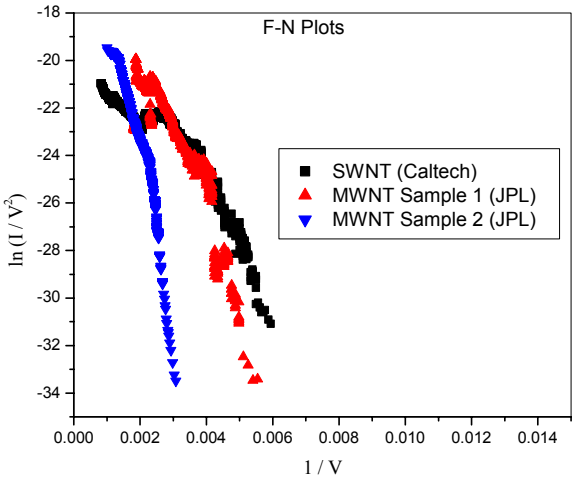

Figure 5. Fowler-Nordheim curves for SWNTs and MWNTs

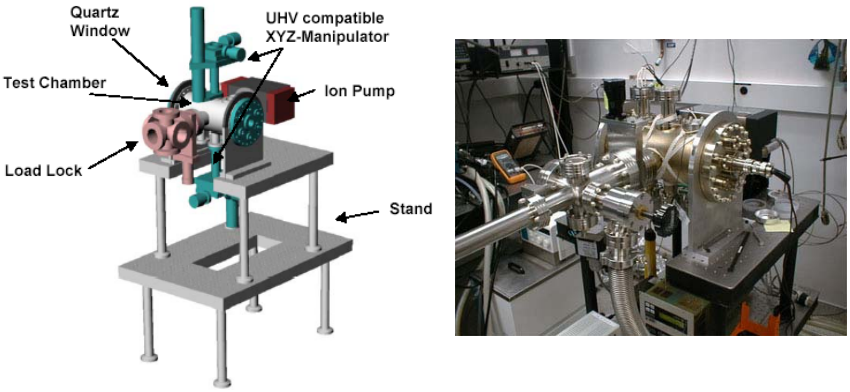

Figure 6. UHV chamber for field emission testing and for nanoklystron assembly and testing

SUBMILLIMETER-WAVE MOMED MIXERS FOR EARTH AND PLANETARY REMOTE SENSING

Interim Report

JPL Task 1025

John J. Gill, John E. Oswald, Peter H. Siegel, Microwave and Lidar Technology Section (386)
Michael Janssen, Earth and Space Sciences (320)

A. OBJECTIVES

In recent years, a new-style device technology, MOMED (Monolithic Membrane Diode) was demonstrated to replace old QUID (Quartz Upside-down Integrated Diode) by our team at JPL. The objective of this project is to analyze, design, fabricate, and demonstrate a 557 GHz fundamental mixer (heterodyne downconverter), based on MOMED technology, which can cover 530-595 GHz with a minimum instantaneous IF (intermediate frequency) bandwidth of 3 GHz. Replacing the QUID technology with MOMED process will substantially improve the repeatability, sensitivity, reliability, and performance of the final circuit. Specific sensitivity goals are <1500 K double sideband (DSB) for the downconverters with local oscillator (LO) power requirements below 3 mW. If successful, the same technology can be applied to 200, 400, 600 GHz receivers MLS (Microwave Limb Sounder), 500-600 GHz receivers for SIGNAL (a proposed Mars Scout mission) and VESPER (Venus Sounder), or future channels on SWCIR (Submillimeter Wave Cloud Ice Sounder) at 900 and 1200 GHz.

B. PROGRESS AND RESULTS

1. Science Data

The first stage of the work focused on the use of analytic tools for the design of the mixer device, the embedding circuitry and the feed horn. The mixer diode was modeled from the device parameters, including the semiconductor doping level and the anode size (see Figure 1). The analytical results suggest the design can achieve a DSB noise temperature of approximately 1000 K with between 7 and 8 dB of conversion loss (not including circuit losses expected to be about 0.5 dB) using an LO power level of about 1 mW (at the diode).

Next, the passive embedding structure (see Figure 2), including the microstrip filter (for signal separation) and a broadband waveguide coupling probe, was analyzed. The circuit parameters were optimized to match the diode operating impedance in order to achieve the desired RF bandwidth (530-595 GHz) while maximizing the IF bandwidth of the mixer.

Simulations of the mixer circuit, which were performed with variations on the LO drive level, the diode size and the semiconductor doping level, have given us the information necessary for effectively laying out a device mask design encompassing an appropriate array of variations to efficiently hone in on the best device design during the empirical phase of this task.

An input waveguide corrugated feed horn was separately designed analytically to achieve low sidelobe levels and E/H plane symmetry across the broad bandwidth of operation. The feedhorn is attached separately to the mixer block during testing.

2. Other Results

Wafer material has been purchased for use in the fabrication of the mixer devices. Planned activities for the final year of this DRDF effort include:

(a) Generation of a device mask set, including variations on anode size, diode finger length, transmission line matching circuitry and beam lead placement.
(b) Fabrication of devices and mounting structures.
(c) Fabrication of feedhorns
(d) Assembly and test of mixers.
(e) Iteration on design, if time permits.

C. SIGNIFICANCE OF RESULTS

Thus far, this task has developed a design for a broadband fundamental mixer, operating at a center frequency of 557 GHz with a DSB noise temperature of about 1000 K with low LO power requirements. This represents a significant improvement (by approximately a factor of 2) over the noise performance of the subharmonic QUID-style mixers at similar frequencies previously made for the MIRO (Microwave Imager for Rosetta Orbiter) and EOS-MLS (Earth Observing System Microwave Limb Sounder) instruments at JPL.

The sensitivity of these mixers can allow for much shorter spectral line observation times, as well as the detection and characterization of weaker lines. The large observational bandwidth of the mixer can allow for a single receiver to measure many more spectral lines. This can lead to a less complex, less costly instrument by requiring fewer distinct receiver systems.

D. FINANCIAL STATUS

The total funding for this task was $274,000.00, of which $96,489.69 has been expended.

E. PERSONNEL

In addition to the personnel listed at the top of this report, Erich Schlecht of the Microwave and Lidar Technology section (386) participated in the design of the mixer, and Aluizio Prata of section 336 participated in the design of the feed horn.

F. PUBLICATIONS

None.

G. REFERENCES

[1] P.H. Siegel, R.P. Smith, S. Martin and M. Gaidis, "2.5 THz GaAs Monolithic Membrane-Diode Mixer," IEEE Trans. Microwave Theory and Tech., v. 47, no. 5, May 1999, pp. 596-604.

[2] Michael C. Gaidis, H.M. Pickett, C.D. Smith, R.P. Smith, S.C. Martin and P.H. Siegel, "A 2.5 THz Receiver Front-End for Spaceborne Applications," IEEE Transactions Microwave Theory and Techniques, MTT-48, no. 4, April 2000, 733-739.

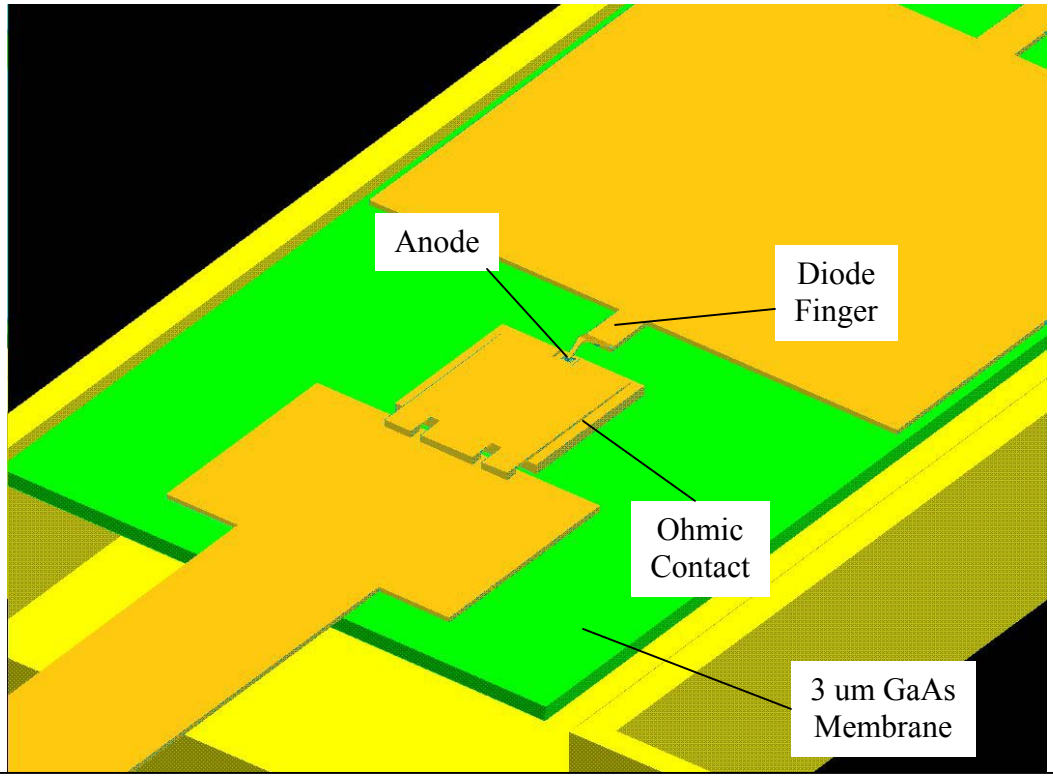

Figure 1: MOMED mixer diode.

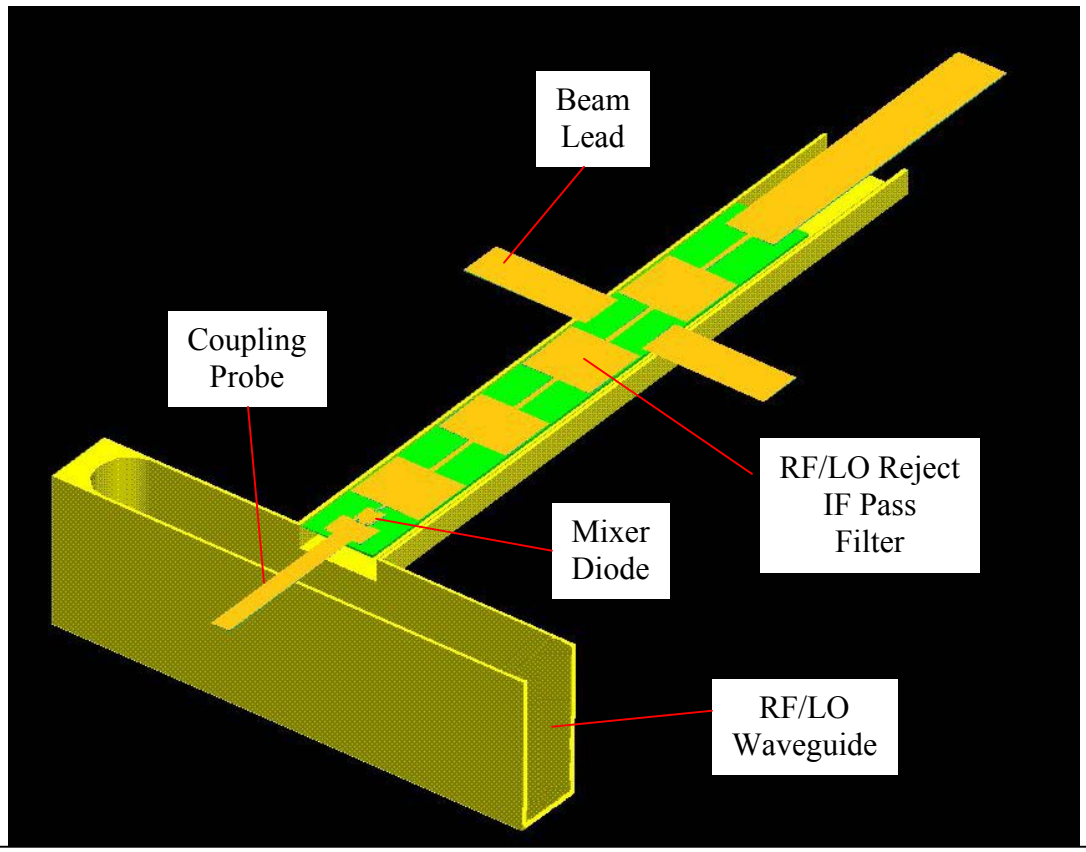

Figure 2: Complete mixer circuit, including device and passive embedding structure.

TOWARD ARTIFICIAL NANOSCALE SYSTEMS: SELF-ASSEMBLED POLYMERIC TEMPLATES FOR FABRICATION OF CARBON NANOTUBE ARRAYS

Final Report

JPL Task 1026

Michael J. Bronikowski, Michael E. Hoenk, Robert S. Kowalczyk, Eric W. Wong,
In-Situ Technology and Experiments Systems Section (384)

A. OBJECTIVES

Nanoscale technology is becoming increasingly important to NASA because it will provide a foundation for advanced spacecraft and instruments with low mass, low power requirements *and* enhanced performance and capabilities. Carbon nanotubes (CNT) hold great promise for a variety of nanoscale applications relevant to future NASA missions. In particular, regularly-spaced arrays of CNT are expected to have wide-ranging applications in the areas of sensing and communications, including high-Q, high-frequency, nano-scale oscillators; local oscillators for high-frequency receivers; nanometer-scale RF filters, signal detectors and analyzers; spectrum analyzers for mechanical vibrations; and filter media for electrophoretic separations of biomolecules (especially relevant to the thrust area of astrobiology).

In this work, we proposed to apply the principles of molecular-scale self-assembly to the creation of regular arrays of carbon nanotubes for applications in nano-scale electrical and mechanical systems. The key to this effort involves assembly on substrates of regular arrays of identically-sized nm-size particles of catalytic metals (Fe, Ni), from which can be grown regular arrays of identical CNT (and potentially nanotubes of other materials as well). The catalyst dot arrays are created using self-assembling molecular templates made from a class of molecules called block copolymers (BCP's). The objective of this work has been to demonstrate the growth of regular arrays of CNT from arrays of catalyst dots, created using self-assembling BCP films.

B. PROGRESS AND RESULTS

Block copolymers of polystyrene (PS) and polymethylmethacrylate (PMMA) were acquired from commercial sources with a variety of lengths of the two different polymer blocks. Thin films of these materials were prepared by spin-coating toluene solutions of the polymers onto Si and SiO_2/Si substrates. The thickness of the film could be controlled by varying polymer concentration or spin speed. Upon annealing for 14 - 18 hours at 165°C, these polymer films were found to self-assemble into ordered structures consisting of alternate zones of PMMA and PS. Figure 1 shows an example, an array of PMMA cylinders in a PS matrix, as imaged by AFM in phase-contrast mode (image is 1µm x 1µm). This film is a 40 nm-thick film of a BCP, consisting of 460 monomers of PS and 210 monomers of PMMA; the PMMA zones are arranged in a hexagonal pattern with a high degree of local ordering. We found that the PMMA blocks in such thin films could be readily removed by exposure of the film to UV light followed by development in acetic acid, leaving a PS film with an array of holes [1].

The next step was to use these arrays of holes as masks through which to deposit an array of dots of metal catalyst for CNT growth. Catalytic metals such as iron or molybdenum would be sputter-coated onto the array of holes, then the PS layer would be lifted off (e.g., by sonication in toluene), leaving an array of metal dots upon the substrate. Deposition of metal dots in this way proved to be somewhat problematic. It was found that the pattern of metal dots replicated the pattern of holes only for very thin polymer films, 15 nm thick or less. However, such very thin films of BCP tended to show irregularities in the size and spacing of the PMMA blocks, most likely because of strong interactions between the polymer layer and the SiO_2 surface, which is irregular on the nanometer scale [2]. We could successfully deposit metal dots only through these thin films, with their irregularities; these irregularities were then reproduced in the resulting metal dot pattern. The result is that, to date, we have been able to deposit arrays of metal dots, but those arrays show some variation in the size and separation between the various catalyst dots. Figure 2 shows a typical example, an array of dots of molybdenum deposited using a 12 nm thick PS/PMMA BCP layer as a mask (image is 1μm x 1μm).

This irregularity in the thin BCP layer most likely arises from differential interaction with the surface of the PMMA block vs. the PS block [2]. It has been demonstrated [2] that one way to overcome such difficulties is to coat the substrate first with a very thin "brush" layer of a random copolymer of styrene and methylmethacrylate (MMA), then spin the BCP layer on top of this brush layer. We have had some success with this approach using commercially-available random PS/PMMA copolymers, but previous work suggests that the exact ratio of styrene to MMA is crucial in achieving the best results with this technique. Ongoing work is in progress, and it may be necessary to acquire custom-synthesized random copolymers in order to perfectly neutralize the substrate surface, and so eliminate irregularities in the BCP film.

The quality of the catalyst dot arrays obtained as above was judged to be sufficient to proceed to the next step, attempting to grow arrays of CNT from these catalyst arrays. In preliminary tests, we coated SiO_2 samples with thin layers of sputter-deposited Fe whose surface-average atom density was approximately the same as that of our catalyst dot arrays. Upon heating, the Fe atoms become mobile and will tend to agglomerate into larger aggregations, or iron particles. Thus a thin layer of Fe, coated uniformly upon a surface should, upon heating, assemble itself into a randomly-distributed array of Fe particles, and thus such a layer should form a reasonable "first order" test of the behavior of our Fe catalyst dot arrays. Such a proof-of-idea test was useful because thin uniform films of Fe can be prepared easily, while the BCP-assembled dot arrays are rather more time-consuming to fabricate. In this step, we sputter-coated SiO_2 samples with Fe layers of nominal thickness 0.1 nm or less, then attempted to grow CNT on these surfaces. The samples were loaded into a tube furnace reactor, then heated to 900 - 1000°C in the presence of flowing CH_4, sometimes diluted with H_2 or Ar. Under such conditions, hydrocarbons are known to catalytically decompose upon nm-size metal particles, and the carbon so liberated forms into nanotubes. Upon exposure to these CNT production conditions, our thin-Fe-on-SiO_2 samples produced sparse arrays of straight CNT, which grew perpendicular to the SiO_2 surface. Figure 3 shows a typical result.

The quality of the nanotubes produced in these preliminary growth tests was highly encouraging, but the process appeared to have a low yield: many fewer nanotubes grew than would have been expected based on the density of Fe atoms upon the surface, which determined the number of catalytic particles that should have been present. Nevertheless, we next attempted to grow CNT arrays using the arrays of catalytic iron dots deposited using the BCP self-assembly technique discussed above. In this stage of the research, we discovered another potential

problem. The process of growing CNT from methane was observed to be highly non-reproducible; some runs gave excellent yield of nanotubes, while other runs gave few or no nanotubes. This irreproducibility of CNT growth from methane has been observed previously [3], and has been attributed to the details of the CNT growth mechanism. Specifically, when CH_4 is used as the carbon source gas for CNT, it is believed that the CNT growth occurs due to decomposition upon the catalytic particles, not of methane, but of higher hydrocarbons into which the CH_4 has been converted while traversing the hot reactor tube. Thus, CNT growth results depend strongly on such experimental parameters as flow rates, heating rates, and even the order in which gases are introduced into the reactor. To date, growth runs using our BCP-prepared catalyst dot arrays have not produced any CNT. Note that in growth experiments with these dot arrays, "witness samples," consisting of thin Fe films on SiO_2, were placed in the reactor alongside the BCP-prepared samples to verify that growth conditions were appropriate to grow CNT. In all experiments on BCP-prepared catalyst dot arrays, these witness samples also failed to grow any CNT, indicating a problem with reaction conditions, not necessarily a problem with CNT growth from the dot arrays. We are currently in the process of optimizing our growth conditions for reproducibility and CNT quality, and once this is accomplished we should be able to grow CNT arrays from our catalyst dot arrays.

C. SIGNIFICANCE OF RESULTS

We have demonstrated the use of BCP templates in fabricating arrays of dots of catalytic metals for growing arrays of CNT, and have begun to investigate the growth of CNT from these arrays. Ongoing work will address specific issues of better ordering and regularity in the self-assembled BCP materials (and resulting catalyst dot arrays), and issues of reproducibility and nanotube quality in the CNT grown from these arrays. Our initial results are encouraging, and indicate that the proposed concept (regular CNT arrays fabricated using self-assembled BCP structures) should be feasible, but clearly more research and fine-tuning is needed.

This ongoing research effort is developing the basic fabrication processes for regular arrays of carbon nanotubes for use in nanotube-based sensors, electronic components, and media for biomolecular analysis. The results of this effort will enable a variety of new sensing and instrumentation technologies, and hold great promise for a variety of nanoscale applications relevant to future NASA missions, including nanometer-scale, ultra-low mass and power sensors, electronic components, components in communications systems, and biomolecular analytical technologies of special relevance to the current thrust area of astrobiology.

The progress made in this seed effort and in complementary programs has already led to follow-on funding from NASA for a new research program aimed at using carbon nanotubes as detector elements in ultra-high sensitivity biomolecular sensors for use in extraterrestrial environments in the solar system such as Mars, Europa, and Titan ("Carbon and Silicon Nanowire Biosensors", NASA Code R, $1.4M over 3 years, starting 10/02).

D. FINANCIAL STATUS

The total funding for this task was $75,000, all of which has been expended.

E. PERSONNEL

In addition to the people listed on the title page, other personnel active in this effort have included Brian Hunt, Maggie E. Taylor, Daniel Choi and Roger Williams.

F. PUBLICATIONS

[1] M. J. Bronikowski, “Regular Arrays of Carbon Nanotubes from Metal-Impregnated, Nano-Structured Block-Copolymeric Materials,” NASA New Technology Report, NPO-30502. (2/02).

[2] M. J. Bronikowski and B.D. Hunt, “Regular Arrays of Carbon Nanotubes Produced Using Templates from Nano-Structured Block-Copolymeric Materials,” NASA New Technology Report, NPO-30240 (5/01).

[3] M. J. Bronikowski et al., "Growth of Aligned Arrays of Carbon Nanotubes from Patterned Catalyst Particles," contributed talk to be presented at the AVS 49th International Symposium, Denver, CO, Nov. 3 - 8, 2002.

G. REFERENCES

[1] T. Thurn-Albrecht et al., *Science*, 290 (2000) 2126.

[2] P. Mansky et al., *Science*, 275 (1997) 1458.

[3] J. Liu et al., private communication.

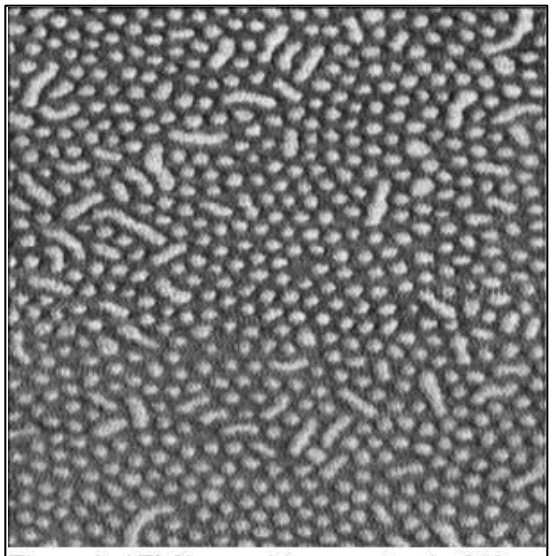

Figure 1: AFM image (phase contrast) of 40 nm annealed film of PS/PMMA, $S_{460}MMA_{210}$

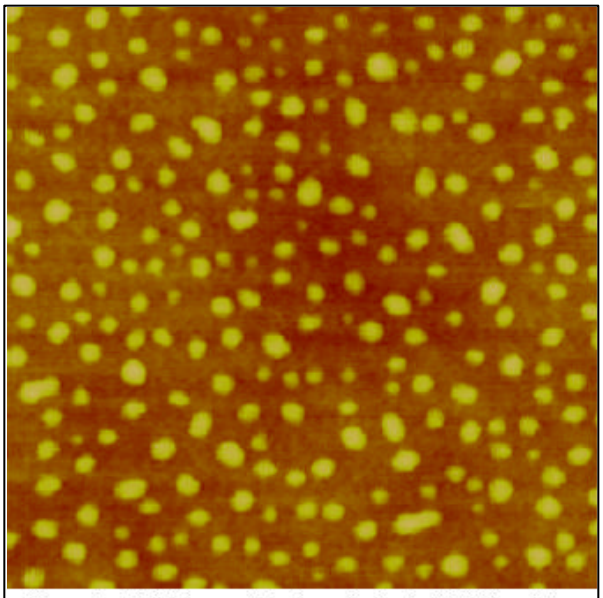

Figure 2: Molybdenum dots deposited using BCP template

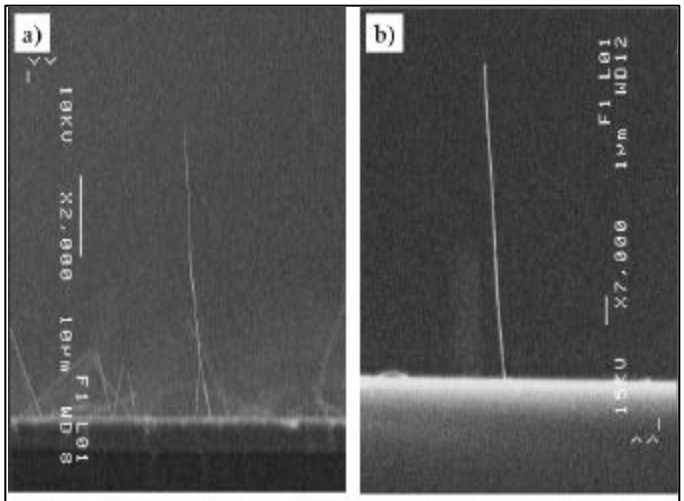

Fig. 3 a) Sparse array of CNT grown from thin Fe on SiO_2
b) Close-up of individual nanotube on this sample

A MICRO TURBINE POWER SOURCE FOR DEEP SPACE APPLICATIONS

Interim Report

JPL Task 1027

Beverley Eyre, In Situ Technology and Experiments Systems Section (384)
Dean Wiberg, Section (384), Kirill Shcheglov, Section (384),
Dr. Phillip Muntz (USC), Eric Moore (USC)

A. OBJECTIVES

The objective of this project is to fabricate a miniature-scale turbine using a novel fabrication method: three-dimensional LiGA using an inverse tomography approach. To put this effort into context, some information on this approach is appropriate.

As micro-fabrication technologies have matured, fabrication approaches have been driven by strategies of how micro-systems should be built. Some paths once thought to be promising, like monolithic electromechanical systems built from one standard process, have been largely abandoned in favor of others that offer solutions to problems that were not originally envisioned. As the strategy of "one process for everything" has faded, micro-systems built from two or more processes with later assembly has come to be thought of as the way these systems should be built. As this strategy has taken root, processes to build micro-parts for later assembly have become more central to whole area of micro-fabrication. Moreover, it has become clear that, while micro-systems are an idea whose time has come, meso-scale and even macro-scale systems can benefit from the use of micro-scale parts in some of their sub-systems.

LiGA (**Li**thographie **G**alvanoformung **A**bformung -- a German acronym meaning lithography, electroplating, and mold-making -- describes the processing steps involved in this technology) has become the prime approach for making precise micro- and meso-scale parts for many systems on all scales. Describing the process in brief: the long polymer chains in a high-molecular-density acrylic are broken up by exposure to soft x-rays generated by a synchrotron source. The acrylic is patterned by blocking some of the x-rays with a patterned gold mask. The acrylic is then placed in a developing bath to remove the exposed acrylic, leaving the unexposed material in the desired pattern. The acrylic is then used as a mold for electroplating (Fig #1).

Figure 1

Efforts to expand the range of parts that can be fabricated by LiGA are ongoing around the world, and JPL is a leader in this research. The limits being challenged are the thickness of the acrylic that can be patterned, and the hitherto inability to pattern parts in the "z" direction.

The technical approach of this project is to expand LiGA technologies into the area of 3-D parts using inverse tomography. Traditional LiGA parts are called 2-D because parts are only patterned in the x-y plane. The z dimension is always a straight vertical sidewall (Fig #1). So gears can be made, but not spheres.

However, tomography, the ability to reconstruct three-dimensional objects using two-dimensional projections, is a natural solution to the problem of fabricating three-dimensional LiGA parts. In theory, by using multiple masks and dynamic scanning techniques, exposed and developable areas within a substrate can assume arbitrarily complex shapes.

This project will use this capability to fabricate the compressor, the key element in the micro turbine power source.

B. PROGRESS AND RESULTS

The milestones for this project are:

- Design and build first-generation scanner module (no computer control).
- Design simple 3-D shape(s) to be fabricated.
- Fabricate 3-D part using first-generation scanning module.
- Design computer-controlled 3-D scanner with multiple degrees of freedom control.
- Software for performing translation from 3-D CAD model to projections to scanning motions.
- Build computer-controlled scanner.
- Design miniature turbine using data on process specifications.
- Design masks for compressor exposure.
- Fabricate compressor.

The initial steps in this project focused on creating a part using the basic idea, but without the computer-controlled scanner. The inverse tomography of the chosen shape, a cone (Fig #2), was straightforward, and only a single mask was necessary. To create this form within the substrate, a complex scanning scheme was used, using two scanners (Fig. #3), one mounted on the other to create the necessary complex motion.

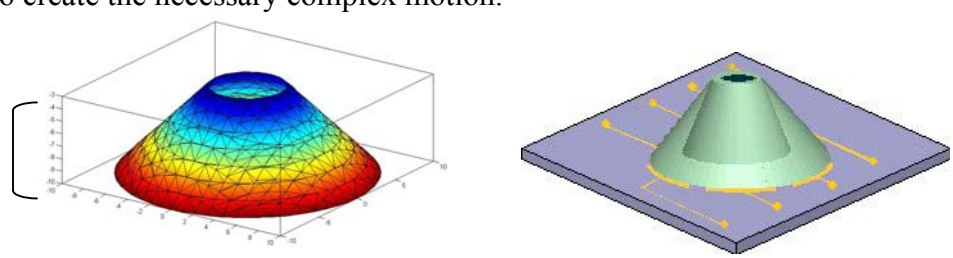

Figure 2: Initial design: simple cone fabricated using one mask and a two degree of freedom scan. The Z axis is no longer a straight sidewall.

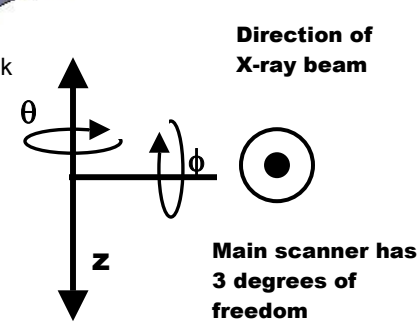

The main scanner (Fig 4) has 3 programmable degrees of freedom: along the z axis, θ rotates around the z axis, and ϕ rotates

around the axis perpendicular to the incoming x-ray beam. However, θ and ϕ rotations can only go 180 degrees, so full rotations cannot be achieved using this scanner alone. To accomplish this, and to implement the fabrication of the cone, another scanner was built to mount on the front end of the larger scanner and sit in the path of the beam (Fig.#4)

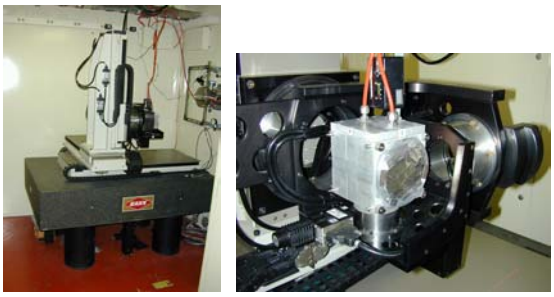

Figure 3: LiGA scanner with 3 degrees of freedom. Samples are mounted on the front block.

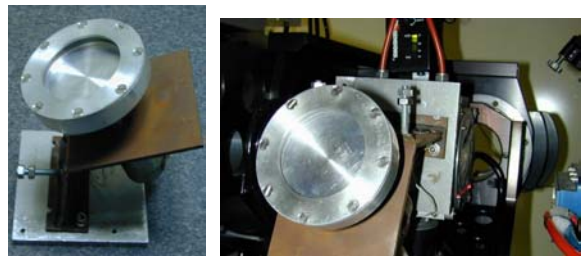

Figure 4: Rotary Scanner is mounted on the LiGA scanner.

This rotary scanner holds the sample at an angle to the path of the incoming beam and rotates. For this sample, two scanning motions were used: along the z axis, and rotation.

The results of the initial experiments were successful in exposing and developing a 3-D LiGA structure (Fig 5,6). Figure 7 shows the results of electroplating, which resulted in only a partially-plated cone. This step is the completion of the first three milestones.

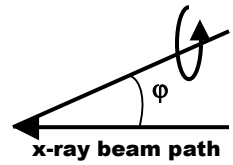

Sample rotates at an angle from the incoming beam. This angle φ defines the vertex angle of the cone.

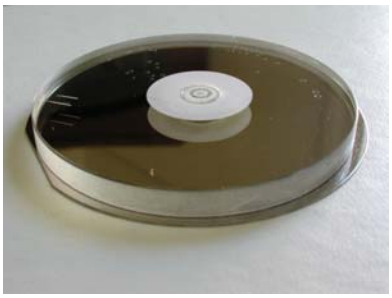

Figure 5: Exposed and developed substrate. 3-D structure is in the center.

Figure 6: Close-up of 3-D micro-mold ready to be electroplated.

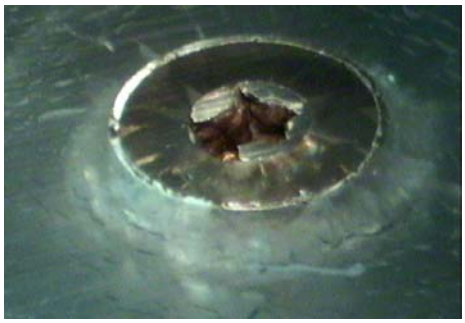

Figure 7: Electroplated cone

A more versatile scanner is needed for true inverse tomagraphic LiGA. The scanner module used in the initial experiments was for a simple proof-of –concept test. The next-generation scanner is also capable of rotation, is adjustable, and with computer control, is programmable. In addition to the rotation, it has 3 degrees of freedom along the x,y,z axes. This scanner is also a module and is mounted on the main LiGA scanner and used in conjunction with the programmable motions of that scanner.

The new scanner was designed in conjunction with Swales Aerospace with finished designs submitted July of 2002. Currently, Swales is awaiting the final contract to build the new scanner.

The software for the project falls into two categories: first, the software to run the scanners, and second, the algorithms to perform the inverse tomography. The scanners are run by LabView, and programming the drivers is currently being done by Cheryl Hauck -- an employee of the Advanced Light Source at Berkeley Labs, who acts as beamline coordinator for our beamline -- and myself. The driver software is in the 3rd generation, and successfully controls the scanner's 3 axes. Currently, we are working on an interface that allows the input from the inverse tomographic calculations.

The second piece of software is for calculating the inverse tomography, given the scanning parameters of our scanners and the shape desired. This code is still in the initial stages of defining the relevant algorithms.

The shape of the turbine is being modeled after an existing compressor. This model will be imported into a computational fluid dynamics program. Using the CFD program, the effectiveness of the compressor blades will be determined, and modifications will be made to the blades accordingly. By varying the shape and size of the blades of the compressor, an optimal blade shape and size can be chosen. Once the optimal shape of the blades is determined, the design will be scaled down to the appropriate size for a LiGA-fabricated micro-turbine. This shape will be represented as a vector array, and used as the input for the inverse tomographic calculation along with the parameters from the scanners.

With the completion of the new scanner and the mathematical representation of the compressor to be used in the design of the masks and scanning strategy, the systems will be in place to fabricate the first of the miniature compressors.

C. SIGNIFICANCE OF RESULTS

If true micro-machines, machines as complex as their macro counterparts, are ever to be made, several steps have to be completed. The fundamental one is discovering methods of fabricating parts on the appropriate scale. MEMS has hitherto been largely concerned with creating simple micro-systems comprised of bending beams or plates with associated strategies for detecting the motion of these elements. There have been attempts to create more complex devices, such as Sandia's comb-drive motors made from a special process, but MEMS devices for the most part are still simple and limited in usefulness. A well-characterized process for creating arbitrarily complex shapes on the micro-scale will revolutionize MEMS, and open up many new areas and applications in the field of micro-systems.

The results: demonstrating that a complex scanning/multiple mask approach, which can create true three-dimensional forms in LiGA, is a significant step towards the fabrication of the miniature turbine using the same process.

D. FINANCIAL STATUS

The total funding for this task was $125,000 of which $75,706.58 has been expended.

E. PERSONNEL

This project is being worked on by Dean Wiberg, Beverley Eyre, Kirill Shcheglov, Dr. Philip Muntz (USC), and Eric Moore (Grad student, USC). Some tasks are being contracted (Swales Aerospace) or assisted by people at the Advanced Light Source at Berkeley Labs.

F. PUBLICATIONS

None.

MICROINSTRUMENTS AND SMALL PAYLOADS

INTEGRATED REFLECTANCE/RAMAN MICROSPECTROMETER

Final Report

JPL Task 979

Pantazis Mouroulis, Space Experiments Systems &Technology Section (387)
Daniel W. Wilson, Paul D. Maker, In-situ Technology & Experiments Systems (384)

A. OBJECTIVES

We sought to prove the feasibility of a miniaturized instrument that would enable correlative reflectance and Raman microspectroscopy, performed on the same sample on the surface of a planetary body, with special reference to Mars. The instrument has two portions, joined by a common optical head which allows extraction of a reflectance or Raman signal from the same position on the sample with only minor repositioning, on the order of 100 μm. The instrument combines the following capabilities: confocal imaging at two different resolution/range levels, reflectance spectroscopy in the 400-2500 nm region with a resolution of 10 nm, and Raman spectroscopy over 4000 cm^{-1} with an average resolution of 3.3 cm^{-1}. The instrument can also serve as an expandable platform for adding fluorescence spectroscopy, or for examining samples from a distance of several meters while using the same spectrometer. In the course of this investigation, an additional capability was added: wide-field color imaging, to solve the problem of providing context for the spectral observations.

B. PROGRESS AND RESULTS

1) Design of front collection optics. This task has been completed successfully. An innovative lens system has been designed that combines not only the optics for the Raman and reflectance spectrometers, as originally envisioned, but also a miniature CCD camera lens, which would be very useful in providing context information. The front optic is shown in Fig. 1. The confocal collection part is a common Schwarzschild reflecting objective that achieves diffraction-limited performance at f/2. This is an obscured design and we take advantage of the obscuration to place the CCD lens in the unused part. The CCD lens is easy to fabricate and align, and the entire system, including fold mirror, sits in a tube that can be cemented to the inside of the reflective objective.

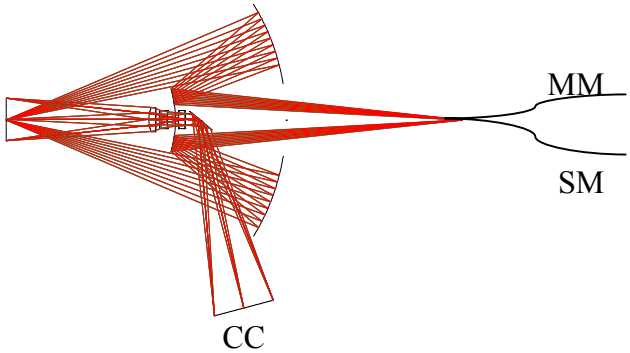

Figure 1: Raytrace of the optical head, combining confocal and wide-field optics. MM is the multimode fiber leading up to the reflectance spectrometer and SM the single mode fiber for the Raman portion. This design represents a significant evolution over our originally-proposed version.

It was not possible to implement this design in practice due to lack of funds. A set of commercial microscope objectives was used for experimentation.

2) Reflectance microspectrometer. As part of this task, we improved the confocal properties of the multimode fiber portion, demonstrating an improvement in vertical resolution by a factor of 2.3 over the earlier version. The vertical and horizontal resolutions are shown in Fig. 2.

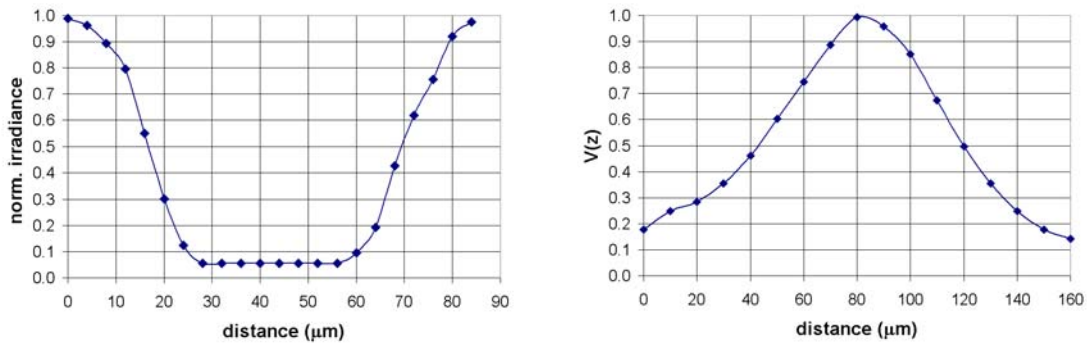

Figure 2. Left: Image of a 50 μm-wide slit through the multimode confocal fiber microscope. The residual signal at the bottom is due to the reflectivity of the glass substrate. 4x (de)magnification. A ~16 μm edge spread is observed at the 10-90% points. Right: Light intensity through a receiving fiber of 50-μm diameter as a function of focus. 4x (de)magnification, 0.35 objective NA. The vertical FWHM resolution shown is ~75 μm.

Lack of funds prohibited the construction of a stable spectrometer module with dedicated detector array. However, we were able to resolve the main question of the research regarding the stability of the signal through the fiber. We used a microbending cladding mode stripper to significantly alter the mode distribution in the fiber, and saw no change in the recorded spectrum. The spectra provided tantalizing hints for further research regarding the sample/optics interaction and the effect of the confocal mode operation on the depth of the observed absorption lines. This portion of the instrument was submitted as a MIDP proposal and received excellent reviews for potential science return and relevance, but was not funded.

3) Demonstration of the utility of fiber Bragg gratings in single-mode Raman spectroscopy. In this part, we examined the means through which two separate fiber Bragg gratings (FBGs) can be made to stabilize the laser diode wavelength and then extinguish the light from the diode. This work highlighted the difficulty of obtaining high-quality FBGs for anything other than telecommunications applications. The low-reflectivity gratings that were to be used for laser stabilization were not of sufficient quality (R too low). We were thus able to experiment only with the high-R grating. This was found to have an extinction of $8x10^{-4}$, which was not up to the specification (10^{-6}). However, it is certain that better gratings can be made; the problem is identifying a manufacturer willing to undertake fabrication. In any case, in order to test the effects of temperature, we subjected this grating to changes in temperature and stress. Both effects produce a shift in the center wavelength. Thus an athermal design where stress compensates for temperature is possible to implement. Figure 3 shows the shift in the spectrum of the FBG as a function of temperature and stress. The data were obtained using the Raman spectrometer module that is discussed in the next section.

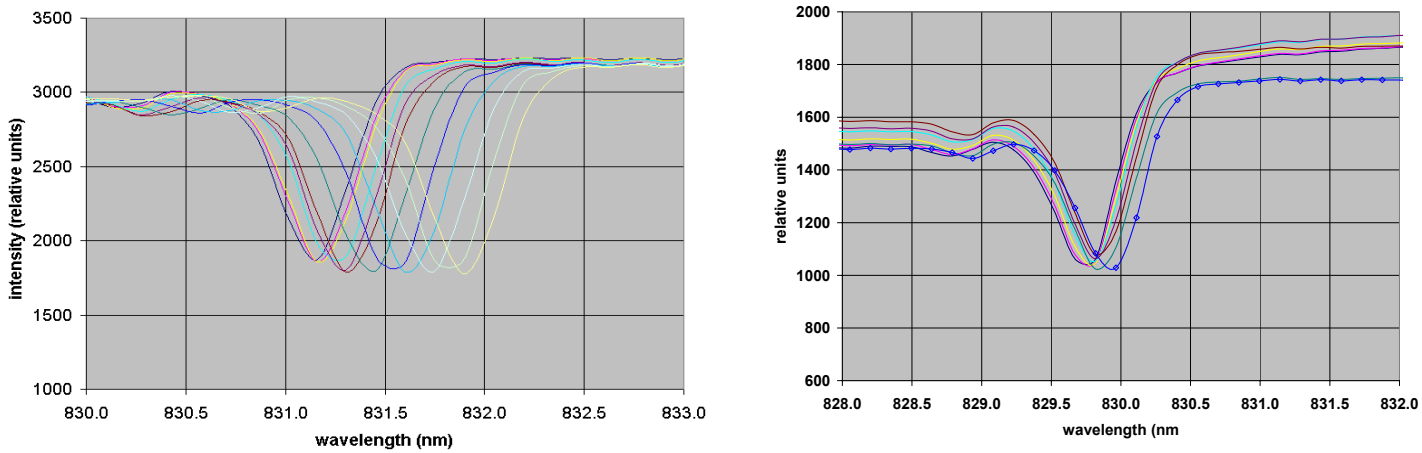

Figure 3. Left: Variation of the FBG spectrum with stress. The background illumination is provided by a superluminescent diode, the spectrum of which is filtered by the FBG. The dip shifts by ~1.7 nm for a total applied strain of $2x10^{-3}$. Right: Variation of the FBG spectrum with temperature. The leftmost curve is obtained for a temperature of 7°C and the rightmost one for 40°C. The observed temperature shift is 0.015 nm/deg. The absolute wavelength scale is only approximate and is not to be compared between the two pictures.

The confocal property of the single mode fiber probe was also investigated. Figure 4 shows the vertical resolution obtained. The horizontal resolution (edge spread) was 4 μm.

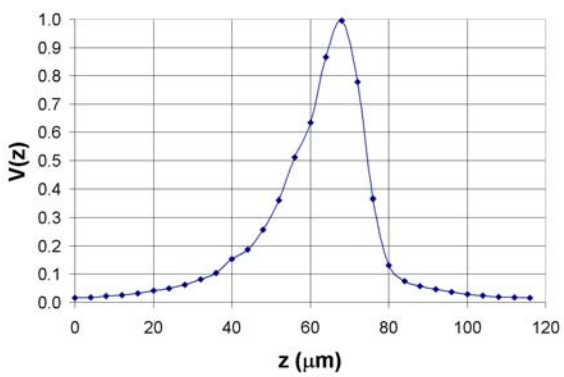

Figure 4. Light collected from a single mode fiber in a confocal arrangement, at 830 nm. A FWHM resolution of about 20 μm is demonstrated for 0.2 NA. The asymmetry in the curve is likely due to spherical aberration in the commercial objectives, which were not corrected for the infinite conjugate arrangement used.

4) Raman spectrometer module. A miniature spectrometer module was demonstrated. A new, fine-pitch (1.4 μm) grating was fabricated at MDL using E-beam lithography. This grating demonstrated outstanding phase continuity between panels (fields). It also was considerably steeper than previous gratings (27 deg. blaze angle compared with typically only a few degrees). The Raman spectrometer was assembled out of stock parts, with the grating being written on the convex face of a small planoconvex lens. A quick interferometric alignment method was developed that enabled alignment of the spectrometer module within ~1hr. The benchtop spectrometer module is shown in Fig. 5.

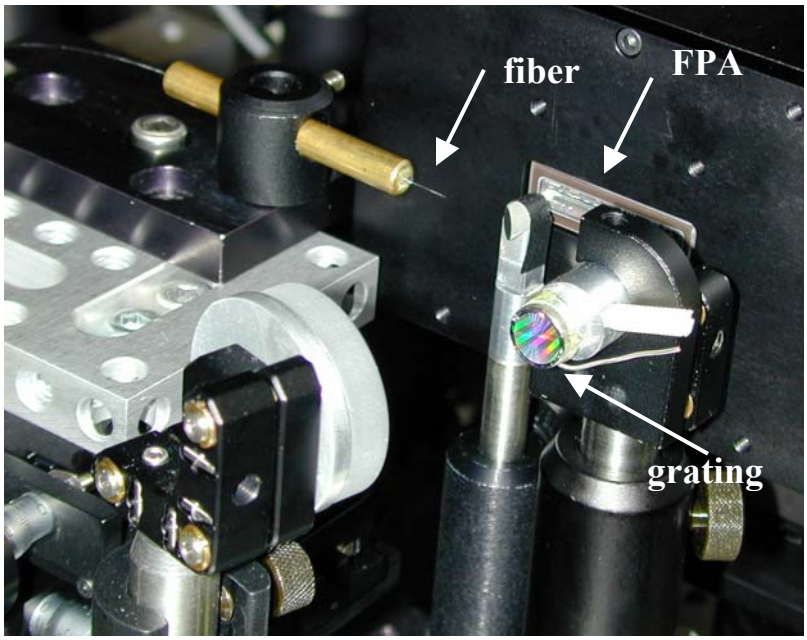

Figure 5. Assembled Raman spectrometer module, used to test resolution and to characterize the FBGs. Room lights diffracted from the grating are seen. For scale reference, the grating substrate is 10 mm in diameter (a dime is 18 mm).

C. SIGNIFICANCE OF RESULTS

These results open the way towards the development of an analytical spectroscopic capability on a rover with unprecedented potential science return, while at the same time reducing the volume and mass over competing approaches. The resulting instrument would be able to map the rover surroundings faster than a thermal IR spectrometer, be simpler to operate, and be more sensitive to water-bearing minerals. The microscopic portion would be able to examine individual mineral grains, map in three dimensions the surface of a rock or prepared sample, provide context information, return orders of magnitude more data than a Raman spectrometer alone, but use the Raman spectrometer whenever the discrimination capability of the reflectance portion fails, and identify iron-bearing minerals like a Mossbauer spectrometer but with high spatial resolution. The combination of all those capabilities in a compact instrument opens the way for smart-rover, autonomous Mars exploration.

D. FINANCIAL STATUS

The total funding for this task was $100,000, all of which has been expended.

E. PERSONNEL

In addition to the investigators, Leonard Wayne of Section 384 provided much-appreciated support with experimental setups and computer hardware and software.

F. PUBLICATIONS

1) P. Mouroulis, “Optical Design of a Reflectance/Raman Confocal Microspectrometer,” SPIE Proc. 4767, in press (2002).
2) P. Mouroulis, “Multimodal Imaging and Spectroscopy Platform”, *NASA Tech. Brief.,* NPO-30650

A PARTICLE SIZE AND CHARGE ANALYZER FOR INVESTIGATION OF THE ELECTRICAL PROPERTIES OF DUST DEVILS

Final Report

JPL Task 980

Gregory Wilson, Geophysics and Planetary Geosciences (3223)
Stephen Fuerstenau, In-Situ Technology and Experiments Systems Section (384)

A. OBJECTIVES

The objectives of the proposal were to develop an end-to-end electromechanical system for the simultaneous analysis of the size and charge of dust-sized particles at a high sampling rate. This included integration of pumping technology, signal-processing electronics, and data-analysis and display software. Included in the objective was to develop the measurement technique to the point where we could credibly propose for future funding from NASA instrument development programs.

B. PROGRESS AND RESULTS

1. Description of the new instrument.

The heart of the particle charge spectrometer (PCS) is a hollow metal tube, which serves as a Faraday cage, connected to the low-noise input transistor of a charge-sensitive preamplifier. A glass capillary (see Fig. 1) guides particles through the tube with a high-speed gas flow induced by a small air pump. Individual particles passing through the sensor generate pulses with amplitude proportional to the charge and width inversely proportional to particle velocity. Signals are analyzed with analog circuitry in the pulse-processing unit (white box in Fig. 2) that reduces each particle event to a pair of voltage values representing charge and transit time. These are digitized and relayed to a laptop computer for immediate display. A power supply completes the system (schematic illustrated in Fig. 3). The PCS requires about 1 watt each for operation of the preamplifier and the air pump. The major power consumption in the instrument is the micro-computer. In the next version of this device, the laptop computer will be replaced with low-power data-logging circuitry.

Because dust particles in the tube are accelerating, their speed at the position of measurement can be related to their aerodynamic diameter, which is a function of particle drag and inertia (Fig 4). A measure of particle size is obtained from each particle event, and is displayed in real time along with the particle charge in a plot of charge vs. size, as indicated in Fig. 5. The data acquisition, analysis, and display system is implemented with LabView software.

The PCS has been used to measure charge on a variety of dispersed dust samples in the laboratory including the JSC-1 Mars soil simulant. The data illustrated in Figure 6 were acquired

in the vicinity of a dust devil during the 2002 MATADOR campaign organized by the University of Arizona.

C. SIGNIFICANCE OF RESULTS

This task developed an end-to-end particle sample and measurement system capable of meeting measurement requirements. While the particle charge spectrometer (PCS) developed is capable of being deployed for field operations, it was only demonstrated in this way on a limited basis, with a handful of data sets collected in the Arizona desert. During prolonged periods of operation, the sensor head was susceptible to overheating in the 105°F temperatures encountered in those tests. Nevertheless, the preliminary observations confirm the predicted charge/size signature of particles in a dust devil. We have since altered the sensor design to reduce the temperature susceptibility. For the case of Mars, this sensitivity to warm temperatures will not be a problem.

The results indicate that the size and charge of dust particles can be measured at a rate greater than 100 particles per second. The minimum charge that can be detected on a particle of any size is 300 electrons with a noise level of 100 electrons. The instrument yields size information for particles in the range from 2 – 200 micrometers. The charge sensitivity of the PCS is at least 1000 times better than the next closest instrument of its type. Most single-particle charge-sensing devices developed for meteorology investigations have historically displayed sensitivities that are 100,000 times weaker than that of the PCS. This capability of the instrument represents a quantum leap forward in measurement capability. In sensitivity and speed, the PCS is matched only by the ESPART analyzer [1], a large instrument strictly intended for laboratory use. One drawback of the PCS approach is that it can only measure particles above the 300 electron threshold limit. Particles with less charge cannot be detected or sized.

The most significant result of research was the demonstration of the technique with a small, field-portable instrument requiring just a few watts of power. This demonstration was fundamental to the success of our Mars Instrument Development Program proposal. That proposal will follow on the groundbreaking work originally funded by this DRDF, including further instrument development and field operations and studies. The ability of the PCS to record charge on particles outside of the laboratory with ultra-sensitivity will open up new areas of research in environmental electrostatics.

D. FINANCIAL STATUS

The total funding for this task was $100,000, all of which has been expended.

E. PERSONNEL

No other personnel were involved.

F. PUBLICATIONS

None.

G. REFERENCES

[1] K.B. Tennal, M.K. Mazumder, D.A. Lindquist, J. Zhang, and F. Tendeku, "Triboelectric Separation of Granular Materials," Conference Record of the 1997 IEEE Industry Applications Society 32 nd Annual Meeting, New Orleans, LA, Vol. 3, pp. 1724-1729, October 5-9, 1997.

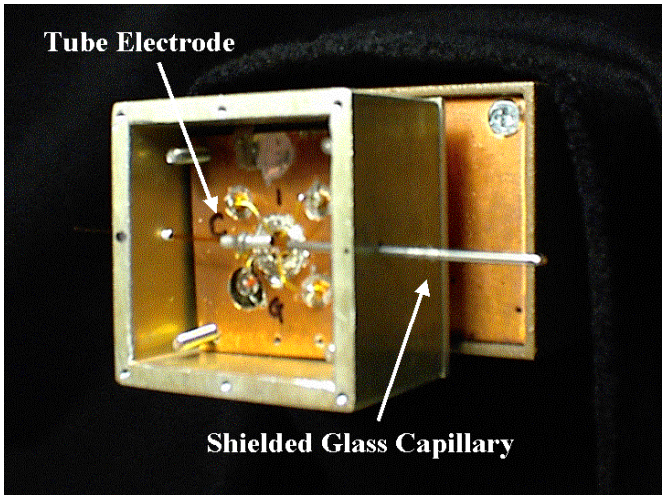

Figure 1. Glass capillary tube and metal tube electrode Faraday cage.

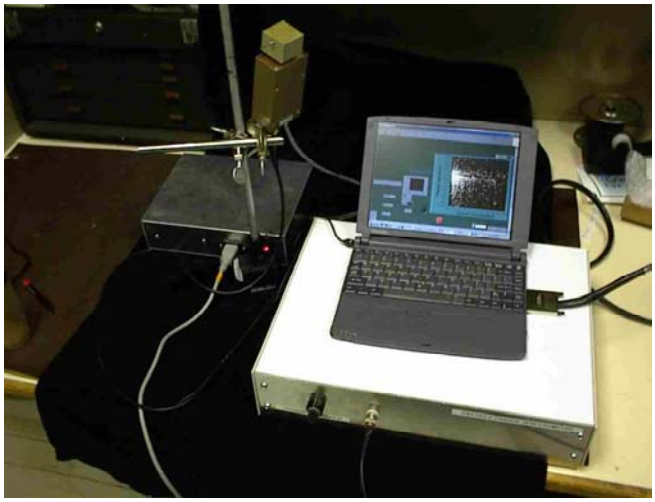

Figure 2. Complete PCS bench-top setup. White box under the computer is the signal-processing electronics.

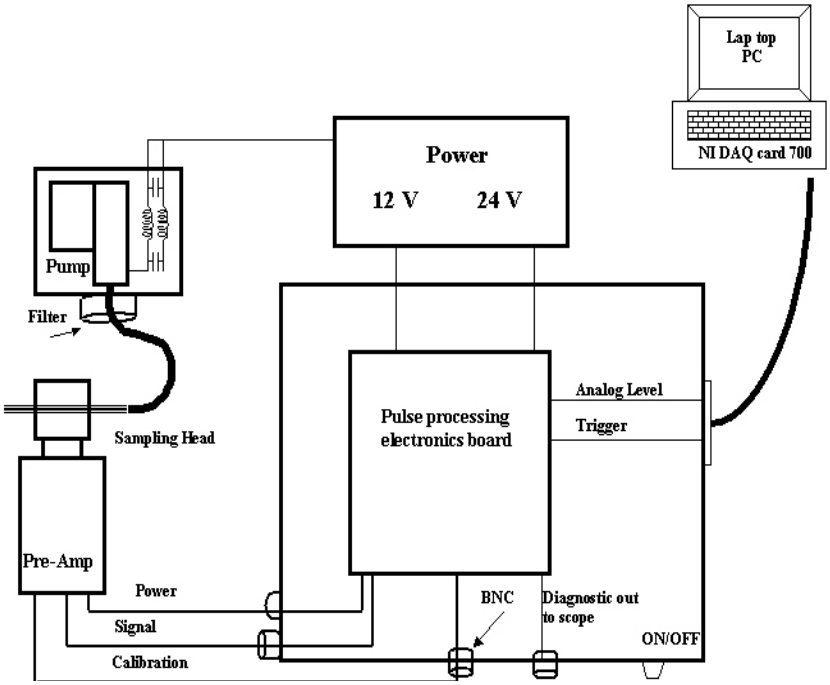

Figure 3. PCS system schematic.

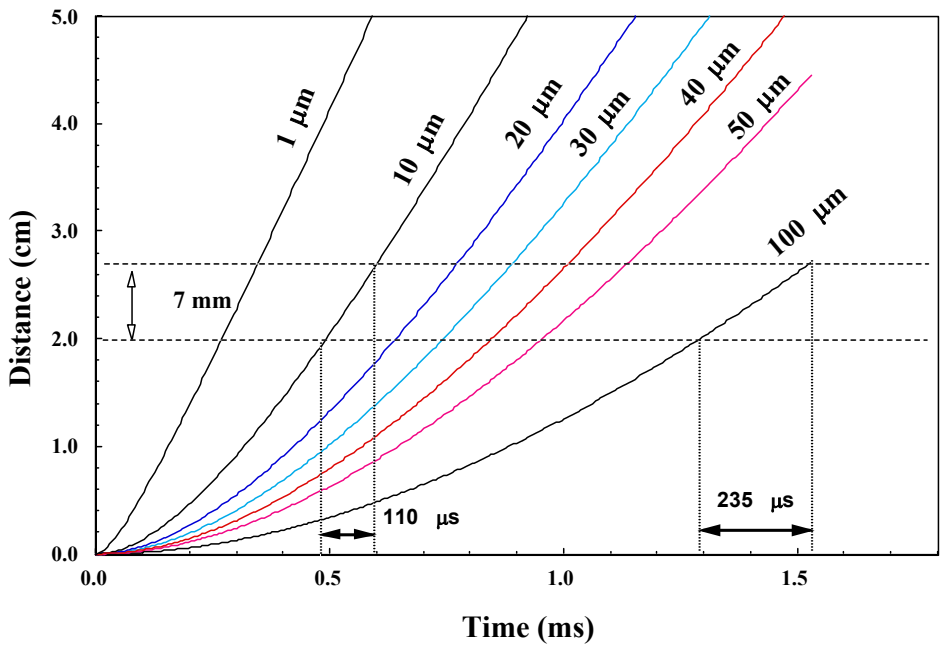

Figure 4. Calculated displacement trajectories for various-size particles accelerated from rest by a 100 m/s flow. All particle trajectories eventually reach the final slope, nearly achieved by the 1 µm trajectory in the first millisecond, which is the velocity of the flow. A 7 mm-long tube electrode, with its entrance placed 2 cm downstream of the inlet, will record a 110 µs transit time for 10 µm particles and a 235 µs transit time for 100 µm particles.

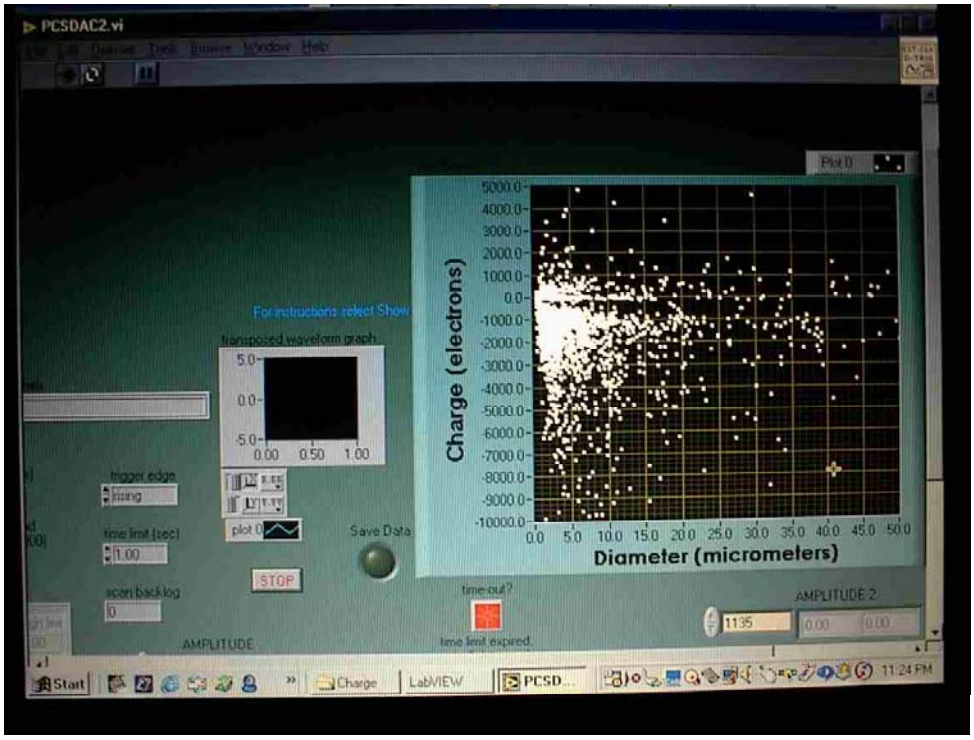

Figure 5. An example of the LabView real-time data analysis and display.

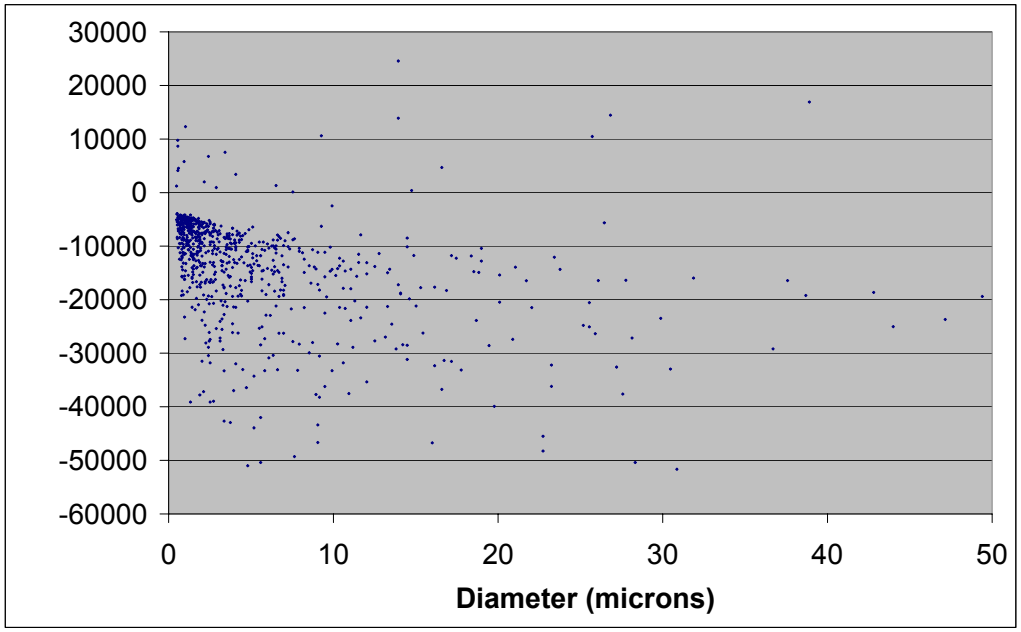

Figure 6. Particle charge and size data acquired in the vicinity of a dust devil during the 2002 MATADOR campaign organized by the University of Arizona.

MINIATURE AGE DATING /MATERIALS CHARACTERIZATION INSTRUMENT FOR MARS EXPLORATION

Interim Report

JPL Task 1017

Soon Sam Kim, Thermal and Propulsion Engineering Systems Section (353)
Stephen W.S. McKeever and Michael W. Blair,
Department of Physics, Oklahoma State University

A. OBJECTIVES

The objective is to develop a miniature age dating/material characterization instrument that will combine the most powerful dosimetric dating techniques, namely thermoluminescence (TL), optically-stimulated luminescence (OSL) and electron-spin resonance (ESR).

B. PROGRESS AND RESULTS

1. OSL Optical System Design

OSL Stimulation: We have gained experience with several Nd:YAG (2nd harmonic) laser diodes, but so far have not found one of suitable size, power and stability. Alternative stimulation sources are high-power LEDs. We have purchased several Nichia Ultra-Bright LEDs and have tested them for radiation sensitivity and stability as a function of temperature. The light output and peak wavelength have been shown to be stable (within 5% and 1 nm, respectively) for absorbed ^{60}Co gamma doses up to 500 Gy (far in excess of the doses expected to be experienced by the instrument). When operated in constant current mode (2.0 mA), the peak emission wavelength remained fixed and the output actually increased initially as the temperature was reduced.

We have used an array of Nichia diodes to successfully stimulate OSL emission from quartz. The diode array pack is shown in **Figure 1**. The array was manufactured by Risoe National Laboratory (Denmark) and consists of 6 clusters each of 6 diodes (36 LEDs in all) producing an estimated 25 mW of optical power at the sample. Figure 1 shows the array fitted with an end-window photomultiplier tube, which is unlikely to be the detector used in the final instrument.

(a) (b)

Figure 1: (a) Diode array, with photomultiplier tube; (b) diode arrays (6 x 6 clusters).

Photodetectors: We have carried out a preliminary search for potential photodetector devices, including photomultiplier tubes, P-I-N photodiodes and Avalanche photodiodes. On the basis of this, we have purchased the followed detectors:

- Hamamatsu Si Avalanche Photodiode S5343
- Hamamatsu Si P-I-N diode
- Hamamatsu H6240 side-window photomultiplier tube with integrated photon counter and power supply.

Selection of these devices was based on wavelength range, quantum efficiency and operational temperature. The devices have not yet been tested. We will conduct back-to-back tests for their wavelength dependence, efficiency and temperature dependence.

Radiation Source: To avoid the use of radioisotopes, we have decided upon an x-ray system for the radiation source in the instrument. We have identified a Moxtek "Bullet" miniature x-ray source (4W, 40 kVp) as a suitable x-ray system (**Figure 2**). This produces up to 40 keV x-rays from a Pd target. The system has not yet been tested. Performance parameters of interest include the divergence of the output beam, scattered radiation, and dose rate.

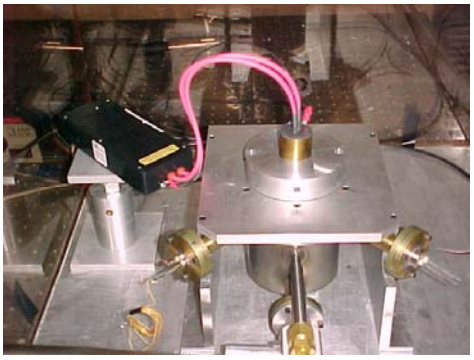

Figure 2: Moxtek x-ray unit and the low-temperature cryostat designed for laboratory characterization of the Martian simulant material

2. Characterization of Luminescence from Martian Meteorites

Our characterization program will include determining the most effective wavelengths of light to use in optical stimulation of the OSL from the simulant materials, tests for anomalous fading (signal instability), sensitivity tests, annealing temperatures, etc. With these characteristics determined at room temperature, we intend to devise measurement protocols (procedures) that will afford maximum utility for OSL stimulation and detection. We then intend to follow this with testing of the procedures at low temperature. For the latter, we have designed a test cryostat (shown in Figure 2) in which we will use the Moxtek x-ray unit.

Simulant materials: To date, we have tested samples from four Martian SNC meteorites, soil simulant JSC Mars-1, a Martian soil simulant (jeweler's rouge), and various feldspars. We have examined their basic TL and OSL properties. The studies investigated the main TL peaks, the OSL dose response curves to determine the maximum estimable radiation doses, and the ability to recover a given laboratory radiation dose (using dosimetric techniques). We have developed procedures for TL and OSL, and the following results have been obtained.

a. SNC meteorites: The TL and OSL results are summarized in Table 1. The SNC meteorites all have TL peaks ~140°C. This is a typical result for Martian meteorites with feldspar in the low-temperature, ordered state (**Figure 3, Left**). OSL dose-response experiments (**Figure 3, Right**) revealed high saturation doses for all the materials that give *theoretical* maximum estimable ages >1 My. We tested our ability to determine a previous absorbed dose by these materials (the so-called "recovered dose"). These tests showed that a laboratory radiation dose can be recovered to within 6%.

b. Feldspars: Most luminescence materials encountered on Mars will probably be of feldspathic origin. While feldpars have been used for terrestrial TL and OSL dating, these materials pose two challenges to the proposed project. Currently, no accepted single-aliquot

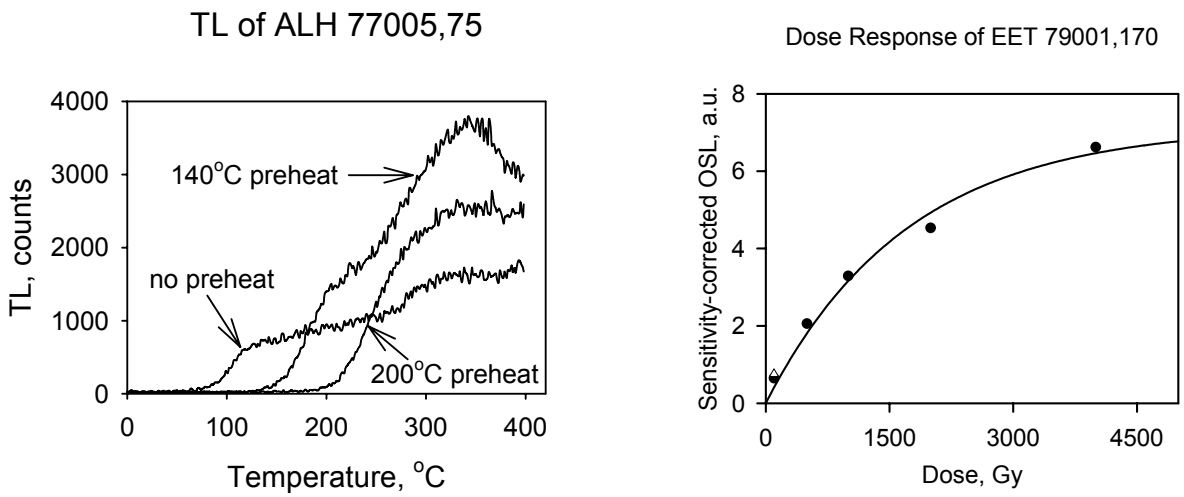

Figure 3: Left TL glowcurve of ALH 77005, 74 showing the effects of preheating. All radiation doses were 300 Gy. **Right** OSL dose response for EET 79001, 170. The open triangle represents the repeat point.

Sample	TL peaks (°C)	Max dose (Gy)	Max age (Mya)	Equiv. Dose Ratio
ALH 77005,74	~140, 340	2500	1.25	0.98
Shergotty	120, 180, 320	6300	3.15	1.04
Zagami	~150, >400	5200	2.6	1.06
EET 79001,170	~150, >400	6000	3.0	0.98
Jeweler's Rouge	140, 350	4300	2.15	0.99

Table 1: The results of TL and OSL experiments conducted on SNC meteorites and jeweler's rouge. The maximum estimable dose was found by fitting the growth curves with a saturating exponential function, and the maximum estimable age was found by assuming a dose rate of 2 $mGy.yr^{-1}$. The equivalent dose ratio is given radiation dose/ recovered radiation dose.

methods (similar to the SAR method outlined above, which was developed for quartz) exist for feldspar dating, and attempts to develop such a method have been unsuccessful (Wallinga et. al., 2000). Also, many feldpsars suffer from anomalous fading whereby thermally-stable signals nevertheless fade with time (Wintle, 1977). Although many suggestions have been made to either correct or eliminate this phenomenon (Huntley and Lamothe, 2001; Lamothe and Auclair, 1999; Vicosekas, 2000), no accepted method has been developed.

To address this issue, a project has been started to develop a single-aliquot procedure for feldspars that also eliminates anomalous fading. Once such a procedure has been developed, further work will be carried out to extend the method to polymineral samples (consisting of quartz, feldspars, and other materials) such as will be utilized for the Mars OSL dating module. The eventual goal is to use the procedure to obtain depositional ages for polymineral terrestrial samples with independent age controls.

One basic requirement for a single-aliquot technique is that repeated cycles with a fixed regeneration dose (including preheating and sensitivity-correction procedures) yield the same OSL or TL result (either the same luminescence signal or sensitivity-corrected ratio as in SAR). Five types of feldspars (microcline, anorthoclase, oligoclase, plagioclase, and andesine) have been tested for this requirement in several different ways.

The samples were first subjected to a measurement of TL to 450°C (to remove any residual signal), followed by 7 cycles of fixed regeneration dose (5 Gy), preheated to 220°C, and TL to 450°C. For all of the samples, the TL glowcurves for repeated cycles overlie each other. However, if the same experiment is conducted with OSL instead of TL measurements, the OSL decay curves do not overlie each other (i.e., there is a sensitivity change).

A subsequent experimental procedure of a measurement of TL to 450°C (to remove any residual signal), followed by 7 cycles of fixed regeneration dose (5 Gy), preheated to 220°C, OSL at 125°C for 100 s, and TL to 450°C yielded identical OSL curves with the notable exception of the first cycle (preceded by the "cleaning TL"). These results strongly imply that performing a TL measurement after the OSL measurement resets the feldspar's sensitivity, and that OSL sensitivity changes are largely governed by the availability of trapping centers (as opposed to the availability of recombination centers).

The latest experiment used the above procedure with regeneration doses ranging from 0.5-100 Gy including a repeat point of 5 Gy to construct a dose-response curve at low doses. All samples showed some non-linearity at low doses (<10 Gy), and the first cycle (after the "cleaning TL") again yielded a much higher than expected response (**Figure 4**). However, the non-linearity at low doses means that a method for sensitivity-correction still needs to be found. The increased OSL response from the first cycle is probably due to high temperature traps (> 450°C) that contribute to the OSL.

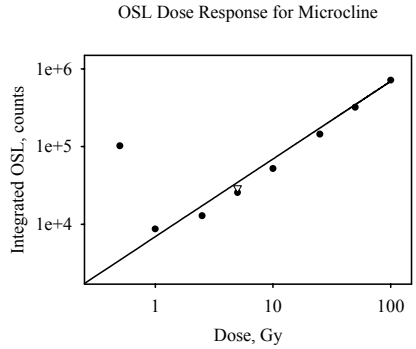

Figure 4: OSL dose-response for Microcline using procedure described in text.

3. ESR Spectrometer Design

We have designed and fabricated components of the miniature ESR spectrometer as shown in Figure 5. The frequency scan ESR spectrometer is achieved by variation of distance (total movement ~ 5 mm) between the two dielectric resonator disks (ε_R = 29, 1.0 cm OD x 0.55 cm ID x 0.35 cm thick) using a small DC motor (MicroMo).

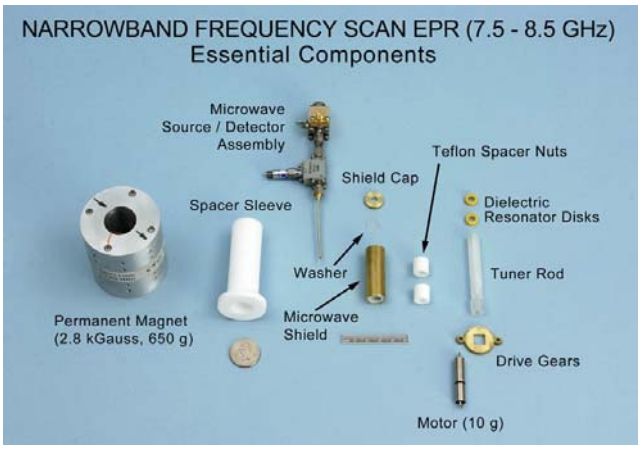

Figure 5. Essential components of the miniature ESR spectrometer that will be integrated into the Age Dating Instrument.

C. SIGNIFICANCE OF RESULTS

A method still needs to be found that fully corrects for OSL sensitivity changes in feldspars. Such a procedure will probably incorporate TL measurements to "reset" the OSL sensitivity, but a test dose correction and preheat procedures still need to be developed. The method will then be incorporated into a polymineral, single-aliquot dating technique that will subsequently be used to date terrestrial depositional events with independent age controls. Instrumentation effort will continue.

D. FINANCIAL STATUS

The total funding for this work was $110,000, of which $84,000 has been expended.

E. PERSONNEL

No other personnel were involved.

F. REFERENCES

D. J. Huntley and M. Lamothe, "Ubiquity of Anomalous Fading in K-Feldspars and the Measurement and Correction for It in Optical Dating," *Canadian Journal of Earth Sciences,* 38, 1093-1106. (2001)

M. Lamothe and M. Auclair, "A Solution to Anomalous Fading and Age Shortfalls in Optical Dating of Feldspar Minerals," *Earth and Planetary Science Letters* 171, 319-323, (1999).

A. S. Murray and A. G. Wintle, "Luminescence Dating of Quartz Using an Improved Single-Aliquot Regenerative-Dose Protocol," *Radiation Measurements*, 32, 57-73, (2000).

R. Visocekas, "Monitoring Anomalous Fading of TL of Feldspars by Using Far-Red Emission as a Gauge," *Radiation Measurements,* 32, 499-504, (2000).

J. Wallinga, A. S. Murray, and A. G. Wintle, "The Single-Aliquot Regenerative-Dose (SAR) Protocol Applied to Coarse-Grain Feldspar," *Radiation Measurements*, 32, 529-533, (2000).

A. G. Wintle, "Detailed Study of a Thermoluminescent Mineral Exhibiting Anomalous Fading, (1977).

POWER AND PROPULSION

A 3-DIMENSIONAL PARTICLE SIMULATION MODEL FOR ION THRUSTER PLASMA FLOW AND GRID EROSION

Final Report

JPL Task 991

Joseph J. Wang, Thermal and Propulsion Engineering Section (353)

A. OBJECTIVES

Ion propulsion is a critical enabling technology for future deep space missions. A key issue in ion thruster development is grid design and thruster service life, which is primarily limited by grid erosion. In recent years, ion optics modeling has become an ever more important tool to help improve grid design, predict thruster service life, and understand thruster failure modes. The objective of this research is to develop a first-principle based, experimentally validated simulation model for ion optics.

B. PROGRESS AND RESULTS

1. Simulation Model

In this research, we developed the first fully three-dimensional ion optics model. The code is designed in such a way that not only single aperture but also multiple apertures can be included explicitly in the simulation domain. In addition, no assumptions are made to simplify the upstream and downstream boundary conditions. The upstream sheath and ion beam extraction from the discharge plasma are determined self-consistently in the simulation. The simulation is extended into the region far-downstream of the accelerator grid. The location where beamlets become neutralized and charge-exchange ions start to backflow are resolved for the first time in the simulation.

The simulation model includes a set of three particle-in-cell (PIC) codes: an ion beamlet code, a neutral particle code, and a charge-exchange ion code. In this model, propellant ions, charge-exchange ions, and neutrals are treated as macro-particles. Out of considerations for computational efficiency for large-scale simulations, these codes are built upon orthogonal grids and a finite-difference-based formulation. The 3-D optics aperture geometry is handled by a method of sub-grid scale placement of boundaries which explicitly includes the location of the optics wall in relation to the grid in the finite-difference form of Poisson's equation. A typical simulation set up is shown in Fig.1. In a simulation, the distances between the upstream/downstream boundaries and the ion optics is successively increased to search for the proper simulation domain size. The final domain size is determined by examining the potential gradient and local charge-exchange ion backflow rate near the boundary. A typical simulation involves over 10 million particles and requires 20-30 CPU hours on the Cray SV1-1A supercomputer.

2. Simulation Results

From the simulation, we may obtain information on the electric field, beam ion flow, and charge-exchange ion flow inside ion optics. For instance, Fig. 2 shows beam ion velocity direction vectors. The distributions of impingement charge-exchange ion current density, incident energy, and incident angle on the ion optics grid surface are also obtained from simulation. Then one would be able to calculate grid erosion based on simulation results.

During the long duration test of the DS1 flight spare NSTAR ion thruster, both laser profilometer measurements and post-test destructive exams were performed to measure accel grid erosion. Fig. 3 compares the measured erosion pattern and erosion depth on the downstream face of the accel grid with that obtained from simulations. The left panel is a photograph of erosion pattern after 8200 hours of operation. The middle panel overlays simulation results on experimental data. The right panel compares erosion depth along the groove. The figure shows that the simulation picks up all of the detailed features shown in the measured erosion pattern. Additionally, the simulation also shows an excellent quantitative agreement with the measured erosion depth.

C. SIGNIFICANCE OF RESULTS

This task developed a fully three-dimensional particle simulation model for ion thruster optics. This 3-D simulation model is applied to study plasma flow and grid erosion for the DS1-NSTAR ion thruster. Grid erosion predicted by simulation is compared against erosion measurements taken during the long duration test of the NSTAR ion thruster.

The results indicate that the simulation not only predicts accurately all the features in the measured erosion pattern, but also gives excellent quantitative agreement with the measured erosion depth. Hence, this experimentally-validated model may be used as a design tool for new ion thrusters currently being developed at JPL.

D. FINANCIAL STATUS

The total funding for this task was $25,000, all of which has been expended.

E. PERSONNEL

Other personnel involved: James Polk, Sec 353.

F. PUBLICATIONS

[1] J. Wang, J. Polk, J. Brophy, and I. Katz, “Three-Dimensional Particle Simulations of Ion Optics Plasma Flow and Grid Erosion,” submitted to *J. Propulsion and Power*, 2002.

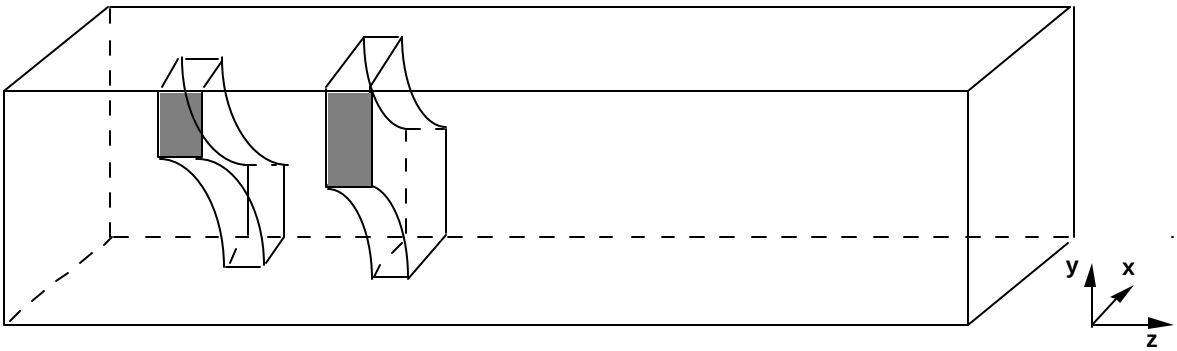

Figure 1: Typical simulation setup: a simulation domain with two quarter-size apertures

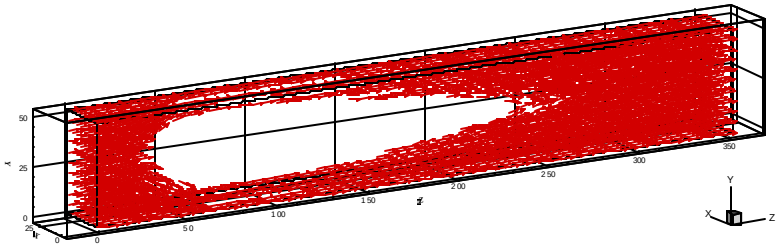

Figure 2: Beam ion velocity direction vectors

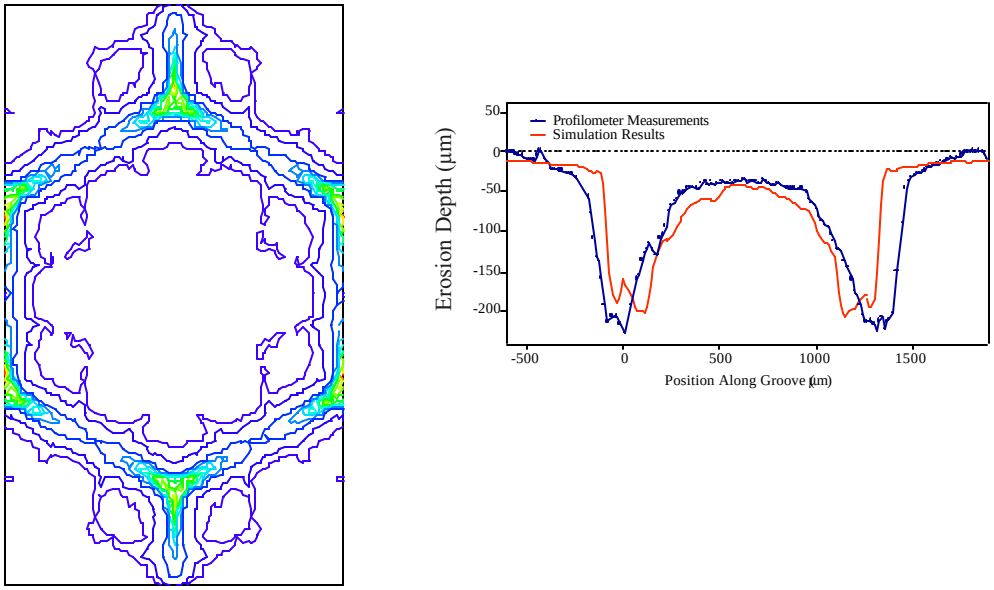

Fig. 3: Comparison of simulation results with experimental data.

NANOSTRUCTURED METAL OXIDES FOR HIGH POWER BATTERIES

Interim Report

JPL Task 1012

Ratnakumar Bugga, Will West, Nosang V Myung, (Section 346)
Jay Whitacre and Marshall Smart (Section 346)
Rachid Yazami and Brent Fultz, Materials Science Dept., Caltech

A. OBJECTIVES

Lithium ion rechargeable batteries are the next-generation rechargeable battery systems for NASA's future needs. Despite their distinct advantages in specific energy, operating temperature range and self-discharge, they have relatively lower power densities than the alkaline nickel systems, attributed mainly to the slow lithium intercalation processes at the electrode. Electrodes with nanostructured features, e.g., Nanofibers, are expected to have much larger effective surface and interfacial areas, and thus higher power densities. The objectives of the proposed work are to synthesize nanostructured metal oxides for cathode applications in lithium rechargeable batteries, using novel template and sol-gel or electrolytic synthetic techniques. Such nanostructured morphologies will enhance the power densities and energy densities of the micropower sources by 1-2 orders of magnitude, compared to the state-of-art devices, while preserving comparable footprints. These nanocathodes will benefit, apart from the batteries, several other electrochemical devices, e.g., electrochromic devices and microsensors.

B. PROGRESS AND RESULTS

High surface electrodes, e.g., nanowires with high aspect ratios, are possible cathode morphologies for high power density applications, as demonstrated with vanadium oxide cathodes.[1] These cathodes were fabricated by sol-gel deposition into nano-channels in porous alumina templates.[2] The procedure adopted by us to get nanowires of transition metal oxides is described below.

We used alumina templates, synthesized in-house with a typical diameter of 20 nm (Fig.1). The porosity and pore diameter of the alumina templates can, however, be varied by changing the anodizing conditions of the aluminum sheet. This in-house capability allows for direct on-silicon fabrication, of interest for micro-power applications. A current collector, either Au or Pt, is deposited on one end of the porous alumina and from the open end, transition metals, either cobalt or nickel, are deposited electrochemically. The template is then digested, leaving nanowires of either cobalt or nickel, as illustrated in Fig. 2. Preliminary attempts to lithiate these nanometallic wires, to form lithium cobalt or nickel oxide nanowires, haven't been successful. Further work is underway to refine the nanostructure and obtain the nanowires in the desired oxidation state. Meanwhile, using a similar approach, we have been able to successfully fabricate freestanding arrays of manganese oxide nanowires from electrolytic sulfate baths (Fig.

3). The stoichiometry (verified via XPS characterization) of the nanowires could be tailored from Mn_2O_3 – Mn_3O_4 – MnO_2 by adjusting deposition potential and bath chemistry. Although the latter composition is most desirable for battery and supercapacitor applications, the other stoichiometries may be of interest for high surface area catalysis applications.

C. SIGNIFICANCE OF RESULTS

We have been able to successfully synthesize various transition metal oxide cathodes, e.g., cobalt and nickel oxides, in the form of nanowires with typical diameters of 20nm. In addition, arrays of free-standing manganese oxide nanowires with comparable electrochemical activity have been synthesized. Combining such nanowire cathodes with a lithium anode in a suitable device, i.e., either with a polymer electrolyte cast from solution, or solid electrolyte, sputter or vapor deposited, will result in a thin film battery with a several-fold increase in the power densities, which is one deterrent factor for polymer electrolyte, or thin film or microbatteries.

D. FINANCIAL STATUS

The total funding for this task was $115,000, of which about $30,000 was spent for in-house efforts and $25,000 was transferred to the collaborator, Caltech.

E. PERSONNEL

No other personnel were involved.

F. PUBLICATIONS

1) W. C. West, N. V. Myung, J. F. Whitacre, and B. V. Ratnakumar, "Synthesis of LiCoO2 Nanowire Arrays from Co Electrodeposits," presented at the Nanophase Materials for Batteries and Fuel Cells Symposium at the American Electrochemical Society Spring Meeting, Philadelphia, May 2002.
2) W. C. West, N. Myung, J. Whitacre, B. V. Ratnakumar, "Direct Electrolytic Deposition of Manganese Oxide Nanowires for High Power Battery and Capacitor Electrodes," an NTR describing processes to fabricate nanostructured electrode materials from templated nanowires, *NASA Novel Technology Report # 30655*, (2002).
3) The group was solicited to present an invited paper describing nanostructured materials for batteries at the NanoEnergy Conference in Miami, FL in Dec. 2002. Will West will present "Freestanding Arrays of Nanowire Materials for High Rate Capability Battery Electrodes."

G. REFERENCES

1) N. Li, C. R. Martin, and B. Scrosati, *Electrochem. and Solid State Lett.*, **3** 316 (2000).

2) For example: F. Croce, C. Sides, B. Scrosati, and C. R. Martin, abstract 172, *May 2002 Meeting of the Electrochemical Society*.

H. FIGURES

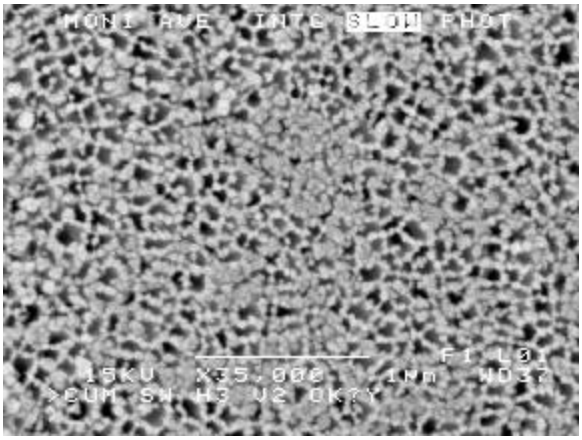

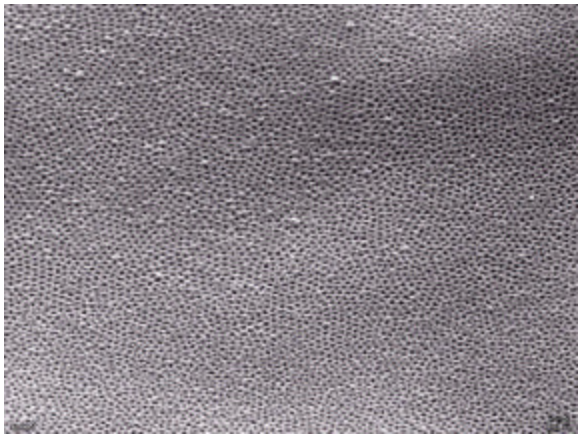

Fig. 1 Whatman Anodisc (100 nm pores) JPL synthesized alumina template (20 nm pores)

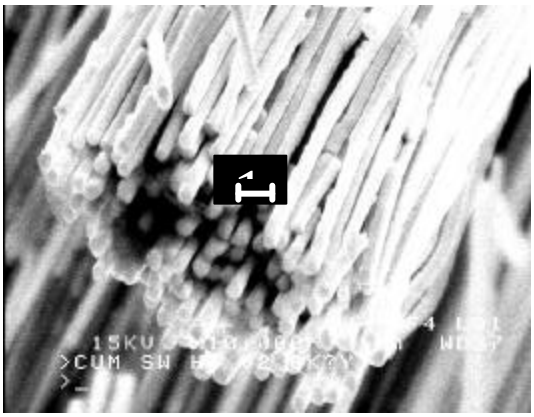

Fig.2. Nanowires of Co(Ni) for fabrication of nanostructured $LiCoO_2$.

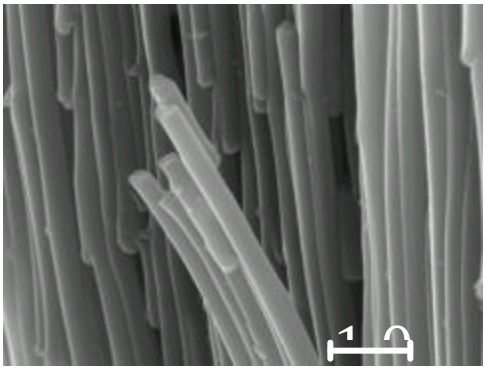

Fig.3. Nanowires of Manganese oxides from sulfate bath

SCIENCE

A STUDY OF *IN SITU* CHRONOLOGY IN THE OUTER SOLAR SYSTEM

Final Report

JPL Task MU994

Leslie K. Tamppari, Mission Systems Engineering Section (314)
Timothy Swindle, University of Arizona

A. OBJECTIVES

Determining the age of a feature on a solar system body is one of the most important tasks that can be done, since any model of its evolution has to include time as one of its parameters. Unfortunately, determining the age of a feature is also one of the most difficult things to do *in situ*, and has not yet been attempted on any planetary body. However, the Beagle2 Mars lander is scheduled to perform crude *in situ* dating, and the University of Arizona has been working (under a Planetary Instrument Definition and Development Program grant, with follow-on work recently approved for funding by the Mars Instrument Development Program) to develop a more sophisticated system for Martian applications. The intent of the present study was to study how *in situ* chronology might be accomplished on solid surfaces in the outer solar system, particularly Europa and Titan. Specific objectives were to 1) perform a conceptual engineering study of a noble-gas-based chronology system for Europa, an extension of the system being developed for Mars; 2) identify some of the key issues in sample acquisition and transfer; and 3) study certain scientific questions that have to be addressed in order for particular *in situ* chronology systems to have a chance of working.

B. PROGRESS AND RESULTS

1. Science Data

Two scientific questions were addressed. The first was a study of ^{14}C production and distribution on Titan, the second a study of production rates of noble gases at the surface of Europa. In each case, it appears that there are prospects for *in situ* chronology. Prospects of dating the surface per se are better at Europa, but one of the more intriguing results found was that production of ^{14}C at Titan may produce effects that could be measured by the Huygens probe. More details are shown below:

(1) **^{14}C on Titan:** The results of this study have been published in *Meteoritics and Planetary Science* (see Lorenz et al. under Publications). The abstract of that paper is as follows: "We explore the likely production and fate of ^{14}C in the thick nitrogen atmosphere of Saturn's moon Titan and investigate the constraints that measurements of ^{14}C might place on Titan's photochemical, atmospheric transport and surface-atmosphere interaction processes. Titan's atmosphere is thick enough that cosmic-ray flux limits the productions of ^{14}C: absence of a strong magnetic field and the increased distance from the

Sun suggest production rates of ~9 atom/cm^2/s, ~4x higher than Earth. The fate and detectability of ^{14}C depends on the chemical species into which it is incorporated: as methane it would be hopelessly diluted even in only the atmosphere. However, in the more likely case that the ^{14}C attaches to the haze that rains out onto the surface (as tholin, HCN or acetylene and their polymers), haze in the atmosphere or recently deposited on the surface would be quite radioactive. Such radioactivity may lead to a significant enhancement in the electrical conductivity of the atmosphere which will be measured by the Huygens probe. Measurements with simple detectors on future missions could place useful constraints on the mass deposition rates of photochemical material on the surface and identify locations where surface deposits of such material are 'freshest.'"

(2) **Europa:** There are two fundamentally different dating techniques which can, in principle, be used at the surface of Europa by measuring the chemical composition of a sample and its content of the isotopes of He, Ne, and Ar. One is K-Ar dating, based on the buildup of ^{40}Ar from the decay of radioactive ^{40}K, which measures the length of time the sample has been cool enough to retain Ar. The other is cosmic-ray-exposure dating, based on the buildup of ^{3}He, ^{20,21,22}Ne and ^{36,38}Ar from nuclear reactions caused by cosmic rays, which measures the length of time a sample has been within 1 to 2 meters of the surface. Various spectroscopic and theoretical studies of Europa have indicated a briny surface for Europa, and the K contents are likely to be enough to make K-Ar dating feasible. This study focused on cosmogenic production, in collaboration with J. Masarik of Bratislava University and R. C. Reedy of the University of New Mexico. Production by high-energy galactic cosmic rays (calculated by Masarik) indicate that production rates comparable to the lunar surface can be expected. Calculations of production by lower-energy charged particles in the Jovian magnetosphere (by Reedy) are in progress. The bottom line is that this should be an effective technique on timescales of 1-100 Ma, which are timescales of interest on the Europan surface. The largest remaining question is the diffusion properties of the noble gases (particularly He) in Europan ice. This work will be submitted as a scientific paper, though it is not complete yet, and no further funding is needed.

2. Other Results

Much of the effort in this study went into trying to define the key engineering considerations for a noble-gas-based *in situ* chronology instrument for the surface of Europa. This study was based on a comparison with the instrument designed for Mars, which utilizes Laser-Induced Breakdown Spectroscopy (LIBS) for elemental analyses; heats a sample to a temperature high enough to release helium, neon and argon (preferably at or above the melting point of the rock); uses a chemical getter to purify the noble gases; and then analyzes the noble gases in a quadrupole mass spectrometry array (QMSA). In considering whether *in situ* chronology can be done on outer solar system bodies, the study started with the Mars concept and considered how working on Europa would be similar or different.

(1) Sample acquisition: D. Yucht of Honeybee Robotics performed tests with existing Honeybee drills into 100 K ice as a part of this study. The results showed that it is possible to drill into such ice using drills Honeybee has already developed. However, there is apparently some localized melting as a result of the process, which can

lead to the drill freezing into the ice if it is stopped. The melting could also be a problem if it heats samples enough to release noble gases, although we had no way to test this in the current study.

(2) LIBS: LIBS has been applied almost exclusively on rock samples so far. However, tests on ice samples are being performed as part of another study by D. Cremers at Los Alamos National Laboratory. The one drawback identified for the LIBS system is that the plume generated by the laser appears to be optimal for pressures of a few torr, like the surface pressure on Mars. In a vacuum, which would be the conditions for a Europan instrument, the plume seems to be comparable to that at Earth's atmospheric pressure. It appears that LIBS would work, although the details of LIBS analyses of ice have not been worked out.

(3) Sample heating: One of the most difficult tasks for the Mars instrument was generating high enough temperatures (1500^0C) in a low-power instrument. Heating will not be a problem for a Europa instrument – the desired temperature will be approximately 0^0C. In fact, the bigger problem will be keeping the sample cold enough until it is ready for analysis.

(4) Gas purification: A key preparation step before analysis of noble gases is removal of the other gases, since noble gases are virtually always only a trace constituent of the gas released. This is often done with chemical getters (the approach planned for the Mars instrument). An alternative approach is to use a cold-trap, at a temperature low enough to condense out the unwanted gases, but high enough not to condense out the noble gases of interest. We would plan to analyze only He, Ne, and Ar, and the high condensation temperature is that of Ar, which is near the temperature of liquid nitrogen. This, in turn, is colder than the temperature of the ice at the surface of Europa, so the cold-trap could simply be a piece of metal in thermal contact with an unheated piece of the surface. The difficulty with this idea is finding a way to get a portion of the instrument in thermal contact with the surface.

(5) Vacuum system: For both the mass spectrometry array and the sample heating and purification portion of the experiment, the gas needs to be in an evacuated, sealed volume. Achieving the necessary vacuum will be easy – the near-surface environment will be at a sufficiently low pressure, so no pumps are required. However, it will be necessary to avoid portions of the spacecraft which may be outgassing, or portions of the surface that are being outgassed by being in contact with the warm spacecraft. In addition, it will be necessary to avoid having surfaces within any vacuum chamber that will be cold enough to act as cold-traps during evacuation, but will then outgas during operation. Finally, high-vacuum valves and seals are required, and none exist that could be expected to perform well at the surface temperature of Europa. This suggests that much of the instrument will need to be in a warm box.

(6) Electronics: The electronics will face two challenges. One is the thermal environment, which will probably require a warm box for virtually all electronics as well. The other, larger, problem is the radiation environment, since Europa is well within the Jovian magnetosheath and is consequently bombarded by energetic charged particles. Radiation hardening is far beyond the present task.

(7) Mass spectrometry: No obvious problems were identified for the mass spectrometry system, beyond those common to all portions of the instrument: the radiation and thermal environment.

(8) Summary: No show-stopping problems were identified. In fact, there are some aspects (reaching the required sample temperature, pumping) that will be far easier on Europa, and those happen to be the activities that require the vast majority of the power for such an instrument on Mars. The most difficult problems are likely to be dealing with the radiation environment (a problem for any instrument operating near Europa) and the thermal environment. The latter is a problem not only because many, if not all, components will need to be warmed above the ambient temperature, but also because the sample will need to avoid that warming.

C. SIGNIFICANCE OF RESULTS

The results indicate that *in situ* chronology on the surface of Europa appears to be feasible, both scientifically and technically, although there are many engineering details left to be solved.

D. FINANCIAL STATUS

The total funding for this task was $100,000, all of which has been expended.

E. PERSONNEL

From the University of Arizona: Dr. Timothy D. Swindle, Dr. Jonathan I. Lunine, Dr. A.J.T. Jull, Dr. Ralph Lorenz, Mr. Rolfe Bode, and Mr. Michael Williams; from Honeybee Robotics, Mr. Daniel Yucht; from the University of New Mexico, Dr. Robert C. Reedy; from the University of Bratislava, Dr. Josef Masarik.

F. PUBLICATIONS AND PRESENTATIONS

[1] R. D. Lorenz, A. J. T. Jull, T. D. Swindle, and J. I. Lunine, "Radiocarbon on Titan," *Meteoritics and Planetary Science,* 37, 867-874, 2002.

[2] T. D. Swindle, "Prospects for Measuring the Age of the Surface of Europa II," Europa Focus Group Workshop 3 (USGS, Flagstaff, Ariz.), May 14-15, 2002.

EXPERIMENT TO DETECT MARTIAN PERMAFROST BASE/GROUND WATER AND BIOGENIC METHANE FROM AN ORBITER AND/OR LANDERS ON MARS

Final Report

JPL Task 1007

Natalia Duxbury, Section 3224

A. OBJECTIVES

I have proposed an experiment to detect subsurface clathrate hydrate by determining local curvature in the melting isotherm (by EM sounding). The task was to investigate the feasibility of my experiment for Mars.

B. PROGRESS AND RESULTS

Partial quantitative analysis for the feasibility of determining a curvature in the Martian ground ice/ground water interface and, therefore, the existence of possible subpermafrost methane clathrate hydrate was performed. For the regime of EM sounding, frequencies less than 1 MHz are recommended as a result of this study.

It was understood that my approach is important in light of the interpretation of continuous permafrost and clathrates as a "lid" for possible subpermafrost reduced biogenic gases. Hence, surface detection of these gases is not possible in spite of their presence at depth. Also, a search was performed for evidence linking Martian geomorphological features and ground water.

As a result of my investigation, the uncertainty in determining the position of ground ice base (melting isotherm) in the Martian subsurface as a function of latitude, using new Mars Global Surveyor Thermal Emission Spectrometer brightness temperature data, was assessed. I have concluded that the accuracy of the annual average Martian surface temperature estimates, prior to the measurement of the Martian surface brightness temperature by the MGS TES instrument, was better than the accuracy to which the other parameters (thermal conductivity and the Martian internal heat flow due to radioactive decay in the core) required to calculate the position of the zero-degree isotherm are currently known.

Secondly, as a result of my investigation, I have concluded that it is better to use the lower-frequency inductive regime rather then the radar regime to obtain an echo from the ground ice/ground water interface globally.

Based on my studies, I make the following recommendations for accessing the Martian subsurface: to drill in the chaotic terrain, which is at the source of Martian outflow channels, for the reason of possible subsurface methane clathrate hydrate deposits. I recommend drilling in the basins not near the equator (where the melting isotherm comes closest to the surface), but in the

mid-latitudes, because the melting isotherm might overlap with the desiccation front, and they have the opposite curvatures.

Thirdly, permafrost features such as thermokarst, polygonal terrain, pingos and rampart craters are very important to determine future landing/drilling sites. They can be identified from the Mars Global Surveyor Mars Orbiter Camera images, which have about 1 m resolution.

Also, I have investigated the possible depletion of the Mars ground water reservoir during the past 3 Ga. From my numerical analyses, I conclude that the best drilling sites to search for Martian ground water would be on the potential intersection of the desiccation front and the permafrost base. From my current investigation, and utilizing terrestrial analogs, I recommend narrowing these "optimal" areas by using the surface manifestation of permafrost/near-surface ground water: pingos, thermokarst, rampart craters. As a result of my investigation, I recommend a concrete region for future drilling missions on Mars: Utopia Planitia, and preferentially its southern part.

To perform this research, I have used the Mars Topographic Globe (constructed using MOLA data) and the book by E. D. Sloan (1998). Despite a previously common concept of a geothermal melting origin of potential Martian subpolar water, I have proven the opposite origin using the MGS MOLA data. I have also investigated the mechanism of sub-ice lake survival on Mars.

C. SIGNIFICANCE OF RESULTS

SHARAD radar on MRO operates in the range of frequencies 15 - 25 MHz, which are higher frequencies than the Mars Express (2003) MARSIS frequencies of 1 - 5 MHz, and thus the penetration depth of SHARAD will be less. The effective sounding depth for MARSIS is about 2 km. As a result of my investigation, for my method, which combines thermoprospecting and electrical prospecting on Mars, I suggest using the inductive rather than the radar regime for subsurface sounding. As a result of this research: I have also co-authored 2 chapters in the book "The Future of Solar System Exploration," one of them on terrestrial analogs for Mars.

My two New Technology Reports were accepted by *NASA Tech Briefs* with the subsequent awards to me as the Class 1 Innovator. I have submitted a proposal "Comparative Studies of Martian Ices, Water, Clathrates and Their Terrestrial Analogs" as a PI to NASA's Mars Fundamental Research program. I have submitted a 2nd proposal, "Mapping Thermal Distribution and Ground Ice Conditions at the Near-surface Martian Landforms," as a Co-I to NASA's Geology and Geophysics program. I have recently reviewed an article about Mars at the request of the *Journal of Geophysical Research.* Additionally, I have co-authored 2 abstracts on the exploration of Mars (to AGU and DPS).

D. FINANCIAL STATUS

The total funding for this task was $25,000, of which $23,700 was expended.

E. PERSONNEL

No other personnel were involved.

F. PUBLICATIONS

1. N. S. Duxbury and V. Romanovsky, "Methane Clathrate Hydrate Prospecting," *NASA Tech. Briefs Journal*, NTR-30257, (in press) (2002).

2. N. S. Duxbury and V. E. Romanovsky, "Permanent Sequestration of Emitted Gases in the Form of Clathrate Hydrates," NASA Tech. Briefs Journal, NTR 30256 (in press) (2002).

3. T. G.Farr and co-authors, including N. Duxbury, "Terrestrial Analogs to Mars," *The Future of Solar System Exploration*, 2003-2013, National Academy of Sciences (NAS), Ed. M. Sykes, (2002).

4. N. G. Barlow, T. Farr, V. R. Baker, N. Bridges, F. Carsey, N. Duxbury et al., "Community Decadal Panel for Terrestrial Analogs to Mars," abstr., September 2002, Birmingham, 33 DPS Meeting.

5. T. Farr and co-authors, including N. Duxbury, "Terrestrial Analogs to Mars: NRC Community Panel Decadal Report," December 2002, AGU conference, San Francisco.

G. REFERENCES

[1] E. Dendy Sloan, *Clathrates Hydrates of Natural Gases* (1998),

TIDAL CORRECTIONS FOR SAR INTERFEROMETRY ON FLOATING ICE SHELVES

Interim Report

JPL Task 1030

Ian R. Joughin, Radar Science & Engineering Section (334)

A. OBJECTIVES

Iceberg calving is the process by which the Antarctic ice sheet discharges most of the annual mass gained by snow accumulation. Much of this iceberg calving occurs along the front of two large floating ice shelves: the Filchner-Ronne Ice Shelf and the Ross Ice Shelf. Loss of the ice shelves would not cause a direct change in sea level because the ice is already floating. Their loss, however, would remove an important restraint on ice stream flow and resulting ice discharge. Furthermore, loss of the ice shelves would produce significantly more open water for sea-ice production, potentially affecting global ocean circulation.

Large ice shelves calve infrequently (every few decades at a given point along the shelf), but when they do, they give rise to the large tabular icebergs that are similar in area to small New England States. Because of the infrequent nature of the calving events, it is difficult to get an adequate sampling of these events with which to detect change. If instead we are able to measure the continuous flow of the ice shelves, we will then be in a better position to understand and predict the long-term viability of the ice shelves in response to climate and other change.

A major problem with measuring velocity on ice shelves using Interferometric Synthetic Aperture Radar (InSAR) is the sensitivity of the measurement to both horizontal and vertical motion. This means ice flow and tidal displacements are ambiguously mixed on the floating ice shelves.

The objective of this task is to modify existing InSAR mapping algorithms to incorporate tidal-displacement estimates from the Circum-Antarctic Tidal Simulation (CATS) Model produced by Laurence Padman of Earth and Space Research. This is a 10-constituent model for Southern Ocean tides. The grid is 1/4 x 1/12 degree (lon x lat), and extends from 86 to 58 degrees S. The 10 constituents are the same as those for the model providing the open ocean boundary conditions in the Oregon State University, TOPEX/Poseidon altimetry assimilation model. The CATS model has been refined using data assimilation techniques to include the tidal displacement of floating ice shelves. The results of this work have demonstrated a method for estimating velocity on floating ice shelves, as well as a map of ice shelf velocity for the large Filchner-Ronne Ice Shelf. In addition, these data will be used for initial science applications such as the estimate of melt beneath the ice shelf.

B. PROGRESS AND RESULTS

Over the last several months, the CATS models were successfully integrated with the existing tools for InSAR mapping of ice velocity. The resulting software was used to produce the map of ice shelf velocity, which is shown in Fig 1.

C. SIGNIFICANCE OF RESULTS

The results demonstrate that when used in conjunction with a tide model, InSAR provides a viable means for mapping ice shelf velocity. These results are now being used to estimate melt beneath the ice shelf. This melt forms Ice Shelf Water (ISW), which is an important contributor to Antarctic Bottom Water formation [Foldvik et al., 1985].

D. FINANCIAL STATUS

The total funding for this task was $25,000, of which $5,600 has been expended.

E. PERSONNEL

No other directly-funded personnel were involved. The tide model that was used in this study is courtesy of Dr. Laurence Padman of Earth and Space Research, Corvallis, OR.

F. PUBLICATIONS

[1] I.R. Joughin and L. Padman, "Basal Melt Beneath the Filchner-Ronne Ice Shelf," presented at the West Antarctic Ice Sheet Workshop, Sterling, Virginia, September 18-21, 2002.

[2] I.R. Joughin and L. Padman, "Melt/Freeze Beneath Filchner-Ronne Ice Shelf, Antarctica," in prep.

G. REFERENCES

[1.] A. Foldvik, T. Gammelsrød and T. Tørrensen, "Circulation and Water Masses on the Southern Weddell Sea Shelf," *Oceanology of the Antarctic Continental Shelf*, edited by S.S. Jacobs, pp 5-20, American Geophysical Union, Washington D.C., 1985.

[2.] I. Joughin, "Ice Sheet Velocity Mapping: A Combined Interferometric and Speckle-Tracking Approach," *Ann. Glaciol.* 34, 195-201, 2002.

[3.] K.C. Jezek, "Glaciological Properties of the Antarctic Ice Sheet From RADARSAT-1 Synthetic Aperture Radar Imagery," *Ann. Glaciol.*, 29, 286-290 (1999).

H. APPENDIX: *Figures*

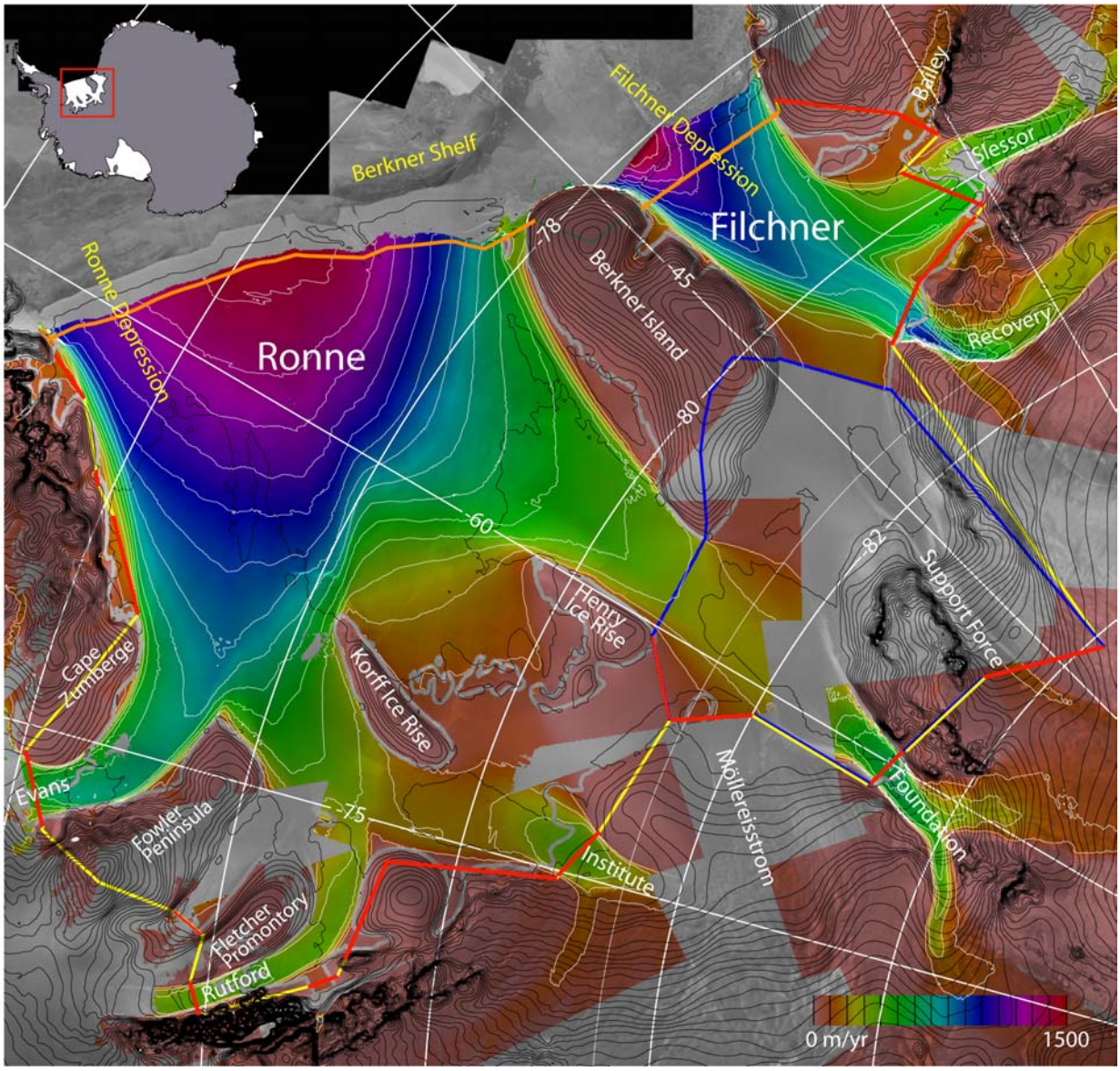

Figure 1. Ice flow speed (color) for the Filchner-Ronne shelf and surrounding ice streams. Speed is also contoured at 100 m/yr intervals (white). Velocities were determined using InSAR and speckle-tracking [Joughin et al., 2002]. Tidal displacements on the floating ice were corrected using the CATS tide model. Surface elevation is shown with 100-m contours (black). The basemap SAR image is from the RADARSAT Antarctic Mapping Mission mosaic [Jezek, 1999]. The red lines show gates where the inflow flux was measured and the yellow lines show gates with negligible flux. Outflow was measured through gates (orange) at the ice shelf front. The gates also surround Berkner Island, ice rises, and some surrounding catchment not included by the ice stream gates. The blue and red lines surround the region downstream of Foundation Ice Stream where the data were insufficient to evaluate melt locally. The velocity data indicate the ice front position in September 2000, while the SAR basemap shows the ice front position in September 1997 prior to the calving of several icebergs.

DISK-AVERAGED SYNTHETIC SPECTRA OF TERRESTRIAL PLANETS

Final Report

JPL Task 1034

Victoria S. Meadows, Planetary And Life Detection Section (322)

A. OBJECTIVES

With the recent discovery of a multitude of planets orbiting other stars, NASA is committed to developing the advanced instrumentation and observing techniques required to characterize other worlds and search for remote-sensing signatures of life. To drive and optimize the development of instruments for characterization of the state of habitation of other worlds, and to understand remotely-sensed information from extrasolar planets, we need to undertake modeling work to better understand the information available to us in disk-averaged spectra of terrestrial planets.

As part of understanding how to characterize extrasolar terrestrial planets, this task seeks to explore what can be learned about a planet's surface and atmospheric properties from disk-averaged spectra at a number of spectral resolutions. This task concentrates on synthetic spectra for Mars, and is part of a larger effort which uses a radiative transfer model and atmospheric and surface data for Earth, Mars, Venus and Titan to generate spatially-resolved synthetic spectra for a range of illumination conditions (phase angles) and viewing geometries. These spectra will then be spatially averaged, and processed with an observing system simulation tool that simulates the spectral and spatial resolution, signal levels, noise sources and other properties of planned extrasolar terrestrial planet observing systems, including nulling interferometers and coronographs.

This task was funded as Dr. Meadows' Lew Allen Award, and was used to fund two SURF students this summer, in addition to covering a small fraction of Dr. Meadows' time to supervise them. In addition to the science goals, it was important to introduce and train these two young scientists to the field of astrobiology, and to hopefully fuel their continued interest in both science and the new field of astrobiology.

B. PROGRESS AND RESULTS

1. Science Data

Two students were trained to use the Spectral Mapping Atmospheric Radiative Transfer Model (SMART; Meadows and Crisp, 1996), including all the ancillary programs and input files, and taught to generate synthetic spectra for Mars. Using their newly acquired skills, they were able to gather available data on atmospheric properties

and surface albedo for Mars, and use this data to generate synthetic spectra for Mars for a given solar illumination, but for arbitrary viewing angle.
In addition to generating the planetary spectra, they also developed a model architecture for the resultant planet simulation model that takes into account user-specified pixellization of the planet. The resultant model, which we completed for a single Mars "day," consists of a selection, pixellization and interpolation architecture, and draws upon a pre-calculated database of synthetic spectra for a range of viewing angles, solar illumination and surface albedos to populate the pixel resolution and viewing geometry specified by the model's user.

This work was written up as a Caltech SURF report and will form the basis for a science poster at the General Meeting of the NASA Astrobiology Institute, and for a paper to be submitted to the Journal *Astrobiology*.

Current work on this model includes generating further "days" within the model, to allow us to generate planetary lightcurves for arbitrary viewing angle, and as seen by astronomical instrumentation.

2. Other Results

In addition to creation of the first cut of this model, we were able to introduce two young scientists to the field of astrobiology. Both enjoyed their work immensely, and are interested in future SURF opportunities on this project. Perhaps most significantly, William has chosen to work in the field of extrasolar terrestrial planet characterization for a reading course term paper at Caltech, and has chosen to be mentored in this further effort by Dr. Meadows.

C. SIGNIFICANCE OF RESULTS

This task developed a proof-of-concept model for a much larger task which seeks to understand the appearance of extrasolar terrestrial planets when viewed in the disk-average, and from arbitrary viewing angle. The techniques developed under this task will now be used and expanded for the larger task of modeling Venus, Earth and Titan. In addition to its science goals of understanding detectability of characteristics for planets that we have data for, this task sets up a validation model for subsequent tasks of a larger project which involves generating disk-averaged synthetic spectra for extrasolar terrestrial planets.

The results indicate that such modeling is feasible on relatively short time scales, and should provide a versatile model which can be used to address the detectability of planetary characteristics in the disk-averaged spectra that will be available to extrasolar planet detection and characterization missions such as TPF.

D. FINANCIAL STATUS

The total funding for this task was $25,000, all of which will be expended by the task end date, which is March ’03.

E. PERSONNEL

This Task funded Caltech/JPL Summer Undergraduate Research Fellowships for Heather Snively of the University of Santa Cruz, and William Fong of Caltech.

F. PUBLICATIONS AND PRESENTATIONS

[1] This work will provide the basis of a conference poster for the General Meeting of the NASA Astrobiology Institute in Feb 2003, and will also provide the basis for the paper on the planetary models that is to be submitted to *Astrobiology* in early 2003.

G. REFERENCES

[1] V. Meadows, and D. Crisp, “Ground-Based Near-Infrared Observations of the Venus Nightside: The Thermal Structure and Water Abundance Near the Surface,” *JGR-Planets,* 101, 1996, 4595-4622.

HIRES FOR SIRTF EXTRAGALACTIC SURVEYS

Final Report

JPL Task 1039

Thangasamy Velusamy, Astrophysics Element (3262)
Charles Beichman, Astronomy and Physics Directorate (700)
George Helou, IPAC (Caltech)

A. OBJECTIVES

SIRTF will provide the most sensitive observations at infrared wavelengths to study light from stars and star formation in high-redshift galaxies. However SIRTF (with mirror size 85cm) is resolution-challenged. SIRTF science will greatly benefit from advanced imaging techniques not presently being developed by the project. At JPL, the Center for Long Wavelength Astrophysics is developing a High-Resolution (HIRES) analysis software tool to enhance the angular resolution in the SIRTF images. Preliminary tests show that an increase in the resolution by factors up to two is achievable. Such increase in resolution offers a tremendous increase in the SIRTF science capability. Our goal is to apply HIRES to the simulated SIRTF images of typical extragalactic surveys and validate its potential to enhance SIRTF science capabilities.

B. PROGRESS AND RESULTS

1. Science Data

Nearly half of the bolometric luminosity of the local universe is channeled through the mid- and far-infrared emission of galaxies. This infrared spectral region probes the youngest star-forming regions and their associated interstellar gas and dust. One of SIRTF's Legacy Science Programs (SINGS: The SIRTF Nearby Galaxies Survey) will survey 75 nearby galaxies to characterize their infrared emission properties. This survey will characterize the large-scale infrared properties of galaxies through complete IRAC (3.6 to 8 μm) and MIPS (24 to 160 μm) imaging instruments on SIRTF. The images will be used to further characterize the discrete infrared-emitting components of galaxies. High-angular-resolution imaging is critical to resolve extra-nuclear IR-emitting regions in the galaxies. HIRES offers a unique opportunity to achieve these goals.

The HIRES algorithm was first developed at IPAC for the IRAS infrared data. At JPL, we have successfully implemented this approach to the SIRTF data. HIRES executes a super-resolution algorithm similar to Richardson-Lucy, with added capability of PSF weighted averaging to fold in redundant pixel coverage. Our implementation has added features to speed up its execution by one order of magnitude. Preliminary tests show an increase in the angular resolution by factors up to two is achievable.

To critically evaluate the use of HIRES for this SIRTF survey, we chose one of our nearby galaxies, M100, as the test target. Using the I Band image of M100 (as truth) we simulated the SIRTF imaging for the MIPS (at 24 μm) and IRAC (at 3.6 μm) instruments. We

used the slow scan mode on MIPS to simulate 56 multiple image frames at 24 μm and the 12 position dither pattern to produce 12 image frames of the central region for IRAC at 3.6 μm. The simulated images at each wavelength were combined to produce conventional co-added images, and were also processed using HIRES to produce high-resolution images. The results of the HIRES image enhancement of M100 SIRTF images are shown in Figs 1 and 2. Fig. 3 shows the truth image assumed for the simulations. The application of HIRES to SIRTF imaging of other galaxies in the survey (e.g. the Large and Small Magellanic Clouds) are also being carried out under this task.

2. Other Results

We use the HIRES results of M100 to evaluate the performance of the algorithm as applied to SIRTF data. The degree of resolution enhancement is dependent on the imaging instrument, pixel sizes, and observing scenario (scanning and dithering) to produce redundant sampling of the image pixels. For example, the effect of HIRES is very significant in the case of IRAC 3.6 μm because of the under-sampling in the raw SIRTF images (the IRAC pixel size ($1.2'' \times 1.2''$) is larger than FWHM of the PSF at 3.6μm). Our results show:

a. Enhancement in the angular resolution: From 6″ to 4″ in the case of MIPS 24μm imaging; from 2.4″ to 1″ in the case of IRAC 3.6μm imaging.
b. Fidelity of reconstructed HIRES image is very good. All the features in the truth image are well reproduced in the image reconstruction, as evident from the difference map between the convolved truth and HIRES images..
c. Dynamic range is high, comparable to that in the truth image, except at regions closest to strong point sources.
d. Photometry: HIRES conserves the flux densities in the raw images on all scales, in point sources as well as in extended regions.
e. Artifacts: HIRES images are generally clean except for a low level (few percent) ringing around a strong point source near the Airy lobes. This can be reduced by characterizing the response to a point source in HIRES images.
f. As few as a dozen images obtained by dithering at 12 positions produce good resolution enhancement and high-quality reconstruction.
g. HIRES results can be used to plan SIRTF observations, optimizing for resolution enhancement.
h. HIRES requires some pre-processing of the raw images from SIRTF Science Center (SSC): Flagging bad pixels (cosmic rays) and correcting pointing errors.
i. Knowledge of the PSF is important to HIRES.
j. In this task, we demonstrate that HIRES will be a powerful general-purpose tool for SIRTF science, providing tremendous improvement in the imaging of debris disks, star-formation in galaxies, and forming galaxies. Increased angular resolution at 160 μm reduces the confusion limit, enhancing SIRTF sensitivity.
k. HIRES will be directly applicable to missions beyond SIRTF, including Herschel and SOFIA.

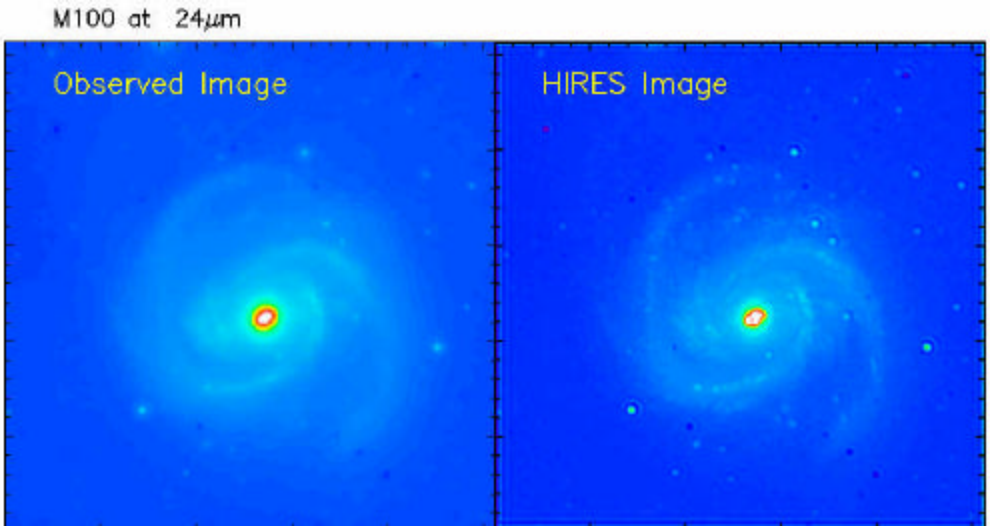

Fig. 1 The 24μm images were obtained from the simulated MIPS frames using the I –band image of M100. A total of 56 SIRTF image frames, obtained in the slow scan mode , were used. Background and noise have been added. The HIRES image shown was obtained after 100 iterations. The observed image is a mosaic of all 56 raw image frames

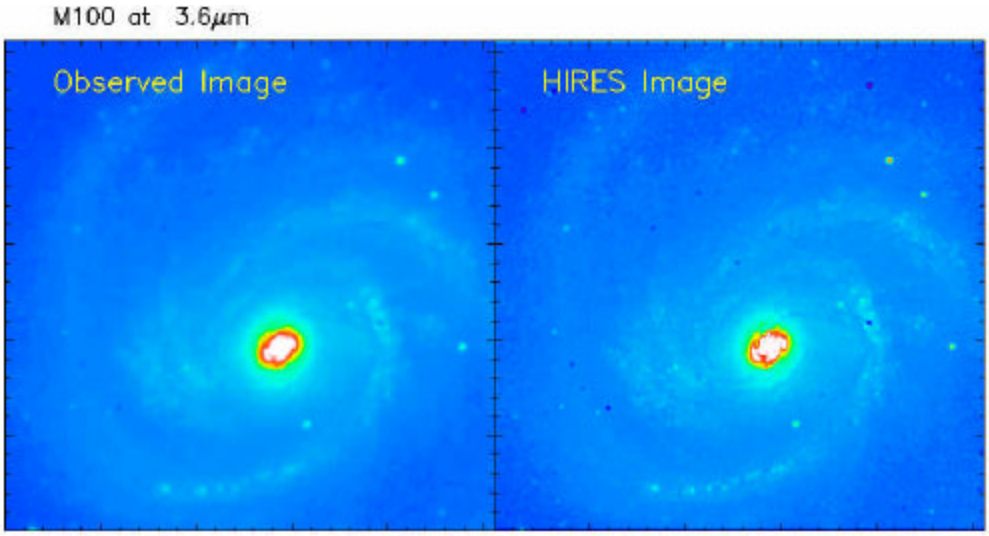

Fig. 2 The 3.6μm images were obtained from the simulated IRAC frames using the I –band image of M100. A total of 12 SIRTF image frames, obtained at 12 dithered positions, were used. Background and noise have been added. The HIRES image shown was obtained after 40 iterations. The observed image is a mosaic of all 12 raw image frames.

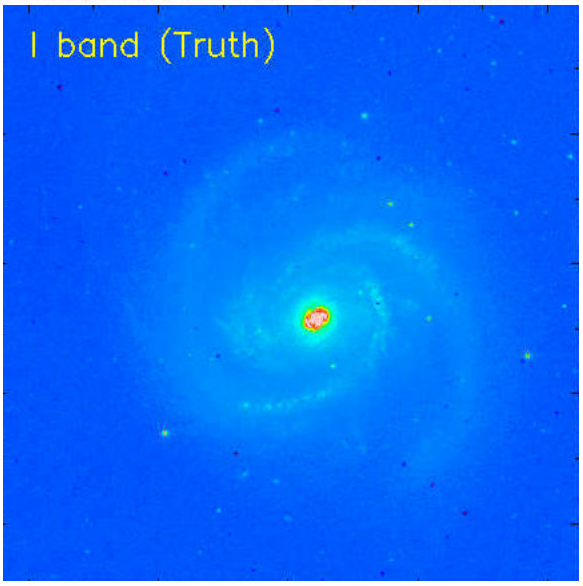

Fig. 3 Truth image used for simulating MIPS and IRAC images: I –band image of M100

C. SIGNIFICANCE OF RESULTS

In this task, we demonstrate that HIRES will be a powerful general-purpose tool for SIRTF science.

The results indicate that application of HIRES to the SIRTF survey of nearby galaxies will provide high-resolution image enhancement to achieve the goals of this survey.

HIRES will be directly applicable to missions beyond SIRTF, including Herschel and SOFIA

D. FINANCIAL STATUS

The total funding for this task was $70,000, of which $46,584 has been expended.

E. PERSONNEL

Timothy Thompson and Charles Backus, both in Astrophysics Element (3262), and Helene Roussel at IPAC were involved.

F. PUBLICATIONS

None.

TELECOMMUNICATION

FAST & ACCURATE PREDICTION OF ANTENNA-SPACECRAFT MULTIPATH EFFECTS

Interim Report

JPL Task 1015

Dr. Vaughn P. Cable, Spacecraft Telecommunications Equipment Section (336E)
Professor Oscar P. Bruno, Applied Mathematics, California Institute of Technology

A. OBJECTIVES

1. Phase 1

The objective of this research project (Phase 1) is to develop a new, fast and accurate electromagnetic (EM) solver [1] of UHF antenna-spacecraft performance (multipath) that significantly reduces the time and memory (e.g., 100 to 1000 times faster and 100 to 1000 times less memory) required to create and iterate an all-metal, antenna-spacecraft design.

2. Phase 2

The Phase 1 effort is necessarily limited to modeling metal-only spacecraft structures because the required theory for efficient (fast and accurate) modeling of radiation and scattering from non-metallic materials is not yet available. An actual spacecraft consists of metallic and non-metallic materials (e.g., composites), hence the primary objective of Phase 2 (proposed for 2003 DRDF funding) will be to develop a new, fast and accurate EM solver for non-metallic materials as well. To further reduce the design time for computing multipath for a full size, multimaterial spacecraft at frequencies up to 2 GHz, a parallel processing capability (Beowulf architecture) will also be added in Phase 2.

3. Background

In recent years, spacecraft antenna design has been a process often requiring many expensive iterations before an acceptable design is obtained. At present, predictions of the combined antenna-spacecraft multipath performance are quite limited, and a mockup of the vehicle with the antenna must be built and tested. In the future, fast and efficient computational modeling of antenna-spacecraft EM performance must play a larger role in the antenna design process and these cut-and-try methods must be used less.

In our approach, we seek to develop accurate and efficient EM solvers of surface integrals based on the Magnetic Field Integral Equation (MFIE) as well as the corresponding Electric Field Integral Equation (EFIE), and their combination [2]. In

attempting to develop accurate and efficient integrators for these surface integrals, two main problems need to be addressed, namely, accurate evaluation of the singular *adjacent interactions* – without undue compromise of speed, and fast evaluation of the voluminous number of *nonadjacent interactions* – without compromise in accuracy.

Our adjacent, high-order integrators are based on *analytical resolution of singularities*. The only alternative approach in existence is based on strategies of refinement around singularities (Canino et al. [3]). The approach we introduce is advantageous since it does not require costly setup manipulations and it leads to substantially more accurate and faster numerics.

The accelerator we introduce for the *nonadjacent interactions*, in turn, is related to two of the most advanced FFT methods developed recently [4]. A number of innovations in our approach, however, lead to very significant memory savings and faster numerics. Our design reduces, significantly, the size of the required FFTs – from N^2 to $N^{4/3}$ points, with proportional improvement in storage requirements and operation count. Further, it results in super-algebraic convergence of the equivalent source approximations *as the electrical size of the body (spacecraft) is increased*.

B. PROGRESS AND RESULTS

1. EM Field Solver

So far, a basic field solver for the acoustic (scalar) problem has been implemented. The results are similar to what can be expected from a full Maxwell solver. These results, for speed, efficiency and accuracy, are presented in Table 1 below. We present comparisons of accuracies and timings produced by our methods versus the well-known Fast Illinois Solver Code (FISC) [5] which uses the Fast Multipole Method [6]. We can see from Table 1 that our new algorithms run with considerably less RAM and yet with a comparable speed.

2. Geometry – Surface Representations

Calculation of EM multipath interactions with our new algorithm will require detailed information on the spacecraft surfaces and edges. This includes not just surface locations, but in some cases continuous higher-order surface derivatives. These data are not readily available from standard CAD programs because these programs focus primarily on mechanical design. Our progress so far with respect to surface representations includes:

i. Edges and corners - Geometry representations for complex spacecraft must include singular-type surfaces with intricate coordinate transformations. Our approach is applicable to such surfaces. In Table 2, for example, we present results on the performance of our approach for the singular scatterers of Figure 1. Errors are computed through convergence studies which, in turn, were checked through comparison with solutions for the same geometries, with "incident fields"

given by point sources within the scatterer – for which the solution is the field of the point source itself.

ii. Spacecraft geometry - The generic lander structure shown in Figure 2 has been implemented. This structure is similar to the test mockup used for measurement of MER Lander UHF antenna performance.

C. SIGNIFICANCE OF RESULTS

The results so far indicate that for scalar acoustics our new, fast and accurate solver technique is performing substantially better than current conventional methods. The work remaining in Phase 1 will focus on implementation and testing of the Maxwell EM (vector) field solver for antenna-spacecraft structures of metallic composition. At the end of this Phase 1 (July 2003), we expect to deliver an initial capability for multipath analysis of complete antenna-spacecraft structures with metallic properties. A follow-on Phase 2 is proposed elsewhere (2003 DRDF call) that will bring this new solver up to full strength and speed by incorporating arbitrary dielectric materials (e.g., composites) and parallel processing.

D. FINANCIAL STATUS

The total funding for this task was $100,000, of which $20,000 has been expended.

E. PERSONNEL

Besides Dr. Vaughn Cable and Professor Oscar Bruno, other personnel involved are Caltech post docs Drs. Matt Pohlman, Randy Paffenroth, and Christophe Geuzaine.

F. PUBLICATIONS

None.

G. REFERENCES

1. Oscar P. Bruno, et al., " A Fast, High-Order Algorithm for the Solution of Surface Scattering Problems: Basic Implementation, Tests, and Applications," *Journal of Computational Physics*, No. 169, pp. 80-110 (2001).
2. Oscar P. Bruno, et al., "Surface Scattering in Three Dimensions: An Accelerated High-Order Solver," *Proceedings of the Royal Society of London*, No. 457,pp. 2921-2934 (2001).
3. Lawrence F. Canino et al., "Numerical Solution of the Helmholtz Equation in 2D and 3D Using a High-Order Nystrom Discretization," *Journal of Computational Physics,* No. 146, pp. 627—663 (1998).
4. Elizabeth Bleszynski, et al., "AIM: Adaptive Integral Method for Solving Large-Scale Electromagnetic Scattering and Radiation Problems," *Radio Science*, Volume 31, No. 5, pp. 1225-1251, Sep-Oct 1996.
5. Jin M. Song, et al., "Fast Illinois Solver Code (FISC)," *IEEE Antennas and Propagation Magazine*, No. 40, pp. 27-34 (1998).

6. Ronald Coifman, et al., "The Fast Multiple Method for the Wave Equation: A Pedestrian Prescription," IEEE *Antennas and Propagation Magazine*, Vol. 35, No. 3 , pp. 7 –12, June 1993.

Algorithm	Diameter	Time	RAM	Unknowns	RMS Error	CPU
FISC	120λ	32x14.5h	26.7GB	9,633,792	4.6%	32 proc. SGI
Our Method	80λ	55h	2.5GB	1,500,000	.005%	Single 1.4GHz proc.
Our Method	100λ	68h	2.5GB	1,500,000	.03%	Single 1.4GHz proc.

Table 1. Scattering from large spheres.

Geometry	Diameter	Time	Unknowns	RMS Error	CPU
Cube	10x10x10	21h	96,774	.049%	Single 1.4GHz proc.
Saucer	42x42x17	53h	290,874	.0045%	Single 1.4GHz proc.

Table 2. Performance of our method on singular scatterers.

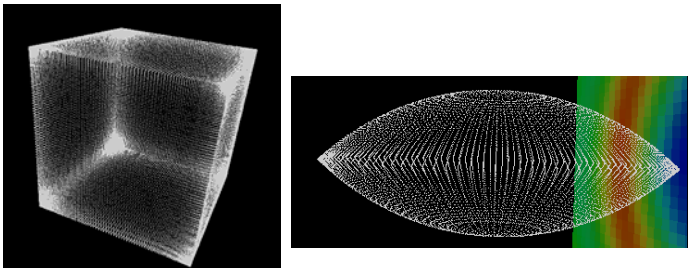

Figure 1: Two singular scattering geometries. Left: cube. Right: Flying saucer.

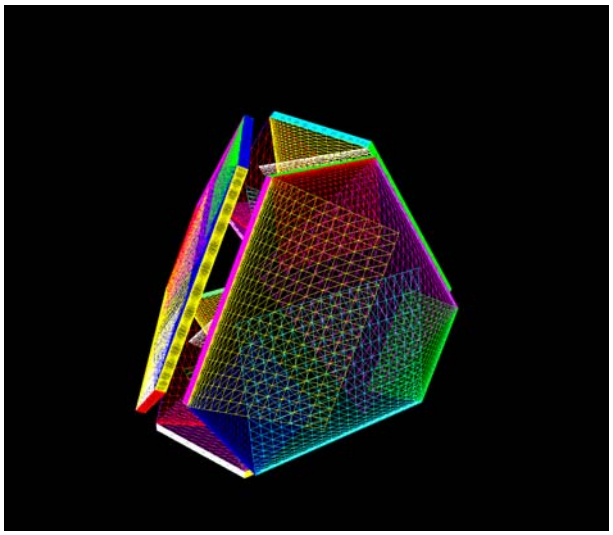

Figure 2: Basic MER Lander mockup geometry.